THE TROPICAL ATLANTIC TRADE WINDS AS RELATED TO DROUGHT IN NORTHEASTERN BRAZIL

by

JAMES CHE-MING CHUNG

S.B., Massachusetts Institute of Technology
(1977)

SUBMITTED TO THE DEPARTMENT OF
METEOROLOGY AND PHYSICAL OCEANOGRAPHY
IN PARTIAL FULFILLMENT OF THE
REQUIREMENTS FOR THE
DEGREE OF

MASTER OF SCIENCE

at the

MASSACHUSETTS INSTITUTE OF TECHNOLOGY

June 1981

© Massachusetts Institute of Technology 1981

Signature of Author _____
Department of Meteorology and Physical Oceanography
March 27, 1981

Certified by _____
Thesis Supervisor

Accepted by _____
Chairman, Departmental Committee on Graduate Students

WITHDRAWN
FROM
MIT LIBRARIES

Lindgren
MASSACHUSETTS INSTITUTE OF TECHNOLOGY
MAR 22 1982

LIBRARIES

THE TROPICAL ATLANTIC TRADE WINDS

AS RELATED TO

DROUGHT IN NORTHEASTERN BRAZIL

by

JAMES CHE-MING CHUNG

Submitted to the Department of Meteorology and Physical Oceanography on March 27, 1981 in partial fulfillment of the requirements for the Degree of Master of Science in Meteorology.

ABSTRACT

Surface wind and sea surface temperature data for the tropical Atlantic Ocean for the period 1911-1972 are analyzed in relation to the precipitation at Quixeramobim, Ceará in northeastern Brazil. The data is summarized into 5°x5° grid squares and long term monthly mean surface wind fields are computed and plotted. Correlations between the deseasonalized values of the u-component of the surface wind and the sea surface temperature are calculated and presented graphically. Stratified correlations between the autumn Quixeramobim rainfall and the December, January, February, and March values of SST, u- and v-components, and wind speed are also presented for the tropical Atlantic. The implications of the correlations are that the months preceding an abnormally dry autumn in NE Brazil are characterized by a strengthened South Atlantic trade flow and a North Atlantic circulation slightly weaker than normal. Cold SST anomalies are found in the South Atlantic and warm anomalies in the North Atlantic, suggesting a wind-induced change in the surface mixing. The divergence over the South Atlantic is seen to be stronger and more extensive preceding a dry season, and the equatorial convergence appears to be compressed northward and also strengthened. This northward compression is concluded to be responsible for the lack of rainfall in Ceara. The data also suggests a connection between the Quixeramobim precipitation and the Southern Oscillation.

Thesis Supervisor: Reginald E. Newell
Title: Professor of Meteorology

The Tropical Atlantic Trade Winds As Related To Droughts In Northeastern Brazil

Table of Contents

Abstract. 2

List of Tables. 4

List of Figures 5

I. The Introduction 7

II. The Tropical Atlantic Ocean

A. The Data and Procedure. 14

B. The Long Term Monthly Mean Ocean. 16

C. The Empirical Orthogonal Function (EOF) Analysis. 17

D. The Wind and the Sea Surface Temperature. 27

III. The Rainfall of Northeastern Brazil

A. The Data. 30

B. The Correlations With the Tropical Atlantic Ocean 33

IV. The Discussion 39

V. The Conclusion. 49

Acknowledgements. 52

References. 53

Tables. 55

Figures 58

List of Tables

Table 1: Summary of results of Empirical Orthogonal Function (EOF) analysis.

Table 2: Basic analysis of Quixeramobim precipitation data.

Table 3: ITCZ latitudinal position during abnormal rainfall, estimated from computer generated wind field plots.

Table 4: Comparison of ITCZ latitude estimates between wet and dry years.

List of Figures

Figure 1: Total number of observations for the period 1911-1972, by 5°x5° grid square.

Figure 2: Number of missing values for each quarter year: 1911-1972.

Figure 3: Standard deviation of raw data for all months, 1911-1972. (a-b)

Figure 4: Standard deviation of deseasonalized data for all months, 1911-1972. (a-b)

Figure 5: Monthly mean surface wind field plots. (a-l)

Figure 6: Unnormalized u-component EOF analysis. (a-d)

Figure 7: Unnormalized v-component EOF analysis. (a-d)

Figure 8: Normalized u-component EOF analysis. (a-d)

Figure 9: Normalized v-component EOF analysis. (a-d)

Figure 10: SST/u-component correlation coefficients using 7 lag relationships ranging from +3 months to -3 months. (a-g)

Figure 11: Time series of Quixeramobim autumn precipitation, expressed as the monthly average for the 3-month season.

Figure 12: Correlation coefficients: Autumn Quixeramobim rainfall with December, January, February and March SST. (a-d)

Figure 13: Correlation coefficients: Autumn Quixeramobim rainfall with December, January, February and March u-component. (a-d)

Figure 14: Correlation coefficients: Autumn Quixeramobim rainfall with December, January, February and March v-component. (a-d)

Figure 15: Correlation coefficients: Autumn Quixeramobim rainfall with December, January, February and March wind speed. (a-d)

Figure 16: (adapted from Hastenrath & Lamb 1977)
(a) - Sea level pressure, illustrating seasonal difference.
(b) - Equatorial convergence, illustrating seasonal difference.
(c) - Total cloudiness, illustrating seasonal difference.
(d) - Equatorial precipitation frequency, illustrating seasonal difference.

Figure 17: Longitudinal cross-sections of simple convergence index using only v-component of wind, comparing dry years' average with wet years' average.

Figure 18: Longitudinal cross-sections of second convergence index, using both u- and v-components, comparing dry years' average with wet years' average.

Figure 19: Second convergence index values for March. Average of 11 rainier than average years.

Figure 20: Second convergence index values for March. Average of 15 drier than average years.

I. The Introduction

In the field of meteorology one of the best approaches to studying the atmosphere is to examine its abnormal behavior. Just as the study of abnormal psychological behavior yields great insights into the workings of the human mind, much can be learned about the atmosphere from the study of its unusual states. It is also often the case that the study of unusual conditions in one small area of the world sheds much light on global meteorology of a scale much larger than the original immediate effects.

Many of the atmosphere's strange behaviors might not have attracted as much attention as they have had it not been for their effect on the human condition. Perhaps if the El Niño phenomenon off the coast of Peru did not have such a devastating effect on the Peruvian economy the urgency for climatological study might not have been so great, and much less would have been known today about the eastern Pacific circulation and its global implications. There are other examples, such as the droughts in the Sahel, but in any case it is unfortunate that we must often rely on the existence of human suffering in the world to direct the focus of our studies.

The annual rainfall of northeastern (NE) Brazil, particularly in the state of Ceará, and its interannual variations is a meteorological phenomenon which causes great distress for the local inhabitants. The large interannual variations often cause severe drought or flood conditions. Droughts may be so severe as to force the mass migration of millions of people to other parts of the country, as in 1958 [Rose 1980], and even if migration is not warranted famine is usually widespread. The immediate goal of meteorological and climatological study in this case, then, must be to ease the suffering of the people of Ceará, mainly through the develop-

ment of predictive aids. As the story unfolds, however, we find that we are apt to learn much about the entire atmosphere and its behavior.

Investigators of the problem have taken various angles of attack. Sampaio Ferraz [1950] sought extraterrestrial explanations and published predictions of drought based on sun spot cycles, although earlier he had labeled the inability of cold destabilizing anticyclones to reach low latitudes as the cause of the droughts [Sampaio Ferraz 1931]. On a more down to earth level, Brazilian rainfall has been connected to the Southern Oscillation by Walker [1928] who suggested using pressure and other data from distant locations as predictors. The Walker circulation, as represented in the Atlantic Ocean by a thermally driven zonal cell, has been discussed in relevance to the Brazilian precipitation by Bjerknes [1969] and Kidson [1975]. Serra & Ratisbona [1942] first noted the relationship between the position of the Intertropical Convergence Zone (ITCZ) and the amount of rain received in NE Brazil. Droughts were concluded to be the result of the ITCZ remaining north of the equator.

Caviedes [1973] has noted the simultaneity of the occurrences of El Niño and of the "sêcas" (droughts) of NE Brazil. He blamed this double hazard on simultaneous unusual behavior on the parts of the South Atlantic and South Pacific subtropical high pressure centers. During a sêca the South Atlantic high remains in an abnormally northern position and prevents the ITCZ from its normal southward movement. Hence, the associated rains do not reach NE Brazil. On the other side of the continent, the South Pacific anticyclone remains at about 35°S rather than moving northward as it normally does. Thus, the southeast trade winds along the Peruvian coast weaken considerably and in rare cases may even disappear. This causes the upwelling to weaken, and warm water to flow into the area from the north.

Meanwhile, the ITCZ and its attendant rains move much farther south than usual. The net result is the destruction of the nutrient rich environment upon which Peru's anchovy industry depends so heavily.

By comparing ten years when NE Brazil was drier than normal with ten wetter than normal years, Hastenrath & Heller [1977] noted a strong negative linkage between NE Brazil rainfall and sea surface temperature (SST) along the coasts of Peru and Ecuador. They suggested that this linkage is related to the Southern Oscillation and the concomitant large-scale mass adjustments, which may cause inverse pressure variations over the eastern South Pacific and South Atlantic Oceans.

Another long-range connection was found by Namias [1972] who discovered that the precipitation at Quixeramobim in Ceará was highly dependent upon the degree of cyclonic activity near Newfoundland and Greenland during the Northern Hemisphere winter and spring. Drought in NE Brazil was found to be associated with intense blocking over North America and the North Atlantic. Namias explained that anticyclones in the Newfoundland-Greenland area are related to a weaker or absent subtropical high. He claimed that the resultant diminished NE trade winds and weaker Hadley cell reduces the rising motion in the ITCZ and decreases latent heat release, and thus places less demand on the SE trades in the Southern Hemisphere. These weakened SE trades then bring less moist air into NE Brazil, and the net result is drought.

Serra's explanation [1946] also involved the circulations of both hemispheres. Noting the symmetry in the occurrences of cold invasions in the Northern Hemisphere and in the Southern Hemisphere, Serra postulated that during rainy years intense cold invasions over the Gulf of Mexico and the Caribbean Sea force the ITCZ to the south. At the same time, cold

invasions in South America, appearing in rapid succession, push the South Atlantic anticyclone farther out to sea. This weakens the SE trade winds, enabling the ITCZ to move southward.

In addition to the linkage with the eastern Pacific, Hastenrath & Heller [1977] also found evidence for inverse behavior of the subtropical highs in the North and South Atlantic Oceans. According to their work the South Atlantic high expands to the north during a rain-deficient season while the North Atlantic high also moves northward. Evidence for this comes in the form of an abnormally northward positioning of the equatorial low-pressure trough, the band of maximum convergence, and the associated bands of maximum precipitation frequency and maximum cloudiness. Wind regimes are also shifted north, with North Atlantic trades weaker than the long term average and South Atlantic trades stronger.

This Northern Hemisphere/Southern Hemisphere dichotomy is also manifested in the sea surface temperatures of the Atlantic. Hastenrath & Heller [1977] found that during drought years the Atlantic is warmer in the north and colder in the south than the long-term mean, while the eastern Pacific is anomalously warm. Markham & McLain [1977] arrived at similar conclusions from their study of the South Atlantic. Their month-by-month correlations of sea surface temperature and an index derived from rainfall in Fortaleza (on the Ceara coast) and Quixeramobim (about 120 km inland) revealed a region of high positive correlation which traversed the Atlantic Ocean at about 10°S from east to west between December and March. They suggested that the sea surface temperature is responsible for the variations in the wind flow over the ocean which is associated with the NE Brazilian rain. Cold water stabilizes the overlying air, decreases the flow, and inhibits convection. The trade-wind inversion thus becomes lower

and less moisture is carried into NE Brazil.

Moura & Shukla [1980] investigate another possible mechanism to explain the sea surface temperature--rainfall link. With a heat source north of the equator (anomalously warm water) and a sink south of the equator (anomalously cold water) there is a possibility of a thermally forced dynamical circulation. This circulation would consist of ascending motion to the north and descending air to the south. The reduced moisture flux convergence and evaporation associated with descending motion over NE Brazil and its neighboring ocean areas would clearly have a negative effect on the rainfall. By using a simple analytical model, Moura & Shukla showed such a thermal forcing would indeed result in a meridional circulation consisting of descending motion and anticyclonic vorticity to the north and ascending motion and cyclonic vorticity to the south. They also performed several numerical experiments using the Goddard Laboratory for Atmospheric Sciences general circulation model, and when sea surface temperatures similar to those illustrated by Hastenrath & Heller's [1977] composite drought maps were specified, the model produced a rainfall reduction over northeast Brazil. Subsequent experiments revealed the dependence of the magnitude of rain deficiency on the position and spatial arrangement of the warm anomaly, as maximum effect (most severe drought) was obtained when the warm water was located in the western part of the tropical North Atlantic, as opposed to lying close to the African coast.

Thus, we have several pieces of a most interesting puzzle which somewhat fit together, but many crucial pieces are still missing. Most investigators seem to agree that it is the position of the ITCZ which determines the rainfall characteristics of NE Brazil. Simply put, when the Convergence does not travel as far south as it normally does, its rains do

not reach NE Brazil and drought and famine ensue. To go beyond this, however, is not so simple, for it is unclear what forces govern the ITCZ's position. What is it that causes the Convergence to occasionally remain northward of its normal position? Is it the behavior of the subtropical highs in the North and South Atlantic Oceans, which may in turn reflect the behavior of the Southern Oscillation or the northern subpolar circulation? Or is the sea surface temperature mainly responsible, with warm anomalies to the north anchoring the ITCZ while cold anomalies to the south reduce the moisture influx over NE Brazil? Then again, perhaps it is not the position of the ITCZ, but the strength of the convergence which determines drought or surplus for the region. Weaker low level convergence over NE Brazil, such as that produced by Moura & Shukla's [1980] thermally driven cell, would surely have a detrimental effect on the precipitation without the need for a translation of the convergence region.

The issue seems to boil down to displacement versus intensity. Assuming that it is some irregularity in the atmospheric circulation which is responsible for producing anomalous precipitation in NE Brazil, one wonders if the irregularity manifests itself as unusual positioning of the ITCZ, or as unusual low-level convergence over the affected region. Perhaps it is both acting together, or perhaps one mechanism is responsible for some of the abnormal rainfall years while the other mechanism is responsible for the rest. And there is always the possibility, however remote, that neither effect is important and that we are barking up the completely wrong tree.

In this report analyses of surface wind and sea surface temperature data for the tropical Atlantic Ocean and rainfall data for northeastern Brazil, all for the period 1911-1972, will be presented in an attempt to

fit another piece into the puzzle. First, the climatology of the ocean as determined by the sixty-two years of data will be discussed. Long-term monthly mean wind fields will be presented, as well as empirical orthogonal function analyses for the period 1949-1972. Correlations between sea surface temperature and surface wind will also be presented in order to gain some insight into the all-too-important interactions of the two parameters. The mainstay of this report will be the correlations computed between the oceanic data and the rainfall. With this type of information the relative influences of the various parameters in the various parts of the ocean may be evaluated. It will be found that the data does not provide incontrovertible evidence for either option in the displacement/intensity issue, but a strong suggestion is made in support of the displacement argument.

II. The Tropical Atlantic Ocean

A. The Data and Procedure.

The oceanic data used in this research was obtained from the United States National Climatic Center and is a subset of Tape Data Family-11. Tape Data Family-11 (TDF-11) is an enormous compilation of over 31 million weather observations covering the entire globe for the period 1800 to the present. The subset used here covers only the tropical Atlantic Ocean, from 30°N to 30°S, and represents only the period 1911-1972. Furthermore, it is a modification of TDF-11, containing monthly summaries of all the observations in each 1°x1° square for the given period. Thus, for each month, one record represents one 1°x1° square and contains data concerning sea level pressure, temperatures, clouds, wind and weather for that square.

For practical purposes it was necessary to further summarize the data into 5°x5° grid squares. Figure 1 illustrates the degree of coverage over the ocean by presenting the number of original wind observations that went into the wind data summary for each 5°x5° grid square. This new dataset contained values of sea surface temperature, sea level pressure, u- and v-components of the surface wind, and the number of observations represented by each value for the entire area of coverage for each month from 1911 to 1972. Since the 5°x5° values were calculated from 1°x1° averages, and not directly from the observations, it is hoped that any bias which may have been caused by clustering of the observations was greatly reduced. If there were no observations in a given 5°x5° grid square during a given month, then that square was represented for that month by a designated missing value. Figure 2 shows the time series of monthly missing values summarized into four 3-month quarters per year. The maximum

value possible is 477 (3 months x 159 grid values per month), and the minimum possible value is zero. The two World Wars are very conspicuous in the high number of missing values associated with those years, whereas the period from 1964 to 1970 shows very few missing values, indicating very diligent data collection.

Once the raw data had been summarized into 5°x5° blocks, the next step was the calculation of the long term monthly means. These means were then subtracted from the raw data to obtain a deseasonalized dataset of deviations from the monthly mean for each parameter. This was the dataset used in most of the subsequent calculations. The data was also averaged into seasonal values, and long term seasonal means and deviations from the seasonal means were also computed. These numbers however, were not used in any of the computations to be discussed here and will not be presented at this time.

Figures 3a and 3b present the standard deviation of the raw data. For the u-component the areas with the largest variances are located on the northern and southern edges of the tropics, illustrating the influence of the extratropical circulation on that of the tropics. Relative minima are located along the east coast of Brazil and under the "bulge" of Africa. The interesting feature of the v-component standard deviation is the relative maximum located in the center of the ocean between the equator and 10°N. No doubt this is an effect of the annual migration of the ITCZ through this area. Maxima are also present along the northern and southern borders. Figures 4a and 4b present the standard deviation of the deseasonalized data. The only real difference between these figures and those of the raw data standard deviation is found in the region of the ITCZ. Since the average annual movement of the ITCZ has been removed in

the deseasonalized data, the large variances associated with this behavior are no longer present. Away from this region the patterns for the raw data and the deseasonalized data are very similar.

B. The Long Term Monthly Mean Ocean.

The long term monthly mean winds for the tropical Atlantic Ocean are presented pictorially in Figures 5a-51. The pictures cover from 30°N to 30° S latitudinally, and from 100° W to 20° E longitudinally. The horizontal and vertical broken lines represent the equator and the Greenwich meridian, respectively. Each vector represents the mean wind for that month in that particular 5°x5° grid square. It should be noted that the presence of missing values often resulted in the means being calculated from less than sixty-two years of data. Extremely poor representation can be found in the center of the tropical South Atlantic during the winter months, where more then half of the sixty-two years may be missing. On the other hand, the ever popular shipping lanes which traverse the ocean are sources of plentiful and reliable observations.

The mean wind field pictures allow us to visualize the flow of the trade winds and its variation through the year. By judging the position of the ITCZ by sight, we can see that the ITCZ reaches its southernmost position in March and its northernmost position in September. In March, the ITCZ is located about 2° latitude south of the equator near NE Brazil. Tracing it eastward, it slopes northward until it hits the bulge of Africa at about 5°N. In September the Convergence appears to have its western end hitting South America at about 10°N, and its African end at about 13°N. Therefore, we see an annual displacement of about 8° latitude in the eastern Atlantic and about 12° latitude in the western Atlantic. Although the

overall wind patterns away from the ITCZ do not differ much between the two months, we notice that the September SE trades are stronger than the March winds, but the NE trades are stronger in March than in September.

Comparison of the January mean surface wind field with the July field reveals striking differences between the two circulation patterns. In both cases the circulation in the summer hemisphere is very strong and well defined, while that in the winter hemisphere shows signs of confusion and weakness. Particularly notable are the differences evident in the vicinity of 20°-30° in both hemispheres. The summer hemisphere shows a definite tendency toward anticyclonic rotation, the center of which would appear to be located just off the picture. The winter hemisphere, on the other hand, shows a more or less unidirectional flow.

C. The Empirical Orthogonal Function (EOF) Analysis.

EOF analysis was performed on the wind component data. This type of analysis transforms the variation through time of a data field into a linear combination of unchanging component fields, each component field being completely independent of all the others. The component fields do not change through time, but the linear combination of them does, and by using the time series of the coefficients for each component field one may completely reproduce the original variation of the data with time. The advantage of using EOF analysis is that it can facilitate the visualization, and thus the understanding, of important physical processes by isolating their effect on the atmosphere from the effects of other processes, and from random noise in the data. Also, EOF analysis allows one to get a good idea of how much of the variance of the original field was actually meaningful and representative of real atmospheric phenomena, and how much was merely noise

in the data.

EOF analysis computes the eigenvalues and eigenvectors of the covariance matrix of the original data. The covariance matrix is a symmetric matrix of order N, where N is the number of data points in the field, and contains the covariance of each location with every other location. Each eigenvector represents a component field, or function, and each is linearly independent of, or orthogonal to, every other vector. Each eigenvalue represents the fraction of the total variance of the original field that can be explained by its associated eigenvector. This explained fraction of the total variance is simply computed by dividing the eigenvalue by the sum of all the eigenvalues. The matrix of the coefficients through time of each component function is obtained by multiplying the transpose of the eigenvector matrix by the original data matrix. For a detailed and more rigorous treatment of EOF analysis, the reader is referred to Kutzbach [1967].

Basically stated, the eigenvector with the largest eigenvalue, usually referred to as the first mode, is the component pattern whose variance explains the largest proportion of the total variance, or whose variation through time most closely matches that of the original data. The eigenvector with the second largest eigenvalue, the second mode, is the pattern which best explains the variance not explained by the first mode; it tries to make up for the deficiencies of the first mode. And so forth and so on—each subsequent mode is the best attempt at explaining the variance that was not explained by all the preceding modes. Finally, the last mode is the function that fills all the holes and reproduces exactly the original data when added to all the preceding modes.

The data used in EOF analysis cannot contain any missing values for

the computations to work properly. There must be some sort of value for every location for every observation, so all missing values in the data to be analyzed must be substituted for by one method or another. A problem arises, then, because one wants to use as many observations as possible in order to obtain the most significant covariances possible. Generally speaking, though, the inclusion of more observations will bring more missing data into the analysis, and no matter how the missing data is filled in, be it by interpolation, substitution, or whatever, the new surrogate value can only have a detrimental effect on the validity of the analysis since it is not the true value. Therefore, one uses the strategy of minimizing the number of missing values in the dataset, and yet maximizing the number of observations. For this reason only the data for the period 1949-1972 were used, for that period represented the best compromise. There was also the additional benefit that many of the missing values within this period were isolated in time and/or space, thus making interpolation feasible.

In substituting for a missing value, the basic aim is to estimate the true value of the variable, which is not known, from information that is known. One desires the best estimate possible so that the EOF analysis is affected as little as possible by the missing data. With the data used here there are basically four ways to fill in a missing value. One can interpolate latitudinally between the missing value's east and west neighbors, interpolate longitudinally, interpolate temporally between the previous and subsequent values for that location, or simply use the long term climatological mean in place of the missing value. Working with Pacific sea surface temperature data, Navato [1980, personal communication] found it wisest to apply the methods in the order stated above, using the latitu-

dinal interpolation as a best guess and the climatological mean as a last resort guess. Tests performed on the tropical Atlantic wind data, however, showed that the four methods could not be positively ranked by accuracy in this case. It was found that an average of the four estimates gave the best overall results over the entire dataset, although such an value might not have been the most accurate estimate in any given case. We opted to use this mean value to replace our missing data in preparation for the EOF analysis.

A cutoff value of 28 missing values out of 288 observations was used to determine the qualification of each grid square, such that if the square was above the cutoff it was not used in the analysis. The cutoff value was quite clearly suggested by the data in the South Atlantic, for as one traversed the boundaries of the shipping lanes extending northwestward from southern Africa, an abrupt change in the number of missing values per grid square was encountered. Within the shipping lanes were relatively low numbers, typically less than twenty missing values, and it was considered acceptable to fill in these values. The regions outside the lanes, however, contained much higher figures, many in the hundreds, and it was felt that filling all these values would introduce too much error into our analysis. The use of this cutoff was necessary to preserve the quality of the data, but also unfortunate in that it eliminated large areas from the analysis. A large portion of the South Atlantic off the coast of Brazil was excluded, as was a region next to Africa encompassing the Gulf of Guinea.

There are two sets of analyses presented here, normalized and unnormalized. The unnormalized analysis uses the basic deviation from monthly mean data, whereas the data used in the normalized analyses have been divided by the monthly standard deviation. Thus, in the normalized

analysis all the locations are weighted equally in the determination of the orthogonal functions, while in the unnormalized analysis those squares with larger absolute variance carry more weight than those with smaller variance.

Some of the results of the four EOF analyses, unnormalized and normalized for u- and v-component each, are presented graphically in Figures 6 through 9. The time series of the modal coefficients are in the units of knots for the unnormalized analyses, and in the units of monthly standard deviations for the normalized analyses. The maps of the modes are dimensionless.

The unnormalized u-component EOF analysis shows a strong extreme at the northern edge of the data in all of the first four modes. This very strong effect is most likely caused by the strong control exerted by the North Atlantic subtropical anticyclone.

Mode U1 shows the anticyclone influence dominating the entire region, so much so that almost all the grid squares are in phase together. South of the equator is seen to be relatively flat and featureless. The associated time series TSU1 does not show much in terms of long term trend, but there is a slightly upward tendency from 1969 to 1972. TSU1 does show a very marked annual behavior in which the early months of the year show a much greater variance than the late months. This could possibly reflect the annual behavior of the North Atlantic anticyclone, the center of which is located close to the African coast in the wintertime and more in the middle of the ocean in the summer.

Mode U2 is interesting in that the North Atlantic is split into opposite phases in the west and east. The longitudinal boundary between the two regions represents either an area of divergence given a positive coef-

ficient, or of convergence given a negative coefficient. The time series TSU2 shows very little in the way of distinctive characteristics. A weakly defined oscillatory behavior may be discerned, but its possible significance is unclear.

Mode U3 is almost all negative, with prominent negative regions located at about 15°N in the center of the ocean, and also in the southeastern corner of the analysis coverage. A localized strong positive area exists in the northeastern corner off the African coast. Time series TSU3 shows definite upward trends in the early and late years of analysis, but not much in between.

Mode U4 is similar to U3 in that very strong extremes are located in the northeastern and southeastern corners of the data. The large southeastern extremes found in U2, U3, and U4 may represent some influence of the South Atlantic high, or perhaps be an artifact which would disappear if the missing squares in the South Atlantic were included in the analysis. A slightly rising oscillatory pattern is shown by TSU4.

Mode V1, the first mode of the unnormalized v-component analysis, shows a division of the North Atlantic into two opposite phase regions. The eastern region contains the largest value found anywhere on the map, as the effect of the subtropical high seems to be showing up in this analysis, also. The time series TSV1 shows a slight downward trend in the long run.

A four-way division of the North Atlantic shows up in mode V2. The largest values appear in the east along the coast of Mauritania. The center of the South Atlantic shows a tendency toward an extreme, but the missing data prevent full definition. An upward trend is seen in TSV2 until the series apparently levels off in the middle years, and then dips down to below normal values during and after 1964.

Mode V3 has a strong positive region in the central North Atlantic and a weaker one in the southeastern corner of the ocean. The strongest negative values are located around the Florida peninsula. The time series TSV3 is somewhat featureles overall and one might suspect that the mode represents a substantial amount of random noise.

Mode V4 divides the ocean at about 10-15°N into a predominantly negative segment to the north and a positive segment to the south. A strong negative extreme is located off the coast of Western Sahara in the northeastern corner. Another strong negative zone is found along the Brazilian southeast coast, but its import is not clear due to the lack of neighboring data. The time series TSV4 does not show any outstanding characteristics.

In the first mode of the normalized u-component analysis NU1 there is no large extreme to the north, indicating that the normalization of the data has reduced the effect of the subtropical high by giving each location equal weight. The function is almost all the same phase and actually quite smooth, save for a mild positive extreme to the east of Puerto Rico. The corresponding time series TSNU1 shows a strong downward trend beginning in 1969, but other than that the behavior is essentially level.

Mode NU2 is composed of quasi-latitudinal belts which progress from a negative extreme in the north to a positive extreme just off the mouth of the Amazon. Time series TSNU2 shows a drop in the long run with the overall trend seemingly modified by a single long-period oscillation.

In the third mode NU3 a strong positive area is located right around Jamaica and large negative values exist in the center of the 30 N northern boundary. The southern half is quite nondescript. Time series TSNU3 is relatively trendless, although oscillations having a period of about seven years do seem to be present.

Mode NU4 shows a region of negative values just north of the equator sandwiched between two positive regions to the north and south. Its time series TSNU4 does not have any overall trend, but does show the presence of oscillations with a period of about five years.

Mode NV1 is the first mode of the normalized v-component EOF analysis, and shows a rather well defined pattern in the North Atlantic, but a relatively poorly defined one in the South Atlantic. The main attractions are a strong negative extreme just northeast of the West Indies, and a positive region located in the Gulf of Mexico. The rest of the ocean is only weakly defined with no strong extremes of either sign. The time series TSNV1 has a slight downward trend from 1949 to 1963, but then rises to a maximum in 1967 and descends from then on.

The majority of the area of NV2 is negative with a strong negative extreme located northeast of the Guianas. Not too far away to the northwest is a strong positive zone. Time series TSNV2 does not show any real long term trend, though there is short term behavior on the scale of several years.

In mode NV3 the most interesting feature is a strong negative area straddling the equator just off northeastern Brazil. The central North Atlantic is occupied by positive values. There is a definite upward trend apparent in TSNV3, and for the last ten years there is in addition a definite oscillation present.

Mode NV4 shows a positive-negative boundary whose position remarkably resembles that of the ITCZ. Perhaps NV4 is related to the strength of the Convergence, for a positive coefficient would represent stronger convergence and a negative coefficient weaker convergence. The only other feature apparent is a negative extreme in the Caribbean Sea. The time se-

ries TSNV4 rises for the first six years and then levels off. Beginning in 1964 some oscillatory behavior is present.

While the EOF analyses presented above are useful in understanding the regime of the tropical Atlantic, there is some room for improvement. It is believed that a monthly or seasonally stratified EOF analysis, i.e. restricting the analysis to the variance of just one month or season, would present much more useful information. When there exist phenomena such as the precipitation in NE Brazil which are very seasonal, information tends to become blurred by the non-stratified analysis. In this case, however, twenty-four years of data, while adequate for a non-stratified analysis (288 observations), was not deemed sufficient for a stratified analysis (24 observations).

An inspection of the modes discussed above shows that in many cases the function may be very well defined in the North Atlantic, but then at the same time be quite featureless in the South Atlantic. Much information is being lost by the exclusion of the large areas in the South Atlantic. This is not surprising, for the fact that they do not lie in the mainstream of shipping activity, and therefore have very few observations, does not necessarily mean that their relationships with the rest of the ocean are unimportant. Indeed, it is expected that the wind data in the central South Atlantic would play a very important role in the determination of the effects of the South Atlantic high. The inclusion of data for the omitted regions would definitely have a major effect on the EOF functions in the south. How the functions in the North Atlantic would change is less clear and may prove very enlightening.

It is not hard to notice the large month-to-month variations apparent in all the time series of the EOF modes. This kind of behavior, prevalent

even in the lowest modes, indicates extreme unsteadiness in the wind data. The inter-monthly variations of the wind data, raw and deseasonalized, is often of the same magnitude as or greater than the actual values themselves. This tends to complicate matters in the examination of any long term trends. Indeed, in studying the EOF time series it was often difficult or impossible to confidently identify any trend-like behavior. Perhaps it would have been judicious, then, to employ some sort of filtering or averaging procedure to clarify matters.

A major question in any EOF analysis is the determination of which modes are actually meaningful and which ones represent noise or random fluctuations. Craddock & Flood [1969] address this problem by plotting the logarithm of the eigenvalues against the eigenvalues' ordinal numbers. They observed that after a certain number of modes the logarithms of the eigenvalues approximate a straight line, and asserted that the noise eigenvalues in meteorology are in geometrical progression. The lower number modes, then, that deviate substantially from the straight line can be safely assumed to consist of meaningful signal predominating over any noise, while those modes close to the line may be assumed to represent non-meaningful signal or noise. This graphical method, when applied to the four analyses discussed above, showed that for the wind components, normalized and unnormalized, modes beyond number 15 probably represent noise, and only modes 10 and below can be thought of as being mostly significant information. Table 1 shows that the first fifteen modes only account for 50%-60% of the total variance, depending on which analysis is being considered. This infers that 40%-50% of the total variance must be random fluctuations. If mode 10 is taken to be the cutoff for meaningful patterns, then only 41%-51% of the total variance has been explained. The four modes

presented graphically only explain 22%-34% of the total variance, and thus only about half of the meaningful variance.

D. The Wind and the Sea Surface Temperature.

Correlation coefficients between the sea surface temperature and the u-component of the wind field are shown in Figures 10a-10g. The problem of the interrelationships between the surface wind and the sea surface temperature is not the main concern of this report, and hence will be only briefly discussed here in terms of the climatology of the Atlantic.

The correlations are calculated for seven different lag relationships ranging from SST values correlated with u-component values three months later, to correlation of contemporaneaus values, to SST values correlated with u-component values three months before. Three main areas of interest become apparent from inspection of the maps. One region extends all along the eastern coast of South America, but the area of maximum effect appears to be near northeastern Brazil. Another region lies close to the bulge of Africa, off the coast of Senegal. The third region is under the African bulge.

The first region shows strong negative correlations throughout the seven lags. The correlations are stronger and more widespread when the SST leads the wind than vice versa, so we conclude that the sea is affecting the wind. The persistence of the SST anomalies tends to extend the correlations through to the other lag relationships. One must keep in mind that a negative correlation means positive SST anomalies connected with negative u-component deviations, and vice versa. Since the winds in this area all have easterly components, the figures imply that warmer water results in stronger easterlies and cooler water results in weaker

easterlies. It might be concluded that such a relationship implies some sort of control on local convergence by sea surface temperature, possibly along the lines of the mechanism proposed by Markham & McLain [1977]. The affinity of the high correlations for the windward coastal regions is somewhat puzzling, though.

The second region, off the African bulge, is one of strong positive correlation, and quite definitely infers a wind-influencing-sea type of relationship. Since this region, too, is in an area where easterly component winds prevail, the positive correlation with u-component values ahead of SST values implies stronger easterlies resulting in cooler water, and weaker easterlies resulting in warmer water. At first guess one might conclude that the stronger winds are inducing a stronger upwelling and thus cooling the water. This seems dubious, however, because calculations of surface divergence such as those performed by Montgomery [1936] show that the actual upwelling region hugs the African coastline quite closely and does not quite coincide with this high correlation region, which is slightly further offshore. Thus, we must hypothesize that the ocean water in this area is cooled through increased evaporation due to stronger wind.

The high correlation region south of the African bulge apparently is also one of wind deviations preceding sea surface deviations. The region has two parts: an area of negative correlations in the Gulf of Guinea, and an area of positive correlations just to the south. Correlations of SST with the u-component are somewhat difficult to interpret here, because the winds on the average are almost directly from the south. It can only be said that a positive u-component deviation, i.e. a stronger westerly or weaker easterly, will yield colder water in the Gulf of Guinea, but warmer water in the area to the south. We feel that these correlations with the

u-component are not very informative in this region of the ocean, and that correlations with the v-component, not computed here, would be more appropriate.

Mention should be made here of the work done by Bakun [1978] concerning the Gulf of Guinea. Bakun explored the interrelationship between sea surface temperature and wind-stress induced offshore Ekman transport in these waters, and found reasonably good correspondence between the seasonal and spatial pattern of the Ekman transport and that of the sea surface temperature. Stronger Ekman transport, due to stronger winds, corresponded quite well with lower SST in both time and space in the Gulf. This supports the negative correlations found in the Gulf of Guinea between SST and the u-component, for since the prevailing winds are SW in this region the negative values indicate a connection between a larger westerly component and a lower SST Bakun also found strong correlation between sea surface temperature and coastal precipitation, suggesting a direct effect of the SST on the stability of the shoreward airflow.

There is an interesting region of high positive correlation in the central South Atlantic which is truly apparent only when the u-component is three months ahead of the SST. The correlations quickly weaken and disappear as the lag becomes smaller and reverses. Somehow the wind in this region is affecting the sea surface temperature three months later such that stronger than normal easterlies bring cooler water. Is it possible that a spin-up of the South Atlantic anticyclone would produce anomalously cold water three months later? Further study is warranted here to fully determine the validity of this correlation and perhaps firmly establish a cause.

III. The Rainfall of Northeastern Brazil

A. The Data.

Unlike the marine surface data which was available on magnetic tape ready for processing by computer, the rainfall data had to be transcribed manually from two collections of data. Data for 1911-1960 were obtained from:

World Weather Records, Smithsonian Miscellaneous Collections, Vol. 79, published by Smithsonian Institution, 1927.

World Weather Records 1921-1930, Smithsonian Miscellaneous Collections, Vol. 90 (cont. from Vol. 79), publ. by Smithsonian Institution, 1934.

World Weather Records 1931-1940, Smithsonian Miscellaneous Collections, Vol. 105 (cont. from Vols. 79 & 90), publ. by Smithsonian Institution, 1947.

World Weather Records 1941-1950, publ. by U.S. Department of Commerce, U.S. Weather Bureau, Washington, D.C., 1959.

World Weather Records 1951-1960, publ. by U.S. Dept. of Commerce, U.S. Weather Bureau, Washington, D.C., 1965.

For the period 1961-1972 rainfall values were obtained from:

Monthly Climatic Data for the World, Vols. 14-25, U.S. Dept. of Commerce, Environmental Science Services Administration, Environmental Data Service, Asheville, N.C.

From these sources rainfall data was collected for thirteen Brazilian stations:

Santarem	2°25' S	54°43' W
Turiacu	1°42' S	45°26' W
Quixeramobim	5°16' S	39°15' W
Fernando de Noronha	3°50' S	32°25' W
Recife	8°04' S	34°53' W
Salvador	12°57' S	38°29' W
Juiz de Fora	21°45' S	43°20' W
Rio de Janeiro	22°54' S	43°10' W
Sao Paulo	23°24' S	46°55' W
Iguape	24°42' S	47°30' W
Curitiba	25°25' S	49°17' W
Brusque	27°05' S	48°59' W
Cuiaba	15°36' S	56°06' W

Only one station, Quixeramobim, will be discussed here as it is the only station which is located in the drought-prone state of Ceará.

Correlation coefficients were calculated for each pair of deseasonalized precipitation time series for the thirteen stations. It is interesting to note that the five northernmost stations: Santarem, Turiacu, Quixeramobim, Fernando de Noronha, and Recife, showed moderately strong positive correlations among themselves. This is not too surprising since the first four all come under the influence of the maritime equatorial type of precipitation regime as described by Ratisbona [1976]. Recife is also very close by, though technically it is in the area of the maritime tropical regime. (The various regimes are distinguished by the source of the air mass which is responsible for the rain.) Thus, while Quixeramobim is the only station analyzed here, it would be interesting to see how the droughts in Ceará are reflected in the precipitation at the other stations. These five stations provide a good spatial distribution which should provide very interesting results.

The basic statistics for the precipitation at Quixeramobim are presented in Table 2. The data seems to be quite complete as only thirteen of the 744 total months are missing. The average total for the year is 742 mm., and the distribution of the rainfall through the year strongly reflects the influence of the ITCZ on the local precipitation regime. March, which is the month of southernmost displacement of the ITCZ, is also the rainiest month, closely followed by April. At the other extreme, September and October, the months of northernmost ITCZ position, are also the driest months.

The autumn season, March-April-May, receives sixty-one percent of the annual precipitation, and it is during this season that the effects of anomalous rainfall most strongly manifest themselves. For this reason most of the computations discussed below will deal with the precipitation for

this season only. The term "dry year" will refer actually to an autumn with below average rainfall, and not necessarily to the entire year. As an aside, Markham & McLain [1977] performed their calculations on the January-February-March rainfall. It can only be speculated that the inclusion of the Fortaleza data along with the Quixeramobim data necessitated their choice of seasons, for it would definitely seem to be inappropriate here. For computational reasons it was easier to deal with the monthly average during autumn instead of the total precipitation for autumn. This value was defined as the average of the March, April, and May values, or in the event of missing values, the average of whichever numbers were present. Only if all three months were missing was the autumn monthly average reported as missing. From Table 2 we see that only one April value and two May values are missing, so at most there are three autumn monthly averages which are not fully accurate representations of the autumn months. Should April and May both happen to report missing in the same year, the March value alone would be used, and this would yield on the average an estimate about eighteen percent too high. This was considered acceptable since this situation could arise at most once during the sixty-two years.

The time series of autumn monthly average precipitation is shown in Figure 11. Several periods of prolonged drought are noticeable, particularly 1918-19, 1930-32, 1941-43, 1953-54, and 1958-59. Rainy years are also discernible, but it appears that above average rainfall rarely lasts more than one year, while dry spells of two or three years duration are not uncommon. It is also quite noticeable that the interannual variations in the first part of the time series are much greater than those of the later part. Could this be more a reflection of the data collection practices than of the actual precipitation? With the lack of any information other-

wise we must presume that these are consistent observations and that all the variations are due to the precipitation only.

B. The Correlations With the Tropical Atlantic Ocean.

Monthly stratified correlations were computed between the autumn (March-April-May) rainfall at Quixeramobim and the sea surface temperature, u-component of the surface wind, v-component, and wind speed for December, January, February and March preceding the rainy season. These are presented in Figures 12 through 15 and are discussed below.

1. Sea surface temperature

Calculations involving December SST and next autumn's precipitation {Figure 12a} show a region of strong positive correlation in the eastern half of the South Atlantic. This region appears to migrate westward in the subsequent months until a maximum correlation of +0.506 is achieved in March {Figures 12b-12d}. A positive correlation associates wetter than average rain conditons with warmer than average sea surface, so apparently a pool of warmer than average water traversing the South Atlantic from east to west is correlated with rainy conditions. Conversely, cool water in the South Atlantic is associated with drought. This is very similar to the results obtained by Markham & McLain [1977], although the correlations are not so strong here. This difference may be attributable to their usage of both Quixeramobim and Fortaléza precipitation and of the January-February-March precipitation in their calculations. Their calculations, also, were confined to the twenty year period 1948-1967, while the values presented here were computed from sixty years of data. Markham & McLain did not pay much attention to the North Atlantic, which we see here to be a region of predominantly negative correlation. The

correlations do not appear to be as well-defined as the migrating region in the south, but they are quite strong. Thus, we find concurrence with the assertion by Moura & Shukla [1980] that warm water in the north and cool water in the south is associated with drought in NE Brazil.

2. Surface wind u-component

Figures 13a-13d present the correlations between the Quixeramobim autumn precipitation and the u-component of the surface wind. Since for most of the area being considered the wind has an easterly component, a positive correlation will associate below average rain with stronger easterlies.

The December figure does not show much of any type of large scale pattern. There are isolated strong correlation regions here and there, but for the most part they seem to have disappeared by the next month. In January, February and March the story is quite different. A region of strong positive correlation has suddenly appeared just off the horn of Brazil. The figures indicate that weaker easterlies blowing just south of the equator in January and February are associated with heavier rainfall in the next three months. The effect seems to have diminished somewhat by March, but is still present.

3. Surface wind v-component

The correlations with the surface wind v-component are presented in Figures 14a-14d. One must keep in mind that a positive correlation will associate either weaker southerlies or stronger northerlies with drought in NE Brazil.

Negative correlations seem to predominate in December, not only in the central Atlantic but also in the vicinity of Cuba and Florida. In January the main region of negative correlation has consolidated into a region

straddling the equator off the northeast corner of Brazil. The situation is much more impressive in February when the negative correlations have strengthened considerably, especially in the central South Atlantic. By March, however, the pattern has become fragmented and somewhat incoherent.

4. Surface wind speed

Correlations with surface wind speed were also computed and are presented in Figures 15a-15d. Through all four months a region of negative correlation is found close to the horn of Brazil just south of the equator. A negative correlation value represents an association between stronger winds and dry conditions. As with the wind component correlations the strongest effect is found in January and February. The correlations for these two months are predominantly negative and contain only weak positive values. The other two months, December and March, contain very significant positive correlations, and an interesting "dipolar" pattern exists in the South Atlantic.

5. Conditions for below average rainfall

As a recapitulation we shall consider the conditions which lead up to below average rainfall or drought as described by the computed correlations.

In December we see a region of stronger SE trades just south of the equator at around 25°W which can be attributed mainly to a stronger southerly component with some contribution also from a stronger easterly. Just southwest of this region, however, is one of slower winds. The wind here is almost directly from the east, and a weaker easterly component seems to be responsible for the decreased wind speed. Stronger winds can be found on the eastern and western flanks of the South Atlantic anticyclonic circu-

lation, primarily due to stronger southerly and northerly components, respectively. In the northern hemisphere stronger ENE winds can be found in the center of the ocean due to both stronger northerly and easterly components. Weaker components are combined in the weaker winds found around 37.5°W 10°N. Just below the equator off the African coast cold water can be found, while to the southwest and northwest lies warm water.

In January the most significant wind speed effects are found straddling the equator. Off the northeastern corner of Brazil stronger easterly and southerly components both contribute to an increase in wind speed. The stronger winds found near the Gulf of Guinea can be ascribed to stronger southerly components. Weaker than average winds, almost directly from the south, are found just west of Angola. On the western side of the ocean stronger east winds can be found, along with a smaller region of weaker northeast winds. Elsewhere in the tropical North Atlantic weaker ENE winds are found near the Golfo de Venezuela. As in December, the central region of the ocean is witness to stronger winds. In regard to the sea surface temperature the most noticeable feature is the region of cold water which trails down from the Gulf of Guinea. Warm water seems to prevail almost everywhere else with especially strong correlations along the southern edge of the analysis and near the Golfo de Venezuela.

February presents us with the most impressive picture yet with its extremely high correlations and the largely one-signed wind correlation analyses. Again the star attraction is the region of strengthened wind located east of Brazil and trailing away to the southeast. The stronger flow also shows itself in the southerly winds which hit Liberia and the Ivory Coast. The northern hemisphere is comparatively plain in terms of wind speed correlations, but the individual components do show some interesting

features. The tongue of strong positive u-component correlation which extends northward across the equator indicates a stronger easterly component, resulting in a veering of the trade winds. The veering is confirmed by the negative v-component correlations which protrude across the equator and which suggest a smaller northerly component. Significant v-component correlations are also found to the north, but it is believed that the effect on the wind flow is not too important since the wind is very close to straight easterly. The SST correlations for February show impressive opposition between the Northern and Southern Hemispheres. Negative correlations and warm water dominate the northern Atlantic, while positive correlations and cold water dominate the south. The region of maximum positive correlation is now west of its January location, suggesting either a transport of the implied cold water or a westward shift in the cause of the abnormally cold water. Several significant strong negative correlation areas have appeared in the North Atlantic indicating large regions of abnormally warm water not present in January.

The March wind situation appears to be not so definitive as that of February. The area of negative correlation and higher wind speed has become somewhat fragmented and disorganized, with a small strong correlation region persisting off the corner of Brazil. Stronger winds also still linger in the Gulf of Guinea and near Liberia. A region of slower wind has developed in the center of the tropical South Atlantic, although its maximum regions are disjointed and quite small. Weaker winds also prevail over much of the North Atlantic, but overall, the correlations are rather weak. Thus, the correlations between the March winds and the March-April-May Quixeramobim precipitation are weaker and much less coherent than for February. There seems to be no real large scale pattern in the correlations

and the regions of relatively strong values are small and localized. The behavior of the ocean water, on the other hand, is somewhat the opposite, and the features of the correlations have strengthened and developed more fully. The region of cold water in the South Atlantic has moved west of its February location and has grown in area and strength. The dichotomy between the two hemispheres which was apparent in the February figure is still present in March, although in March the negative northern correlations have slightly weakened.

IV. The Discussion

The correlation computations presented above for the four parameters, u-component, v-component, wind speed, and sea surface temperature, by themselves suggest an interesting scenario for the months preceding a drought season. The first act of this scenario is an intensification of the anticyclonic circulation in the South Atlantic Ocean. It is important to note that while the correlations do indicate below average strength in the NE trades of the North Atlantic, a greater effect is found in the Southern Hemisphere where correlations are stronger and more widespread. The immediate cause for such an intensification is not known, but in light of the connections found by Caviedes [1973] and Hastenrath & Heller [1977] between Brazilian precipitation and the sea surface temperatures and the El Niño off the coasts of Peru and Ecuador, and in light of the seemingly stronger influence in the Southern Hemisphere than in the Northern Hemisphere, it may be speculated that the Southern Oscillation in the South Pacific and its long-reaching global effects are responsible for the variations in the flow. Indeed, Stoeckenius [1980] did find strong connections between Brazilian rainfall and the Southern Oscillation. To go back one more step and specify the underlying cause of the Southern Oscillation is, of course, much more difficult.

The intensification of the Southern Hemisphere flow yields stronger SE trade winds blowing up from Southwest Africa, and the weaker Northern Hemisphere circulation yields lighter NE trades blowing down from the Azores. It is thought that the opposite phase behavior exhibited here by the two hemispheres is due to the response of the Northern Hemisphere to the Southern Hemisphere's variations. In an attempt by the tropical motion

systems to maintain a uniform level of relative angular momentum over the tropical Atlantic the increased relative angular momentum of the slower NE trade winds will compensate for the deficit caused by the faster SE trades with their decreased relative angular momentum. There is also the possibility of extratropical causes in both hemispheres which through some sort of teleconnection act synchronously to produce concurrent but opposite behaviors in the two hemipheres. We feel, however, that the relative strengths of the correlations, stronger in the south than in the north, argue for a south/north--stimulus/reponse relationship.

This is in opposition to the contention put forth by Namias [1972] that it is the increased blocking in the Newfoundland-Greenland area and its resultant weaker NE trade winds which are the stimulus, with weaker SE trade flow as the response. He argued that it is the diminished SE flow and the concomitant diminished moisture flux which cause lighter than normal rains in northeastern Brazil. Thus, two points of disagreement found here are the correct stimulus/response link and whether the two trade regimes act in parallel or in opposition.

What, now, is the role of the sea surface temperature? Markham & Mclain [1977] proposed that a warm SST anomaly in the western part of the tropical South Atlantic would increase evaporation, speed up the trade winds, raise the trade inversion, and bring more moisture and rain to northeastern Brazil. A cold, anomaly would have the opposite effect and result in drought. Moura & Shukla [1980] credit a warm-cold SST anomaly dipole with being the driving force behind a meridional thermal cell which affects the convergence and precipitation over northeast Brazil.

Both of these papers cite SST anomalies as being responsible for changes to the normal flow, and thus responsible for changes in precipita-

tion. The correlation maps presented here suggest something quite different. In the south, under the intensified circulation, cold water anomalies prevail. In the north, where the circulation is weaker than average, warm water anomalies prevail. The explanation taken here is that increased surface wind stress causes turbulent mixing, thereby mixing surface water with deeper than normal water, and the result is that the surface water becomes unusually cool. The west to east migration of the cold water in the south is not fully understood, but it is interesting to note that the position of the cool water patch for a given month roughly coincides with negative windspeed correlation regions for the previous month. Also, a perusal of the SST/u-component correlations {Figures 10a-10g} will show that in the southeast sector of the tropical Atlantic, strong positive correlations are present when contemporaneous values are used and when the wind values lead the SST values. Perhaps computations using the wind speed, and not just the one component, would have yielded even stronger correlations, since in this region the wind also has considerable north-south component. In any event, it is believed here that the sea surface temperature anomalies are by-products of the wind anomalies, and do not play the role of the provocateur of the abnormal situation.

Heretofore, no mention has been made of what real, direct effects the aforementioned anomalies would have on the rainfall of northeastern Brazil. By what mechanism does an anomalous trade wind circulation effect an anomalous rainfall regime? Let us first examine normal conditions, and perhaps some insight will be gained pertaining to this question.

The seasonal variation of the atmosphere over the tropical Atlantic is illustrated in Figures 16a-16d. In these figures the September positions of the equatorial trough, and the bands of maximum convergence, maximum to-

tal cloudiness, and maximum precipitation frequency are all seen to be north of their March positions. Other parameters, including sea surface temperature, sea-air temperature difference, wind stress curl, relative vorticity, and wind steadiness, are all seen to exhibit similar north-south annual movement of their equatorial bands [Hastenrath & Lamb 1977]. One notices, also, that the fields of convergence, sea-air temperature difference, wind stress curl and relative vorticity show interesting behavior in that the eastern end of the thin band of equatorial extreme in each case seems to be anchored in place while the western end shows relatively large seasonal movement. For example, in Figure 16b the band of maximum convergence seems to move very little on its eastern end between March and September. The western ends for the two months, on the other hand, indicate quite a significant variation between the seasons. Thus, it is seen that the African end of the band of equatorial extreme changes very little or not at all in position with the change of seasons, although variations in strength are possible. On the other end, though, the band appears to be much freer to move in response to the seasons. The other parameters do not seem to have this character of one-ended anchoring, and in these cases the entire region is free to move with the seasons.

With such noticeable seasonal differences in the atmosphere and ocean, we must consider the possiblity that interannual variations in the climate are basically extensions of the seasonal variations with essentially the same forces causing each. Is it not possible that the atmospheric differences which distinguish a wet year from a dry year are basically the same atmospheric differences which distinguish the wet season (autumn) from the dry season (spring)? The seasonal differences discussed above demonstrated that the major difference between the autumn tropical atmosphere

and the spring atmosphere is the latitudinal displacement of the ITCZ and all its various manifestations. Perhaps, then, it is not so unreasonable to look for the cause of the interannual abnormalities in the position of the ITCZ, also.

This explanation is quite appealing for two reasons. Since Quixeramobim is situated so close to the average southernmost position of the ITCZ, the amount of rainfall received there is very sensitive to the actual behavior of the ITCZ and its deviation from the norm. Small differences in the latitudinal position of the ITCZ would be expected to have very conspicuous consequences regarding the precipitation amount. Secondly, it would not be hard to reconcile a strengthened South Atlantic circulation and a weakened North Atlantic circulation with an abnormally northward ITCZ position, but as will be discussed below, one must be very careful with this reasoning since such atmospheric changes do not necessarily have to result in the such a shift.

Another explanation for rainfall variations, which also merits examination and is subtler than the first, is variation in the strength of the convergence which produces the rain. Of course, this is implicit in the displacement argument, for as one moves away from the ITCZ one also moves away from the region of strongest convergence. It is conceivable, however, that changes in the maximum strength of the convergence with no positional change also could produce rainfall anomalies. If the ITCZ were at its normal position, but with weaker convergence, one would expect less intense precipitation. Or if the ITCZ were farther away, but with a stronger maximum convergence, one might very well see normal rainfall. The subtlety of this argument is that convergence is a tricky quantity which depends not on wind speed but on the gradient of wind speed. Thus, while a stronger

southern flow and a weaker northern flow might suggest the ITCZ being pushed northward, it does not say anything about the strength of the convergence, and thus, can be quite deceptive.

The solution proposed by Moura & Shukla [1980] revolves around the existence of a small thermally driven cell which modulates the convergence over northeastern Brazil and thus affects the precipitation. This type of convergence strength argument is quite interesting, but there has been no observational evidence for the existence of such a cell. It also goes against the contention put forth here that the SST anomalies are a consequence of changes in the circulation, and are not themselves the cause of the circulation changes. Strong supportive evidence does come, however, from simple numerical models and GCM simulations, and one must not be too quick to dismiss this proposal. We feel that while our data here does not support this hypothesis, it does warrant further attention and study.

To get a handle on the strength of the displacement argument the March wind fields for fifteen drier than average years and eleven wetter than average years were examined. For each wind field the latitude of the ITCZ for each 5° longitudinal strip was estimated, and these values are tabulated in Table 3. For each longitude the mean of the ITCZ latitudes for dry years was compared with that for the wet years, and the results are shown in Table 4. The significance of the difference represents the probability that the two samples, wet and dry years, were actually taken from populations with different means. It is seen that while the dry ITCZ latitudes are indeed north of the wet ITCZ locations on the average, the significance of the differences of the means is very low and nowhere near the 95% confidence level commonly used as the cutoff value for hypothesis acceptance. Therefore, the comparison is rather inconclusive in that one

cannot talk of a difference between the ITCZ location during dry years and wet years with very much confidence.

It is felt that the method used to estimate the ITCZ location of visually sighting the region of confluence from the wind field plots may have been too vague and inexact to yield good, statistically significant results. Difficulties were caused in some cases by the presence of missing data, and in others by an inability to judge precisely the position of the confluence. Also, a slight complication is added by the fact that the region of confluence does not have to always coincide exactly with the region of maximum convergence, which is usually used to define the ITCZ. Thus, the fact that the statistical t-test performed does not give much significance to the dry-wet ITCZ latitude differences does not necessarily discredit the latitudinal displacement hypothesis, but instead points to the need for a more objective and exact method of determining the ITCZ location.

A step taken in this direction was the computation of a crude convergence index to obtain a rough measure of the convergence. The index was simply calculated by subtracting the v-component of a given grid square from the v-component of its southern neighbor. Thus, a positive value indicates convergence in the medial region, and a negative value indicates divergence. Figure 17 presents five meridional cross sections of this convergence index, comparing the average of fifteen dry years with the average of eleven wet years.

Is there a difference between the convergence pattern of an average dry year and that of an average wet year? From Figure 17 only a tentative answer can be obtained. The cross-section for 22.5°W does show a difference, with the wet years having their convergence distributed to the south

of the dry years. The 27.5°W distribution does not show any significant difference, but 32.5°W indicates that the "center of gravity" of the rainy convergence is to the south of the one for dry years. The cross-sections for 37.5°W and 42.5°W are the ones most pertinent to Quixeramobim precipitation, but unfortunately they only can give half of the picture since the data was not included for the land regions to the south. The 42.5°W plot only weakly suggests a southward shift of the wet convergence, and the 37.5°W plot makes no statement either way.

Once again there seems to be evidence for a northward shift of the drought convergence compared to the wet conditions, but it is still not definitive or convincing. In an effort to perhaps obtain stronger evidence, a more complete convergence index was calculated, this time incorporating both components of the surface wind and adjusting for the convergence of the meridians away from the equator. The cross sections of this new improved convergence index are presented in Figure 18, and values for the entire tropical Atlantic are shown in Figures 19 and 20. Evidence for latitudinal displacement of the ITCZ is more definite here. The cross-sections for 42.5°W, 32.5°W, 27.5°W, and 22.5°W all suggest southward shifts during wet years and northward shifts for dry years, but still the differences are not as apparent as we would like.

Perhaps, though, things may not be as bad as they might appear. This is only a very crude indicator of the convergence. The resolution of this analysis is only five degrees of latitude or longitude, but judging from the highly localized distribution of convergence and rainfall frequency {Figures 16b and 16d} a displacement of only about two degrees could result in major changes in the local precipitation regime. Therefore, an analysis that resolves down to five degrees will inevitably blur the evidence of

such a small amplitude effect, and a seemingly insignificant difference on a five-degree scale may actually reflect quite significant differences on smaller scales. Thus, it is heartening that the differences between wet and dry regimes, as shown by this data analysis, are along the expected lines, even though their statistical significance leaves much to be desired.

The question of the role of convergence strength, as opposed to convergence location, in determining precipitation regimes of northeastern Brazil can best be addressed by examining Figures 19 and 20. These maps present the fields of the second, more complete convergence index for the average rainier than normal March and the average drier than normal March. A dry versus wet comparison is very interesting and revealing. First consider the equatorial convergence region. The northern boundary is located at almost the same latitude in the two cases, but the southern boundaries do show some difference. Particularly, on the western side of the ocean the convergence zone extends farther to the south in the wet case than in the dry case. The eastern side appears to be at approximately the same latitude in both situations. In the South Atlantic dry years appear to have stronger divergence on the average than wet years, and this stronger divergence may contribute to the northward shift of the convergence zone boundary. The North Atlantic, on the other hand, shows very little difference between the two situations. The strengths and distributions of the divergence there are very similar, and as was mentioned before, the boundaries with the equatorial convergence coincide almost exactly. So, the features which distinguish a typical dry March from a typical wet March are a narrower, compressed, more intense equatorial convergence zone, and stronger, more widespread divergence in the South Atlantic. Meanwhile, the

North Atlantic contributes relatively little to differentiating the two conditions.

These differences fit together rather nicely with the circulation changes discussed previously. The intensified circulation in the South Atlantic during the dry spells produces more vigorous and more extensive divergence over the region. The equatorial convergence region appears to be compressed northward, in a sense pressed up against the comparatively unchanging North Atlantic circulation. The net result is stronger convergence confined to a more northward area. It is interesting to note that the western end of the equatorial convergence is more affected by this compression than the eastern end which seems rather stable. We recall that this type of behavior was also detected in the seasonal differences of several climatological parameters over the equatorial Atlantic.

In summary, the evidence presented here, derived from sixty-two years of surface wind data for the tropical Atlantic region, suggests that droughts in northeastern Brazil are the result of an abnormal northward compression of the equatorial convergence region. The compression of that region, caused by an intensification of the South Atlantic anticyclonic circulation, is also associated with stronger convergence which usually indicates stronger rising motion in the atmosphere and increased rainfall. The sensitive location of Quixeramobim, being just on the edge of the ITCZ's southernmost excursion, however, makes the precipitation amount there much more responsive to the northward compression than to the increased convergence, and the net result is decreased rain, or drought in the more severe cases. The cause for the initial intensification of the South Atlantic circulation is not known at this time.

V. The Conclusion

The intent of this study was to contribute knowledge and information toward the total understanding of the phenomenon of drought in northeastern Brazil. Analysis of surface wind data for the tropical Atlantic was performed in an attempt to seek answers in the atmospheric circulation. The main thrust of the results is that it is the strength of the South Atlantic anticyclone and its attendant SE trade winds in the tropics which are ultimately responsible for the amount of rain received in northeastern Brazil. These components determine the latitudinal position of the ITCZ, and variations in this position are felt very strongly in the Quixeramobim precipitation. It is also found that the atmospheric circulation over the North Atlantic is relatively unimportant in the scheme of things. Its behavior appears to be more of a response to the South Atlantic variations than a contributing factor to the equatorial changes. Sea surface temperature changes were also seen to be more of a side effect of the circulation changes than a cause for them. The correlations calculated suggest that the increased trade winds during dry seasons cause increased mixing in the ocean surface layer, thereby reducing the sea surface temperature.

The analysis presented here conflicts with several other theories. For one thing, the stimulus for the precipitation variations appears to originate south of the equator, not in the vicinity of Newfoundland and Greenland, as suggested by Namias [1972]. Also, the contention by Markham & McLain [1977] that cold SST anomalies in the tropical South Atlantic reduce the wind flow and moisture influx to northeastern Brazil does not jibe with results found here correlating cold SST anomalies with increased wind. Thirdly, the hypothesis of Moura & Shukla [1980] of the existence of a me-

ridional cell driven directly by SST anomalies has only theoretical support at this point, and corroborative empirical evidence has yet to be found. The apparent dominance of the Southern Hemisphere suggests concurrence with teleconnections between northeastern Brazil precipitation and conditions in the southeastern Pacific Ocean discussed by Hastenrath & Heller [1977] and Caviedes [1973], and argue for some kind of influence by the Southern Oscillation phenomenon.

The climatology of the tropical Atlantic Ocean was also discussed, and perhaps the most interesting aspect was the surface wind--SST correlations. The relationship between wind speed and sea surface temperature was found to vary spatially over the ocean, and also with various lags between the two quantities. Only correlations between the u-component of the wind and SST were calculated and presented here, since for the most part the winds over the tropical Atlantic are very close to easterly. There are some regions, such as along the African coast, where v-component correlations would have been more appropriate. Or perhaps correlations with the wind speed would have been better, since it is the simple wind speed and not its horizontal components that figure into the heat budget of the sea surface.

The predictive aspects of the situation were not discussed above, and of course this is one of the more pressing considerations involved in this problem. Markham & McLain [1977] achieved reasonably good results using sea surface temperature as a predictor of dry seasons. The evidence indicates, however, that the SST anomalies, like the precipitation anomalies, are products of the circulation anomalies. This suggests that some indicator of the circulation might make a better predictor than the SST. Further research should be conducted investigating the possibility of using, say, sea level pressure as a predictor, or possibly a Southern Os-

cillation index, should such a teleconnection be firmly established.

Acknowledgements

The author is immeasurably indebted to Professor Reginald E. Newell for his invaluable guidance and support. Appreciation is also expressed to Drs. Alfredo Navato and Long Chiu who were very helpful in the data reduction and analysis. Thanks are given to Ms. Nancy Striniste for her time-saving assistance in the preparation of the figures and for her editorial advice.

References

Bakun, A., 1978: Guinea Current upwelling. Nature, 271, 147-150.

Bjerknes, J., 1969: Atmospheric teleconnections from the equatorial Pacific. Mon. Wea. Rev., 97, 163-172.

Caviedes, C.N., 1973: Secas and El Nino: Two simultaneous climatical hazards in South America. Proc. Assoc. Amer. Geogr., 5, 44-49.

Craddock, J.M., and C.R. Flood, 1969: Eigenvectors for representing the 500 mb geopotential surface over the Northern Hemisphere. Quar. J. Roy. Met. Soc., 95, 576-593.

Hastenrath, S., and L. Heller, 1977: Dynamics of climatic hazards in northeast Brazil. Quar. J. Roy. Met. Soc., 103, 77-92.

-----, and P.J. Lamb, 1977: Climatic atlas of the tropical and Eastern Pacific Oceans, Madison, Univ. Wisconsin Press, 115 pp.

Kidson, J.W., 1975: Tropical eigenvector analysis and the Southern Oscillation. Mon. Wea. Rev., 103, 187-196.

Kutzbach, J.E., 1967: Empirical eigenvectors of sea-level pressure, surface temperature and precipitation complexes over North America. J. Appl. Meteor., 6, 791-802.

Markham, C.G., and D.R. McLain, 1977: Sea surface temperature related to rain in Ceara, north-eastern Brazil. Nature, 265, 320-323.

Montgomery, R.B., 1936: Computation of the transport of surface-water due to the wind-system over the North Atlantic. Trans. Amer. Geophys. Union, 17, 225-229.

Moura, A.D., and J. Shukla, 1980: On the dynamics of droughts in northeast Brazil: Observations, theory and numerical experiments with a general circulation model. unpublished manuscript, 66 pp.

Namias, J., 1972: Influence of northern hemisphere general circulation on drought in northeast Brazil. Tellus, 24, 336-342.

Ratisbona, L.R., 1976: The climate of Brazil. in Climates of Central America, W. Schwerdtfeger, (Ed.), World Survey of Climatology, H.E. Landsberg, (Ed. in chief), Vol. 12, New York, Elsevier, 219-294.

Rose, N., 1980: A persisting misconception about the drought of 1958 in northeast Brazil. Climatic Change, 2, 299-301.

Sampaio Ferraz, J., 1931: Causas Provaveis das Secas do Nordeste Brasileiro, Diretoria de Meteorologia, Ministerio da Agricultura, Rio de Janeiro, 30 pp.

-----, 1950: Iminencia duma grande seca no nordeste. (Imminence of a great drought in Northeast). Revista Brasileira de Geografia, Rio de Janeiro, 12(1), 3-15.

Serra, A., 1946: As secas do nordeste. Servico de Meteorologia, Ministerio da Agricultura, Rio de Janeiro, 148 pp.

-----, and L. Ratisbona, 1942: As massas de ar da America do Sul, Servico de Meteorologia, Ministerio da Agricultura, Rio de Janeiro, 137 pp.

Stockenius, T.E., 1980: Interannual variations of tropical precipitation patterns. S.M. Thesis, Massachusetts Institute of Technology, 75 pp.

Walker, G.T., 1928: Ceara (Brazil) famines and the general air movement. Beitr. Phys. Frein Atmos., 14, 88-93.

MODE NO.	UNNORMALIZED U-COMP EXP %	UNNORMALIZED U-COMP CUM %	UNNORMALIZED V-COMP EXP %	UNNORMALIZED V-COMP CUM %	NORMALIZED U-COMP EXP %	NORMALIZED U-COMP CUM %	NORMALIZED V-COMP EXP %	NORMALIZED V-COMP CUM %
1	16.4	16.4	6.9	6.9	11.7	11.7	7.3	7.3
2	6.8	23.2	5.4	12.3	7.3	19.0	6.5	13.9
3	6.2	29.4	4.8	17.1	6.1	25.1	5.4	19.3
4	4.4	33.8	4.5	21.6	4.6	29.7	4.5	23.8
5	3.9	37.7	4.1	25.7	3.4	33.1	3.6	27.4
6	3.6	41.3	3.5	29.2	3.2	36.3	3.1	30.5
7	2.6	43.9	3.4	32.6	2.8	39.1	2.9	33.4
8	2.5	46.4	3.1	35.7	2.3	41.4	2.7	36.1
9	2.3	48.7	2.9	38.6	2.1	43.5	2.4	38.5
10	2.3	50.9	2.7	41.3	2.0	45.5	2.3	40.8
15	1.6	60.2	1.9	51.9	1.5	54.1	1.6	49.7
20	1.3	67.0	1.5	60.1	1.3	60.7	1.2	56.5
30	0.8	77.0	1.0	71.8	0.9	71.0	0.9	67.2
40	0.6	83.9	0.7	79.9	0.7	78.6	0.7	75.3
50	0.4	88.8	0.5	86.0	0.5	84.4	0.6	81.6
60	0.3	92.3	0.4	90.4	0.4	88.9	0.4	86.6
70	0.2	94.9	0.3	93.6	0.3	92.3	0.3	90.4
80	0.2	96.7	0.2	95.9	0.2	94.9	0.3	93.5
90	0.1	98.0	0.1	97.6	0.2	96.8	0.2	95.9
100	0.1	98.9	0.1	98.7	0.1	98.2	0.1	97.6
110	0.1	99.5	0.1	99.4	0.1	99.2	0.1	98.9
120	<0.05	99.9	<0.05	99.9	<0.05	99.8	0.1	99.7

Table 1. Summary of results of Empirical Orthogonal Function (EOF) analysis.

Table 2. Basic analysis of Quixeramobim precipitation data.

MONTH	NO. YEARS	MEAN (MM)	STD.DEV. (MM)	MINIMUM (MM)	MAXIMUM (MM)
JANUARY	62	77.99	121.41	0.0	880.0
FEBRUARY	62	95.51	68.37	0.0	270.8
MARCH	62	178.08	94.72	29.0	479.6
APRIL	61	166.97	86.01	14.0	523.1
MAY	60	107.38	71.88	9.0	288.4
JUNE	61	46.16	38.37	0.0	137.1
JULY	60	27.52	27.92	0.0	121.1
AUGUST	61	9.70	15.82	0.0	80.0
SEPTEMBER	61	3.51	6.37	0.0	27.5
OCTOBER	60	2.35	5.80	0.0	37.7
NOVEMBER	60	7.16	13.48	0.0	60.0
DECEMBER	61	19.75	25.96	0.0	102.0

Table 3.

ITCZ latitudinal position during abnormal rainfall, estimated from computer generated wind field plots.

YEAR	42.5W	37.5W	32.5W	27.5W	22.5W	17.5W	12.5W
YEARS WITH BELOW AVERAGE RAINFALL							
1911	-	2	-2	0	1	2	7
1915	-	-	1	-	-	13	-
1918	-	-	-	-	-	-	-
1919	-	7	4	3	5	-	-
1930	-	-2	-1	-2	4	-	4
1931	-	-2	0	0	-	9	7
1932	0	0	3	3	3	-	7
1942	-2	0	2	-3	-3	4	6
1943	-	-2	-3	-	2	4	-
1946	-	-	2	0	-	-	2
1951	-	-1	0	1	4	4	6
1953	-	0	1	0	2	2	7
1954	-	-2	-1	-1	3	3	6
1958	-	1	3	4	4	6	7
1970	-	-2	0	1	1	4	-
YEARS WITH ABOVE AVERAGE RAINFALL							
1917	-	-	-	-	-	-	-
1922	-	-	1	-1	1	-	7
1924	-	-	-2	-3	-2	3	5
1934	-	-2	-1	-2	-	-	3
1936	-	4	3	3	4	4	7
1938	-2	-1	-1	-1	1	3	7
1940	-	3	-	-	-	2	10
1950	-	-2	1	1	-1	2	7
1960	-	-	-5	4	3	3	7
1964	-	-3	-1	-2	0	3	6
1969	-	-	-1	-1	4	3	7

Table 4.

Comparison of ITCZ latitude estimates between wet and dry years.

LONGITUDE	MEAN ITCZ LATITUDE DRY	WET	SIGNIFICANCE OF DIFF. (%)
42.5 W	-1.00	-2.00	33.3
37.5 W	-0.08	-0.17	4.6
32.5 W	0.64	-0.67	82.6
27.5 W	0.50	-0.22	52.2
22.5 W	2.36	1.25	70.1
17.5 W	5.10	2.88	90.8
12.5 W	5.90	6.60	62.5

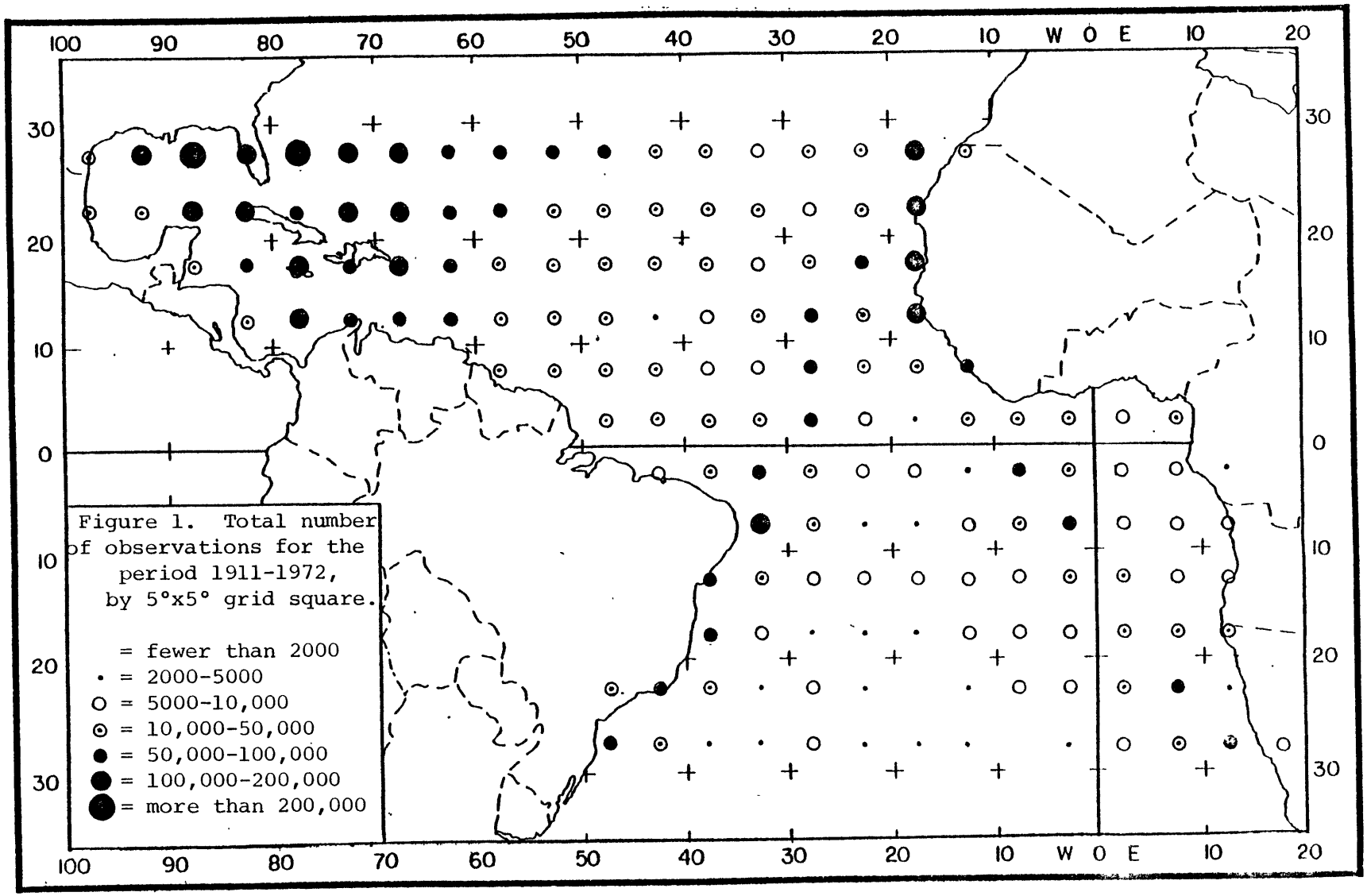
100 90 80 70 60 50 40 30 20 10 W 0 E 10 20
30
20
10
0
10
20
30
Figure 1. Total number of observations for the period 1911-1972, by 5°x5° grid square.
= fewer than 2000
. = 2000-5000
O = 5000-10,000
⊙ = 10,000-50,000
● = 50,000-100,000
● = 100,000-200,000
● = more than 200,000

Figure 2. Number of missing values for each quarter year: 1911-1972.

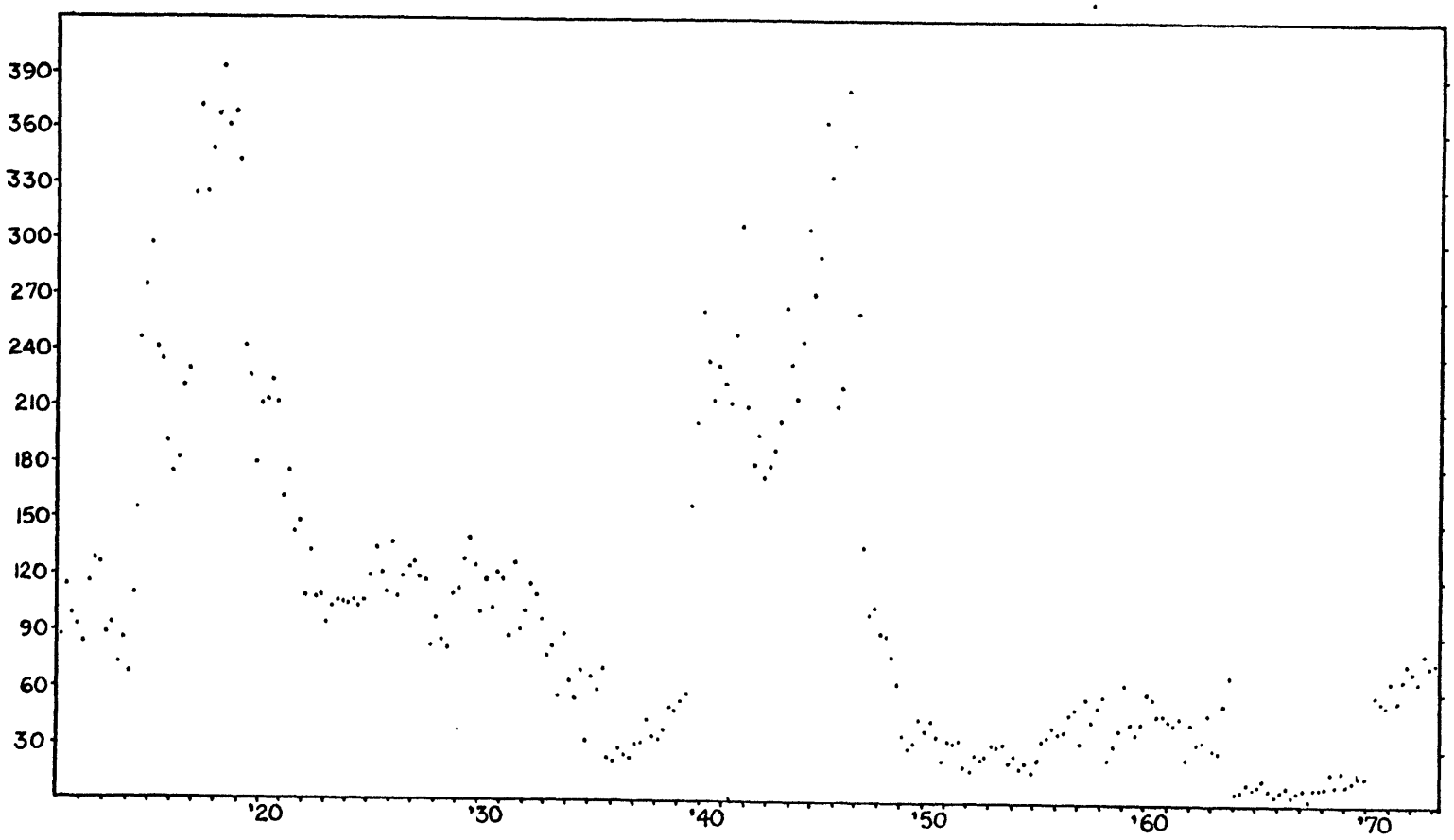

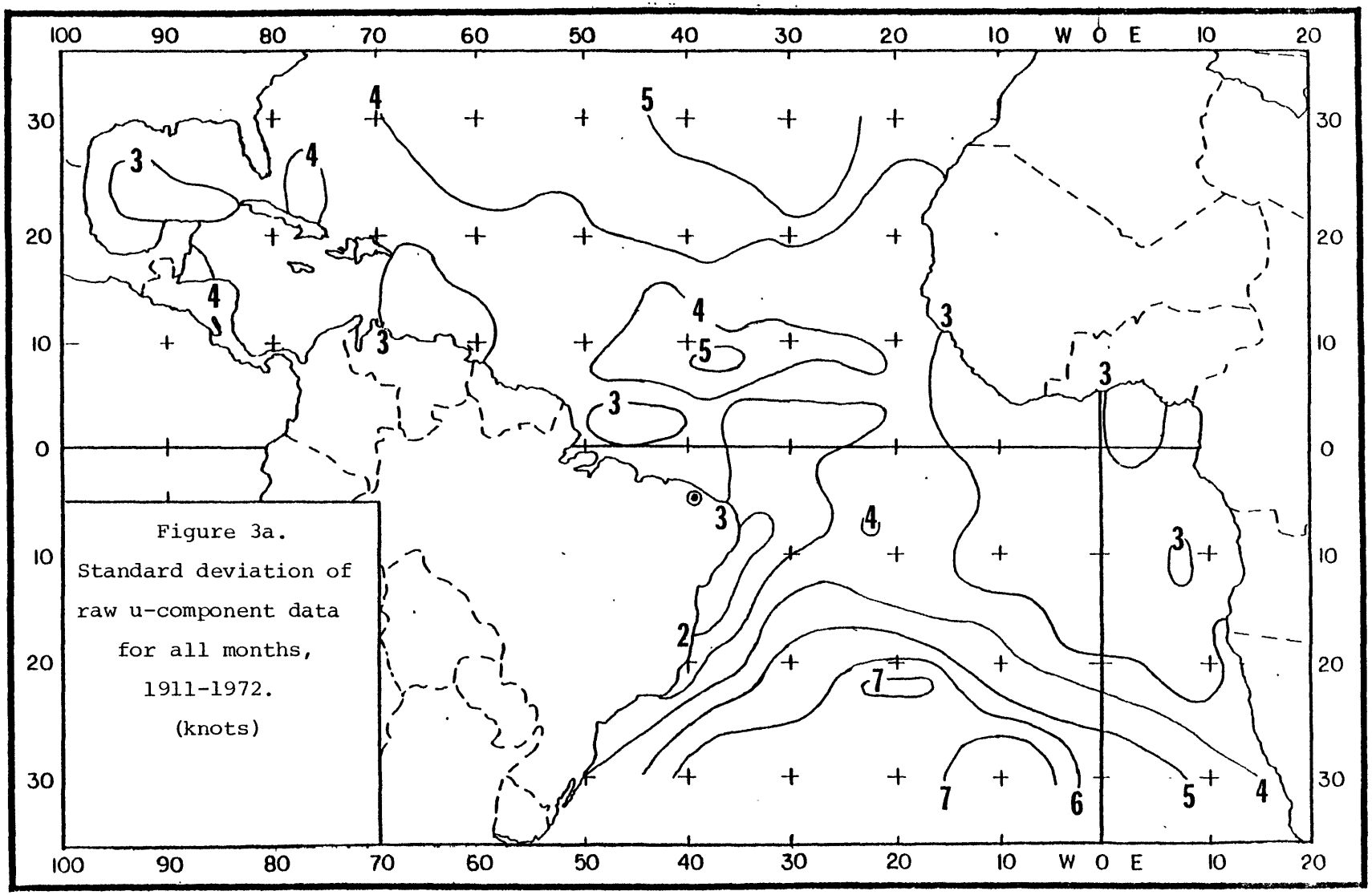
100 90 80 70 60 50 40 30 20 10 W 0 E 10 20
30
20
10
0
10
20
30
Figure 3a.
Standard deviation of
raw u-component data
for all months,
1911-1972.
(knots)

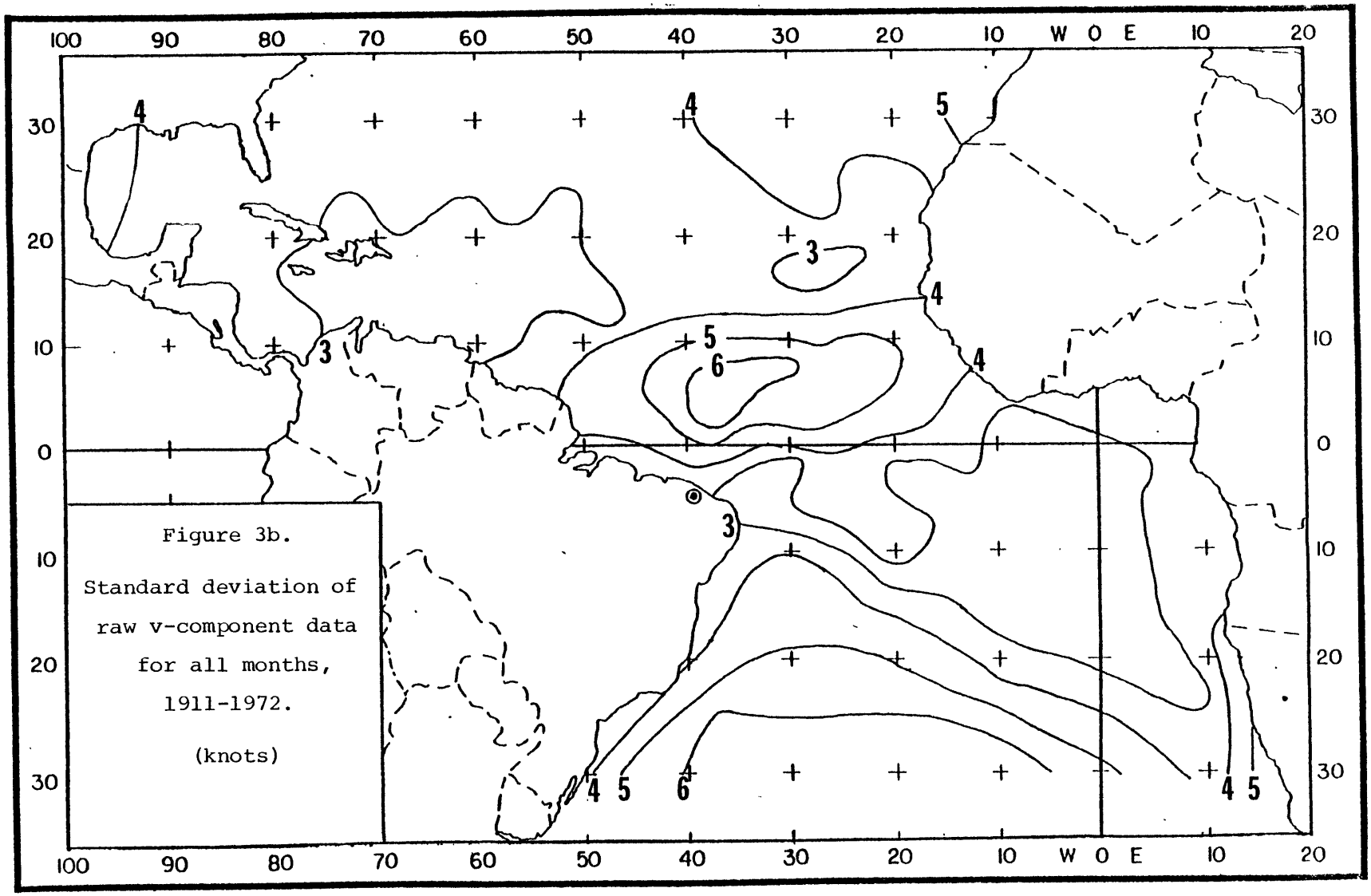
100 90 80 70 60 50 40 30 20 10 W 0 E 10 20
30
20
10
0
10
20
30
4
4
5
3
4
5
6
4
3
3
4 5 6
4 5
Figure 3b.
Standard deviation of raw v-component data for all months, 1911-1972.
(knots)

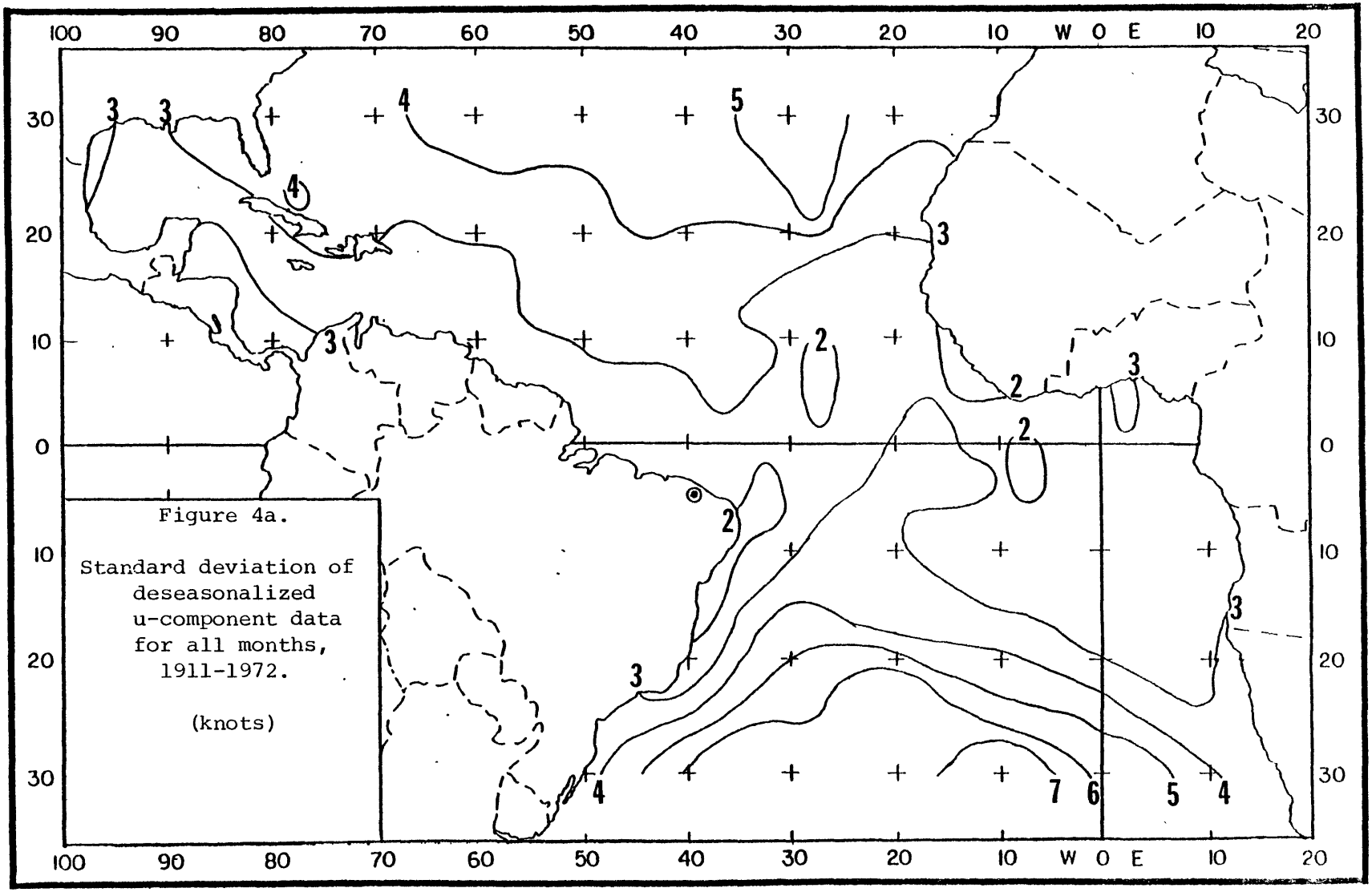
100 90 80 70 60 50 40 30 20 10 W 0 E 10 20
30
20
10
0
10
20
30
3 3 4 5 4 3 3 2 2 3 2 2 2 3 4 7 6 5 4
Figure 4a.
Standard deviation of deseasonalized u-component data for all months, 1911-1972.
(knots)

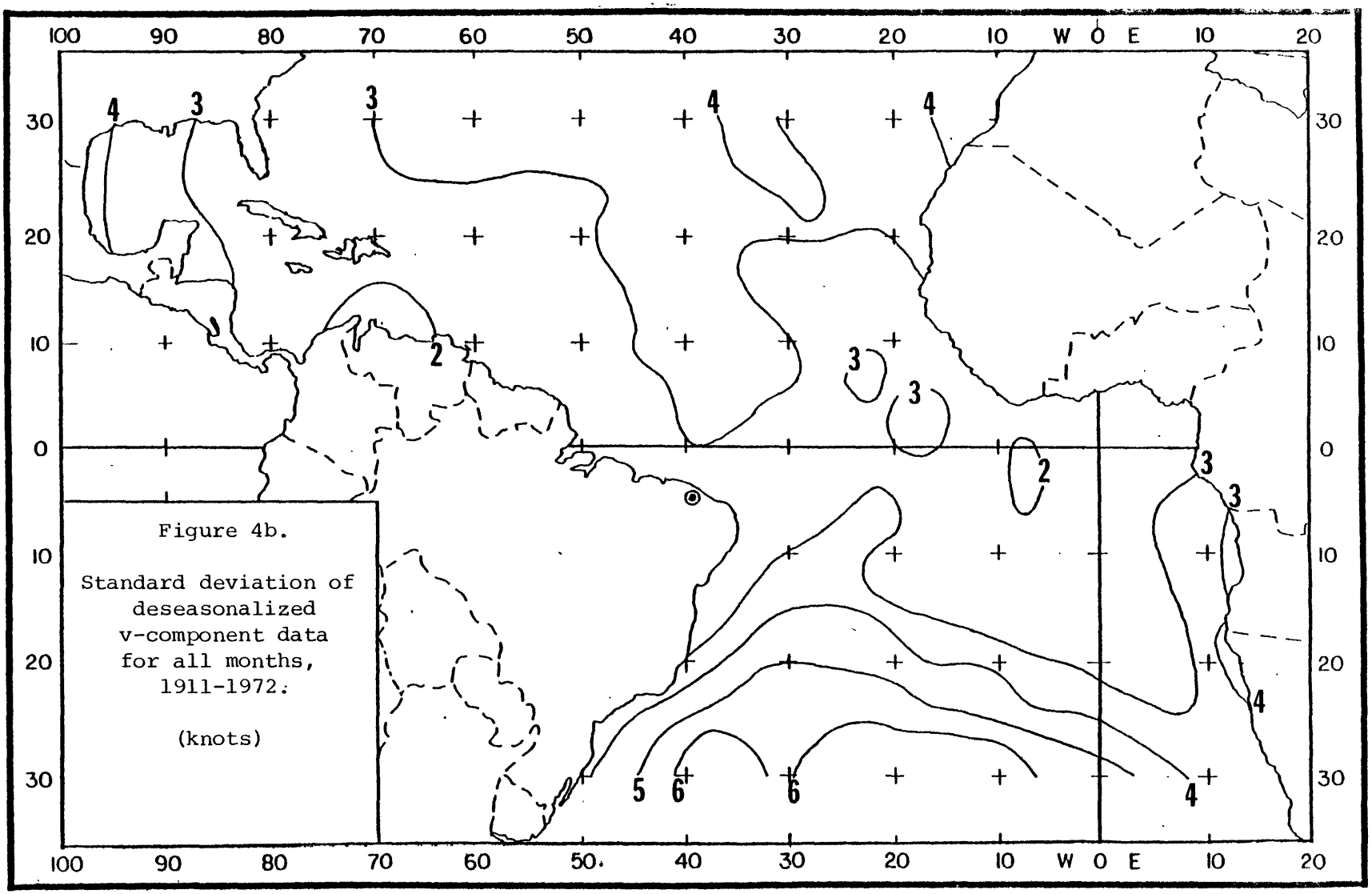
100 90 80 70 60 50 40 30 20 10 W 0 E 10 20
30
20
10
0
10
20
30
Figure 4b.
Standard deviation of deseasonalized v-component data for all months, 1911-1972.
(knots)

Figure 5a.

** JANUARY **
MEAN SURFACE WIND FIELD

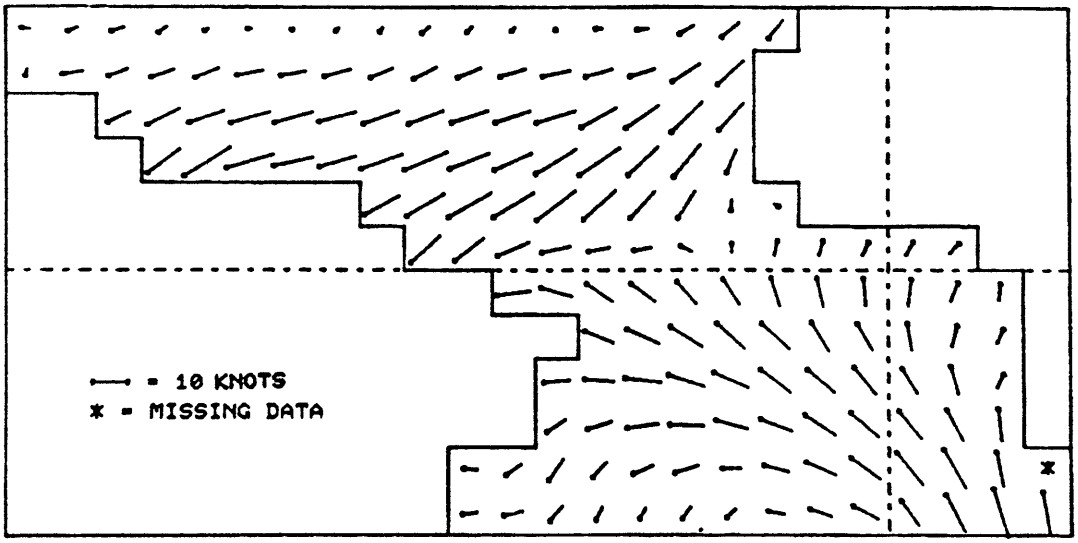

Figure 5b.

** FEBRUARY **
MEAN SURFACE WIND FIELD

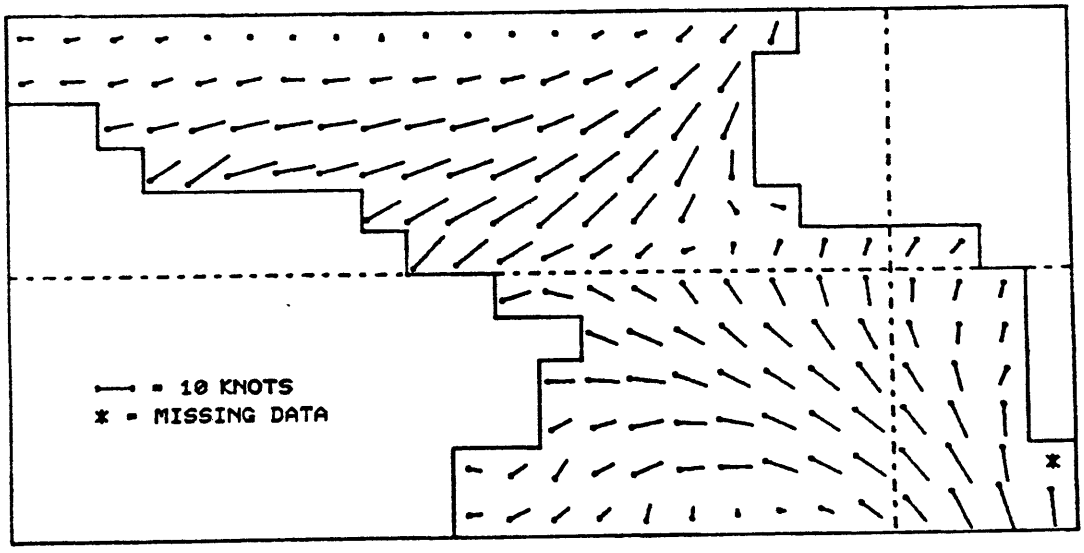

Figure 5c.

** MARCH **

MEAN SURFACE WIND FIELD

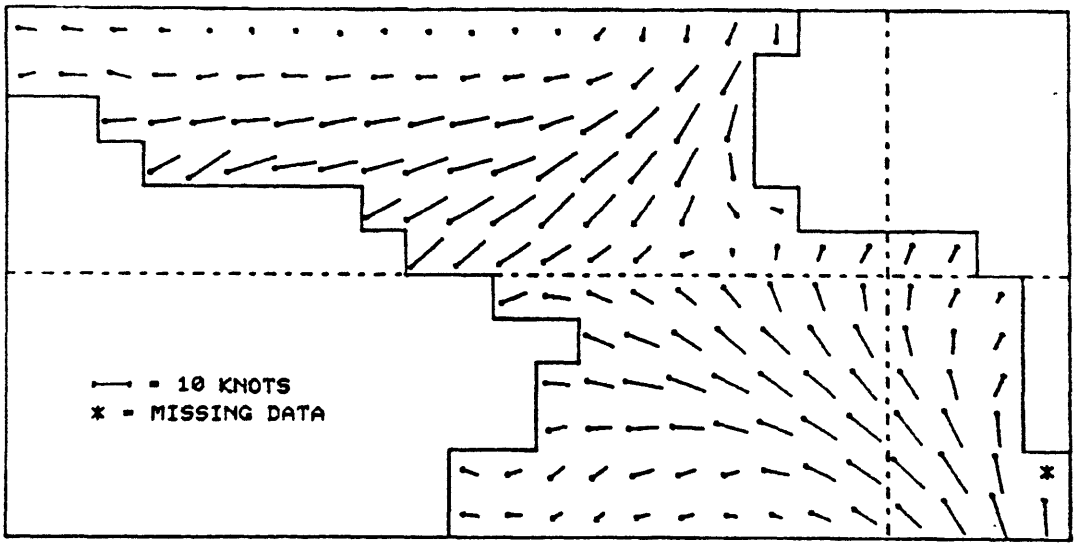

Figure 5d.

** APRIL **

MEAN SURFACE WIND FIELD

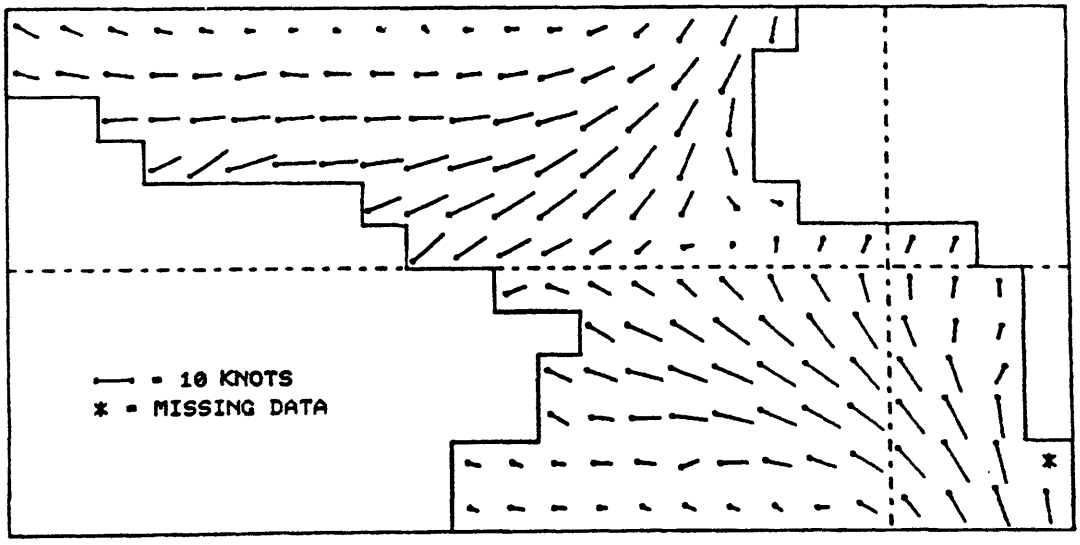

Figure 5e.

** MAY **

MEAN SURFACE WIND FIELD

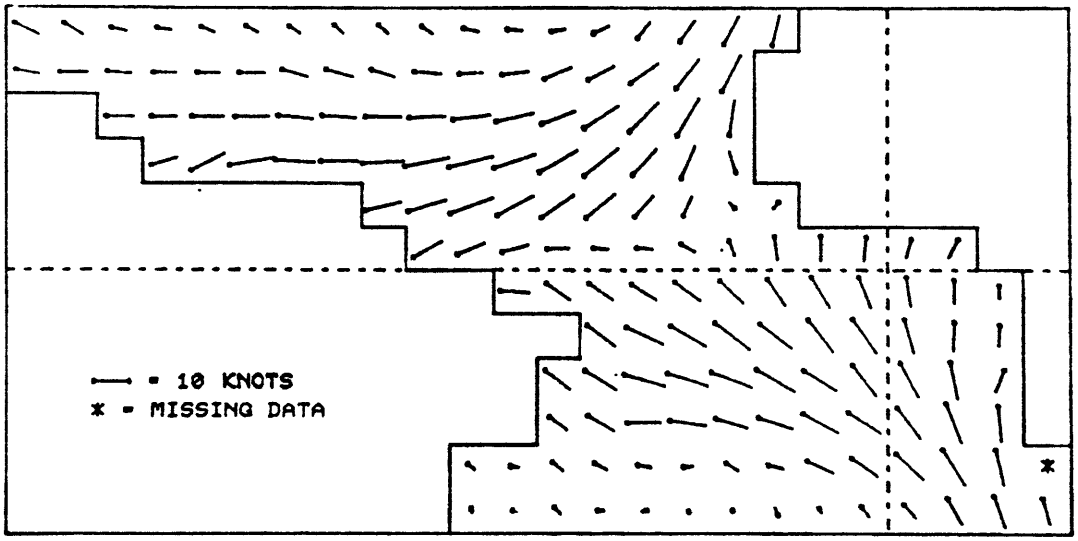

Figure 5f.

** JUNE **

MEAN SURFACE WIND FIELD

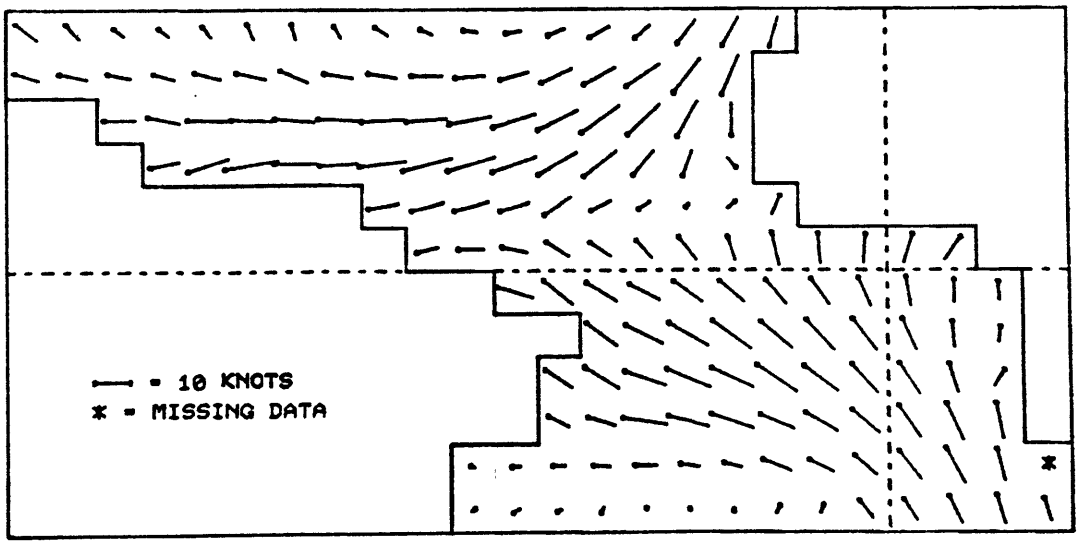

Figure 5g.

** JULY **

MEAN SURFACE WIND FIELD

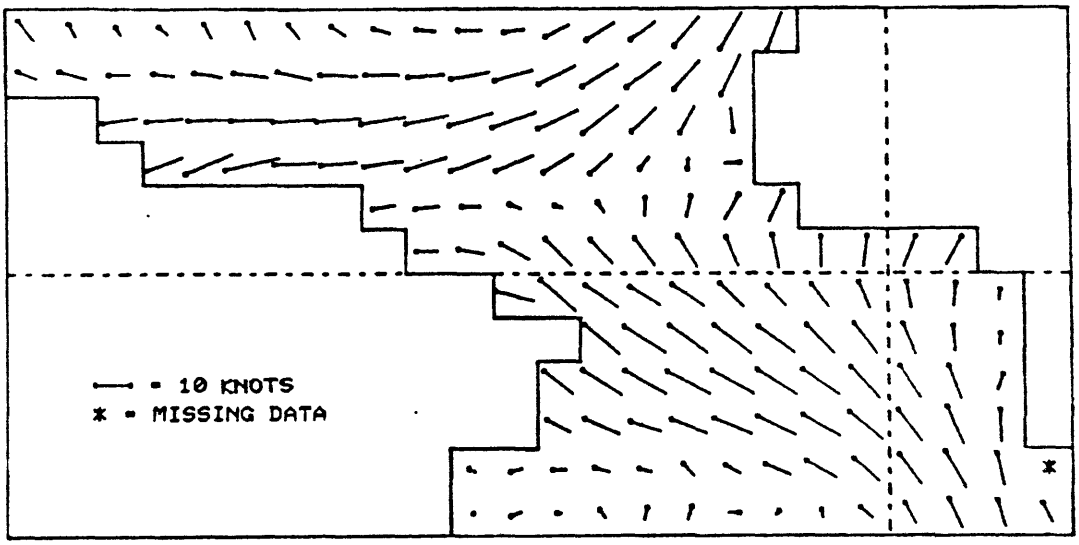

Figure 5h.

** AUGUST **

MEAN SURFACE WIND FIELD

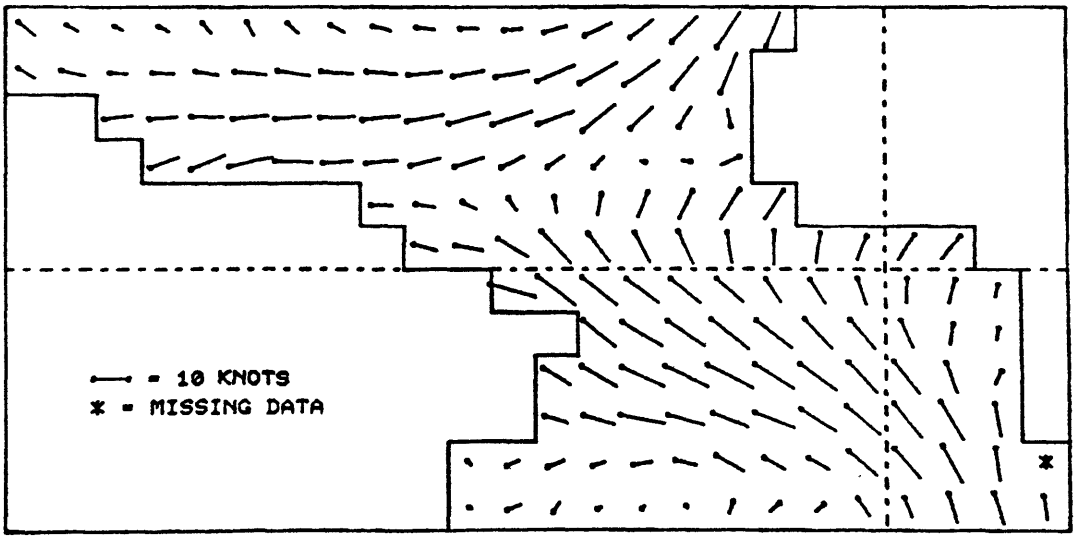

Figure 5i.

** SEPTEMBER **

MEAN SURFACE WIND FIELD

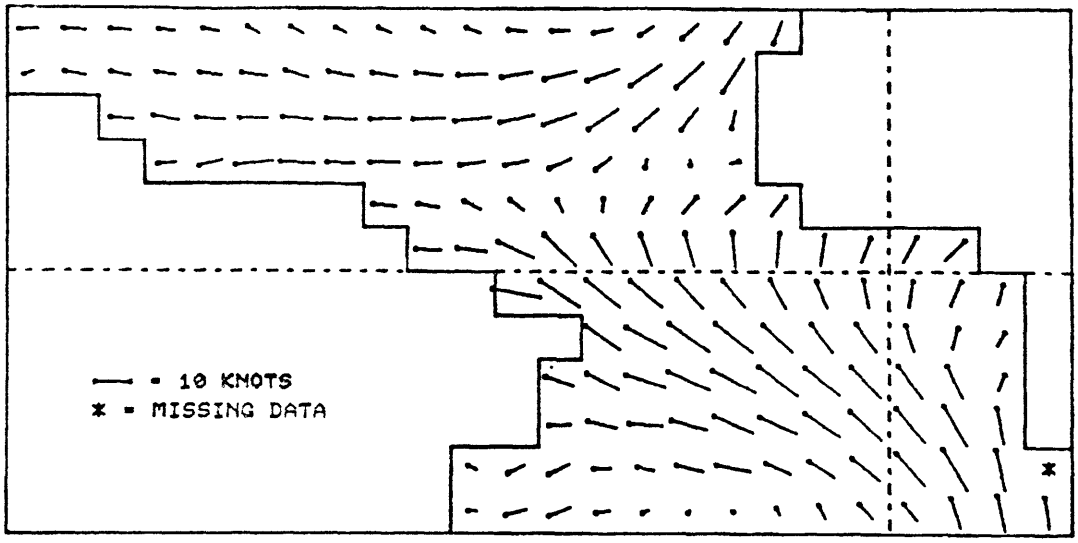

Figure 5j.

** OCTOBER **

MEAN SURFACE WIND FIELD

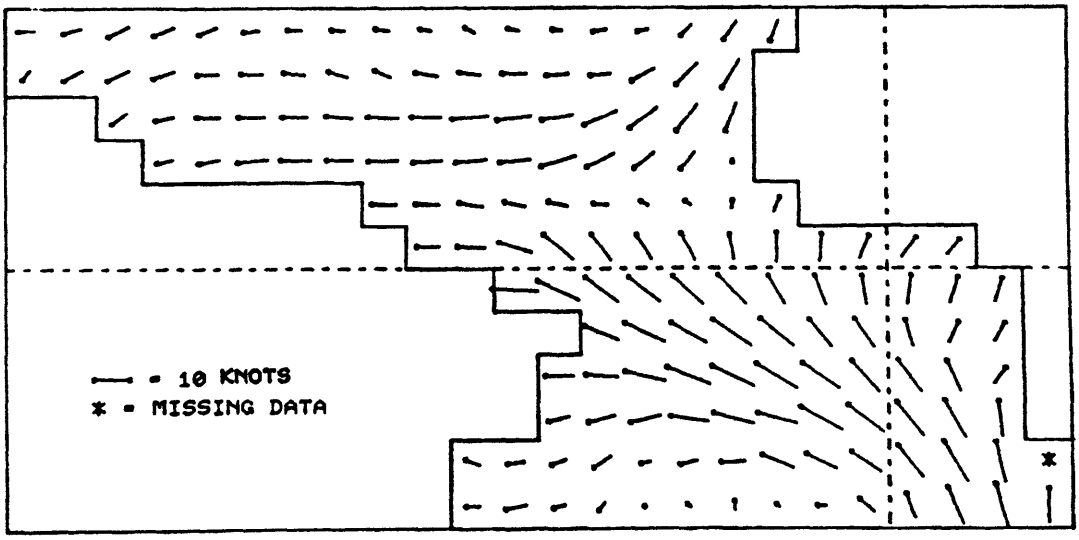

Figure 5k.

** NOVEMBER **

MEAN SURFACE WIND FIELD

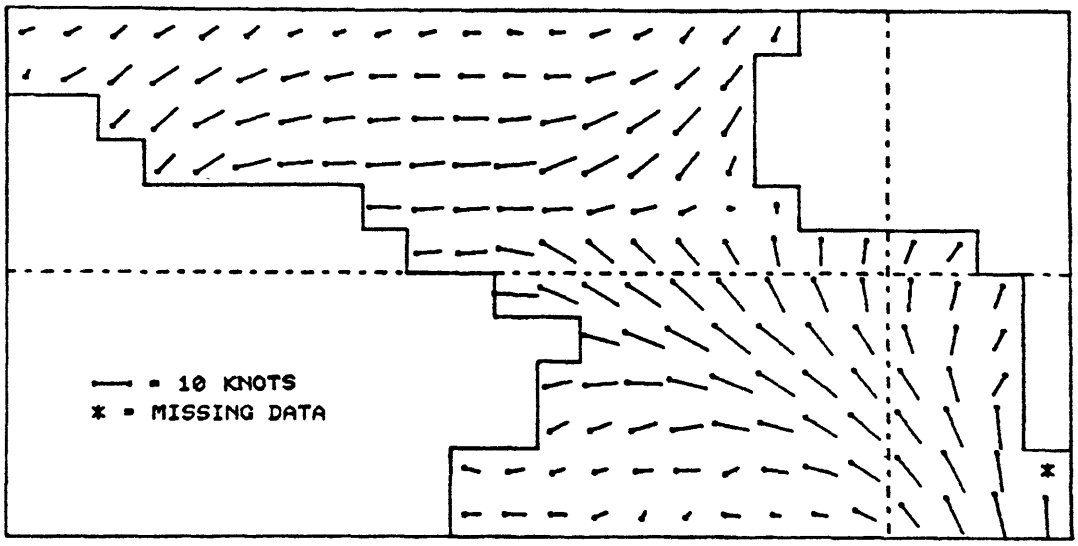

Figure 5l.

** DECEMBER **

MEAN SURFACE WIND FIELD

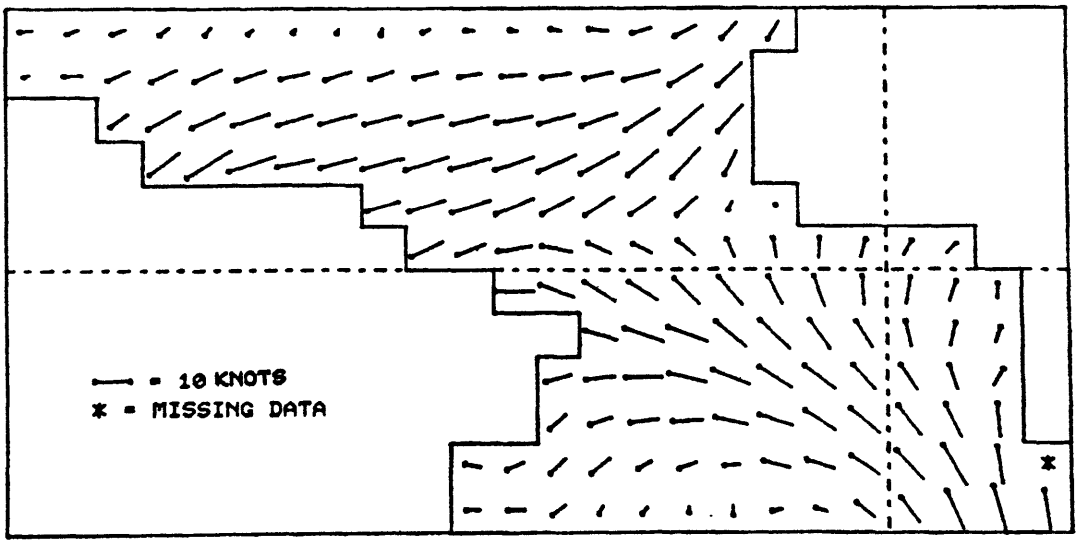

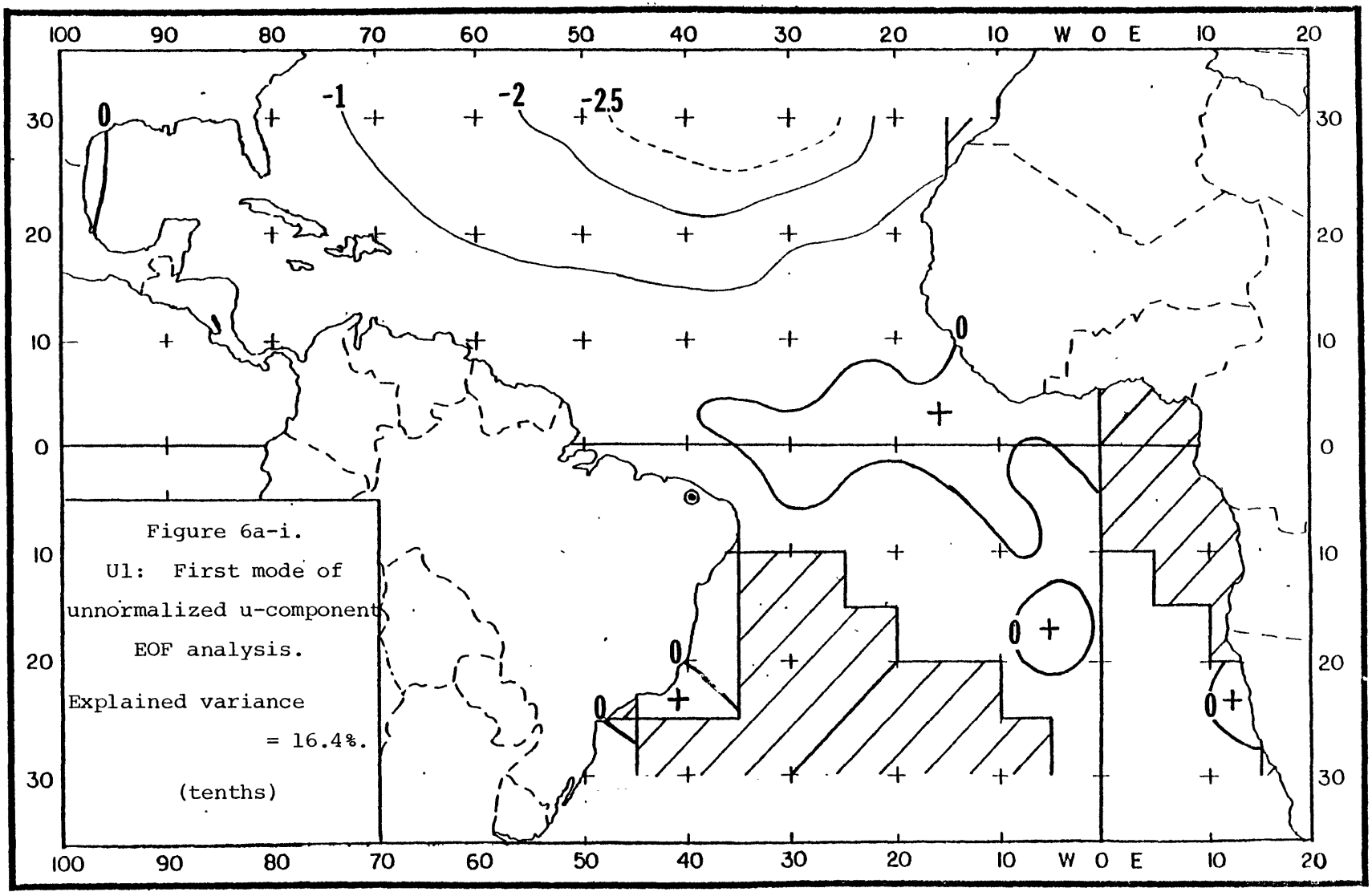
100 90 80 70 60 50 40 30 20 10 W 0 E 10 20
30
20
10
0
10
20
30
-1
-2
-2.5
0
Figure 6a-i.
U1: First mode of unnormalized u-component EOF analysis.
Explained variance = 16.4%.
(tenths)

Figure 6a-ii. TSU1: Time series for U1. (knots)

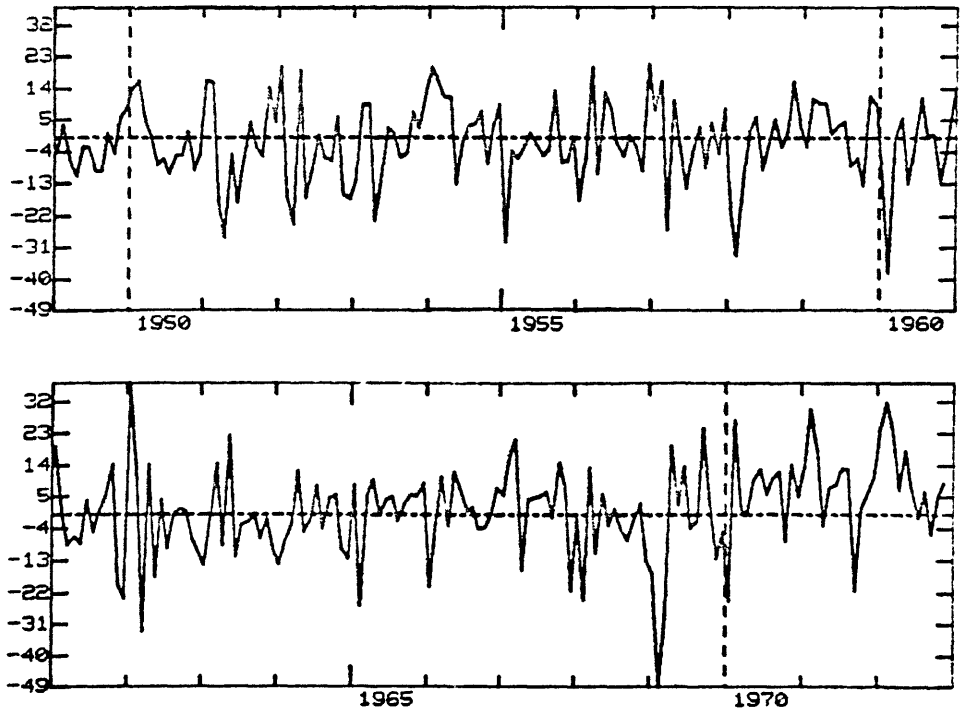

Figure 6b-ii. TSU2: Time series for U2. (knots)

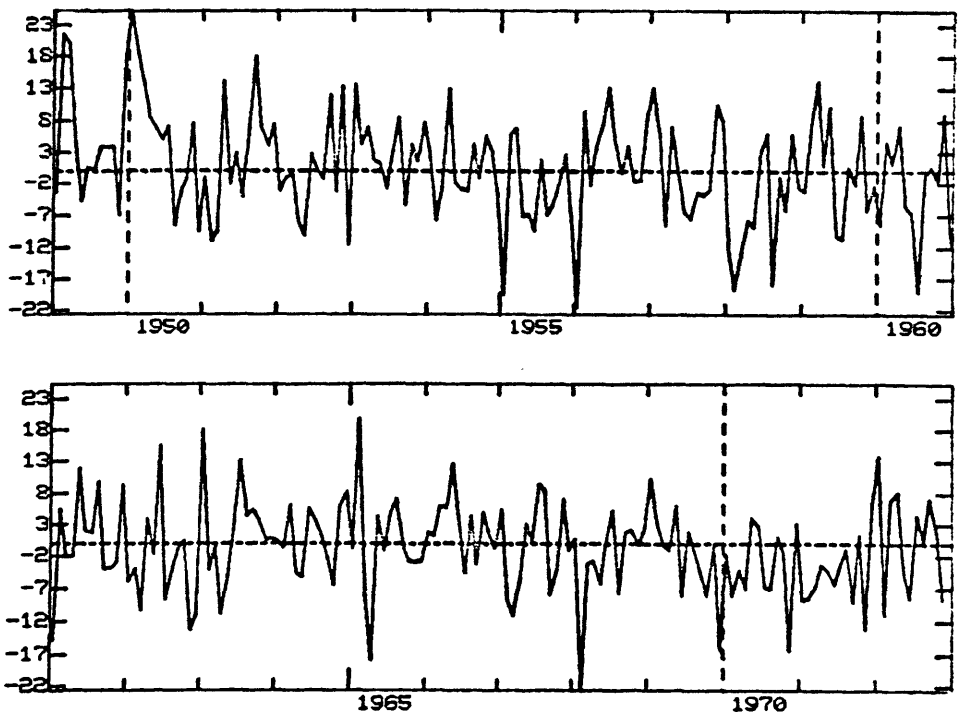

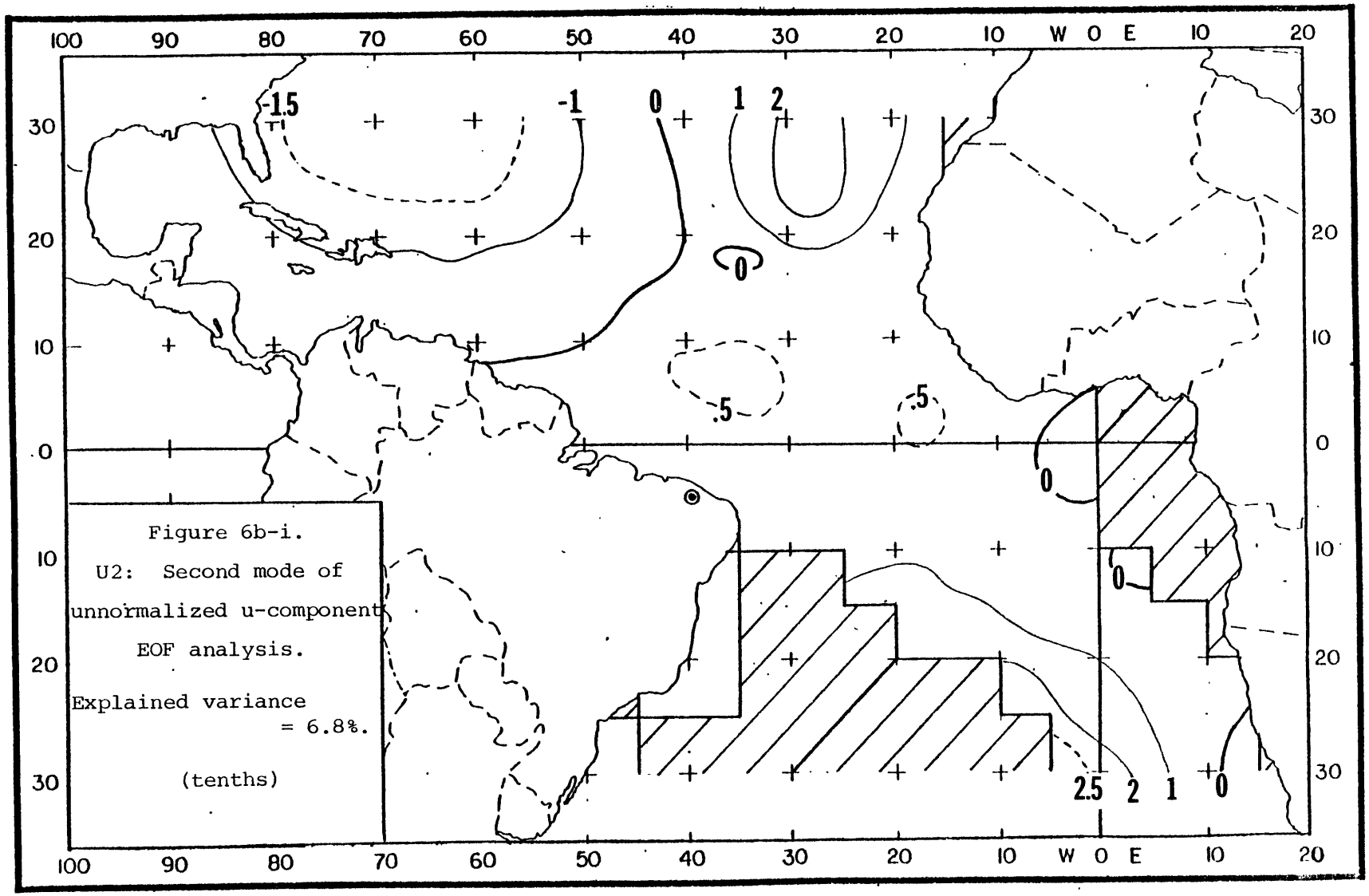
100 90 80 70 60 50 40 30 20 10 W 0 E 10 20
30
20
10
0
10
20
30
-1.5
-1
0
1 2
0
.5
.5
0
0
2.5 2 1 0
Figure 6b-i.
U2: Second mode of unnormalized u-component EOF analysis.
Explained variance = 6.8%.
(tenths)

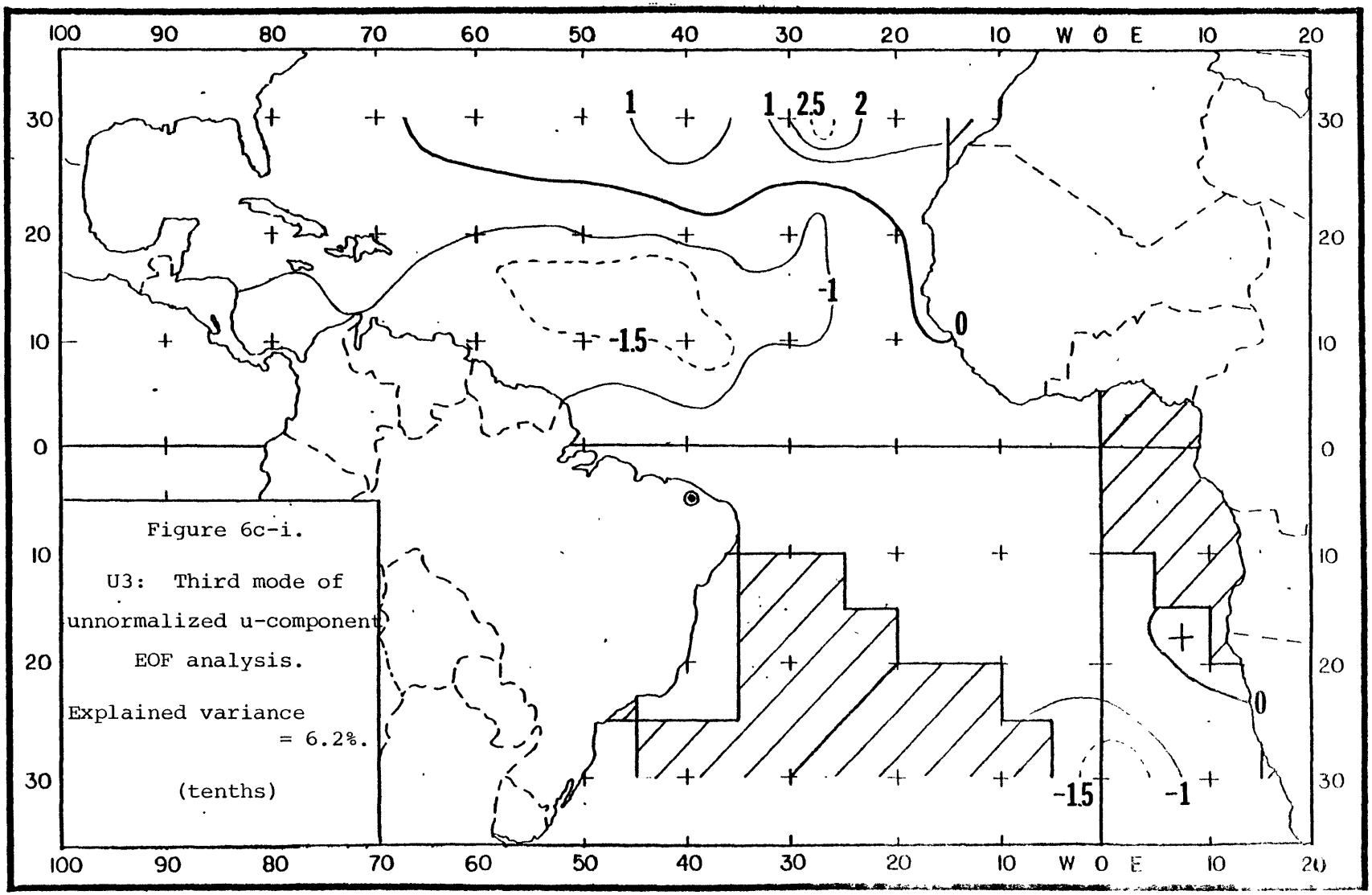
100 90 80 70 60 50 40 30 20 10 W 0 E 10 20
30
20
10
0
10
20
30
1
1
2.5
2
-1
-1.5
0
0
-1.5
-1
Figure 6c-i.
U3: Third mode of unnormalized u-component EOF analysis.
Explained variance = 6.2%.
(tenths)

Figure 6c-ii. TSU3: Time series for U3. (knots)

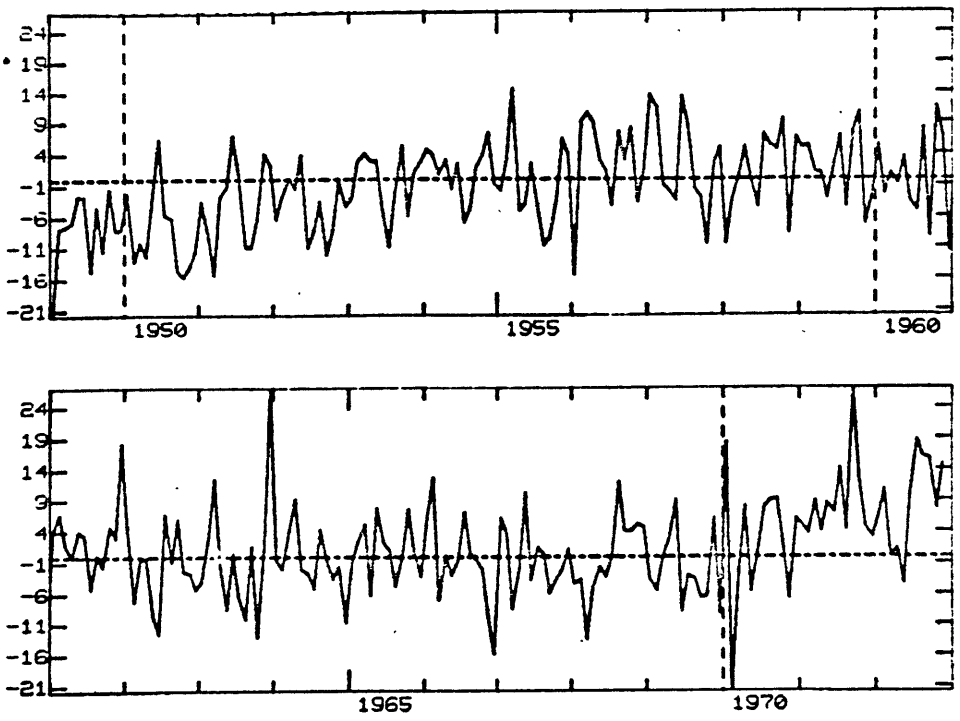

Figure 6d-ii. TSU4: Time series for U4. (knots)

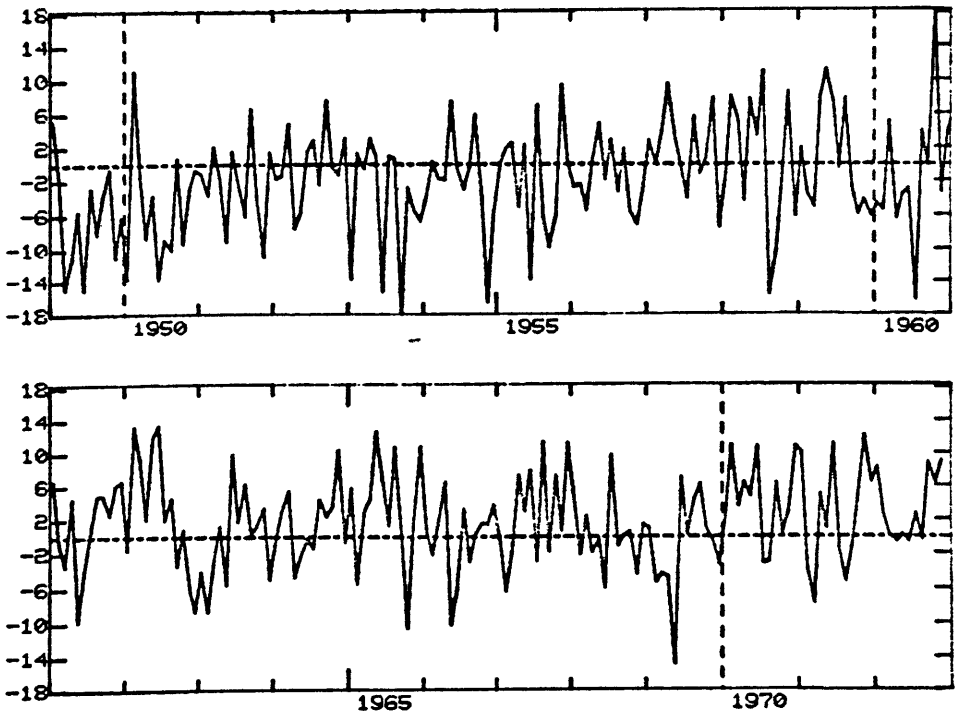

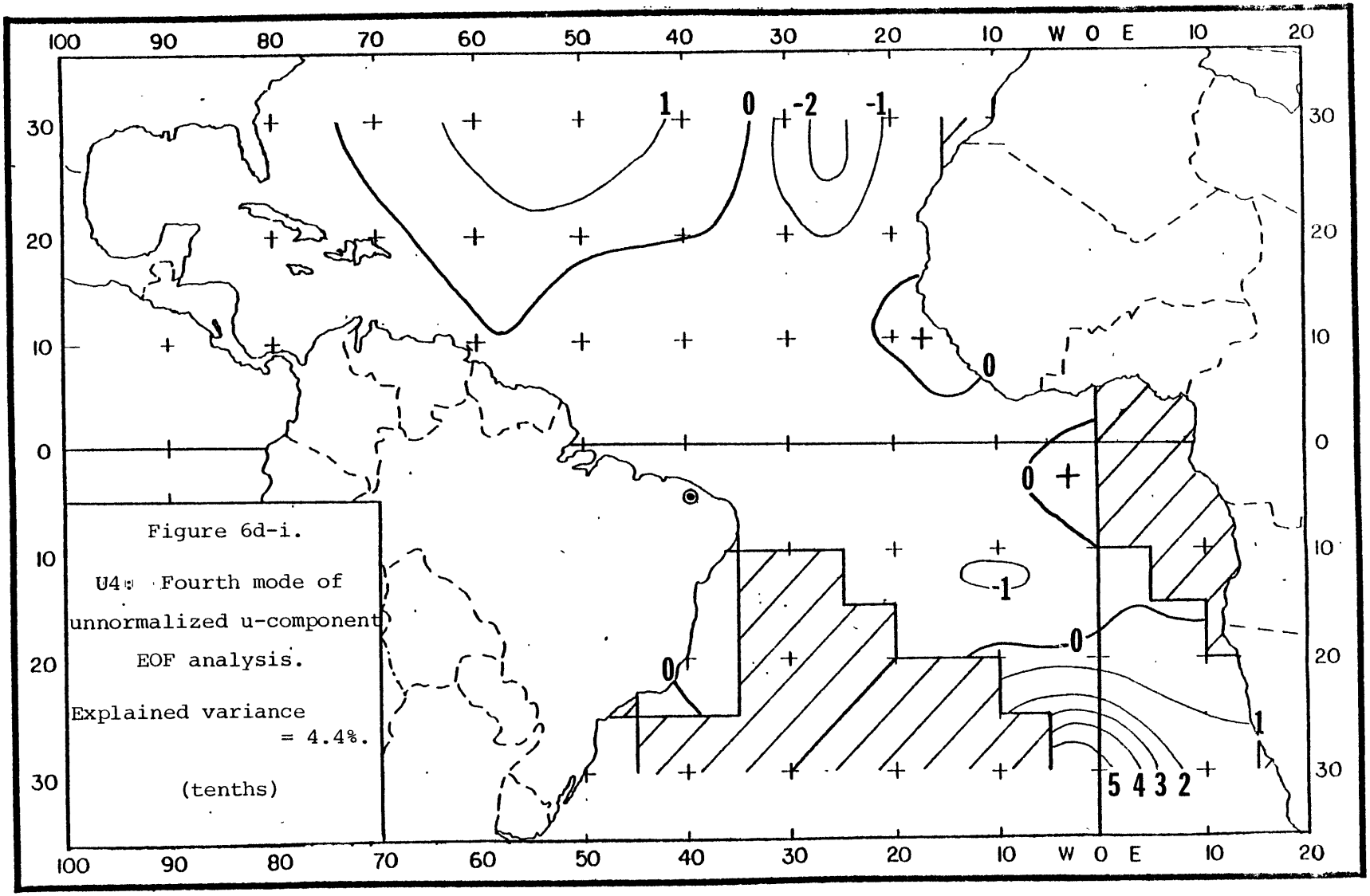
100 90 80 70 60 50 40 30 20 10 W 0 E 10 20
30
20
10
0
10
20
30
1
0
-2
-1
0
0
-1
-0
1
5 4 3 2
Figure 6d-i.
U4: Fourth mode of unnormalized u-component EOF analysis.
Explained variance = 4.4%.
(tenths)

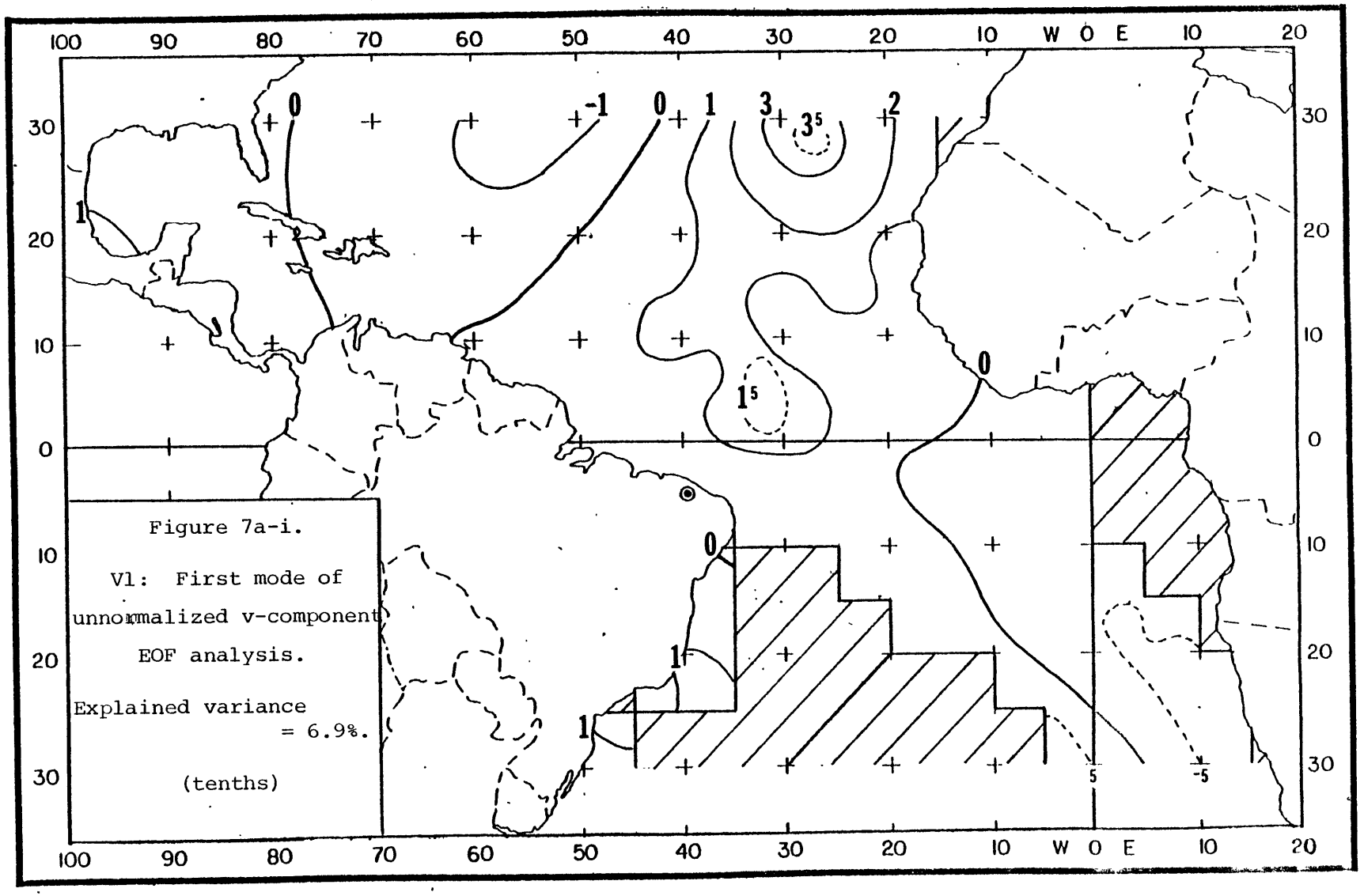
100 90 80 70 60 50 40 30 20 10 W 0 E 10 20
30 20 10 0 10 20 30
0
-1
0
1
3
3.5
2
1
1.5
0
0
1
1
5
-5
Figure 7a-i.
V1: First mode of unnormalized v-component EOF analysis.
Explained variance = 6.9%.
(tenths)

Figure 7a-ii. TSV1: Time series for V1. (knots)

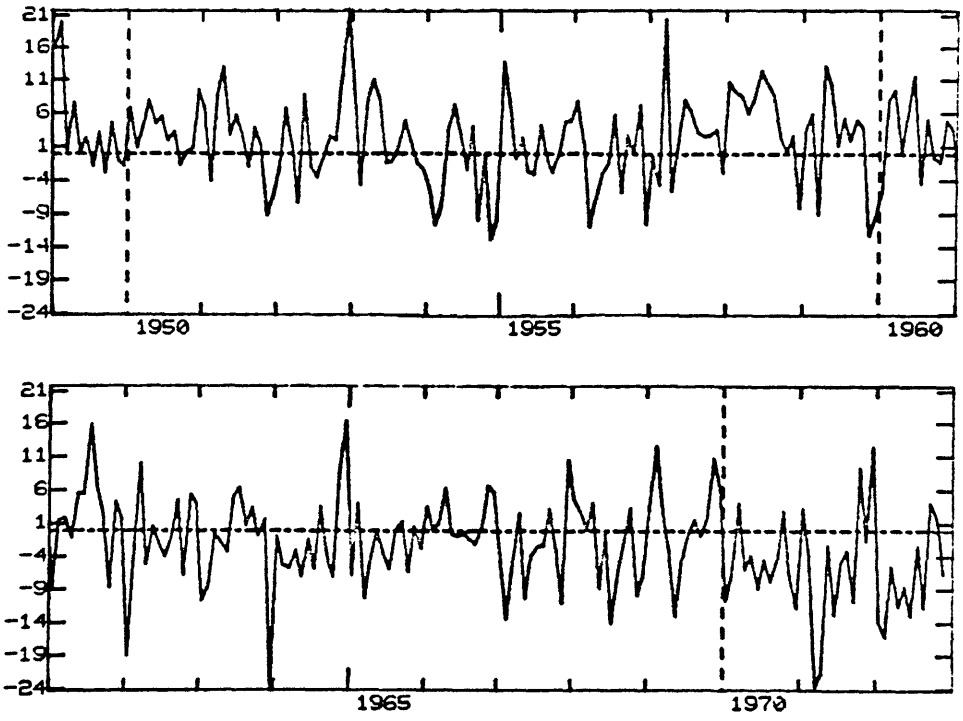

Figure 7b-ii. TSV2: Time series for V2. (knots)

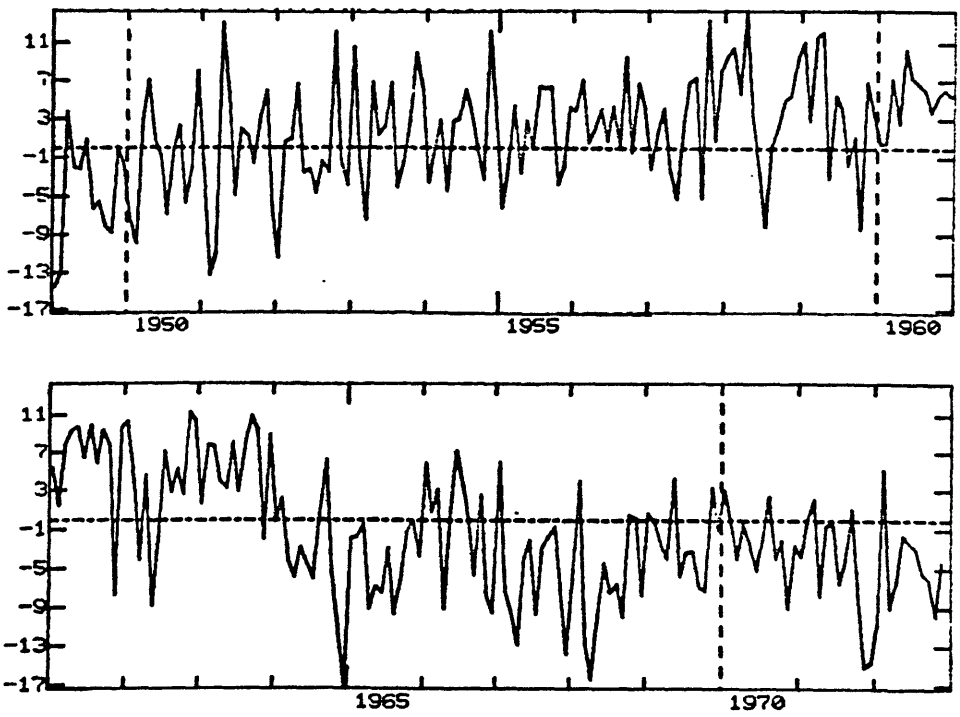

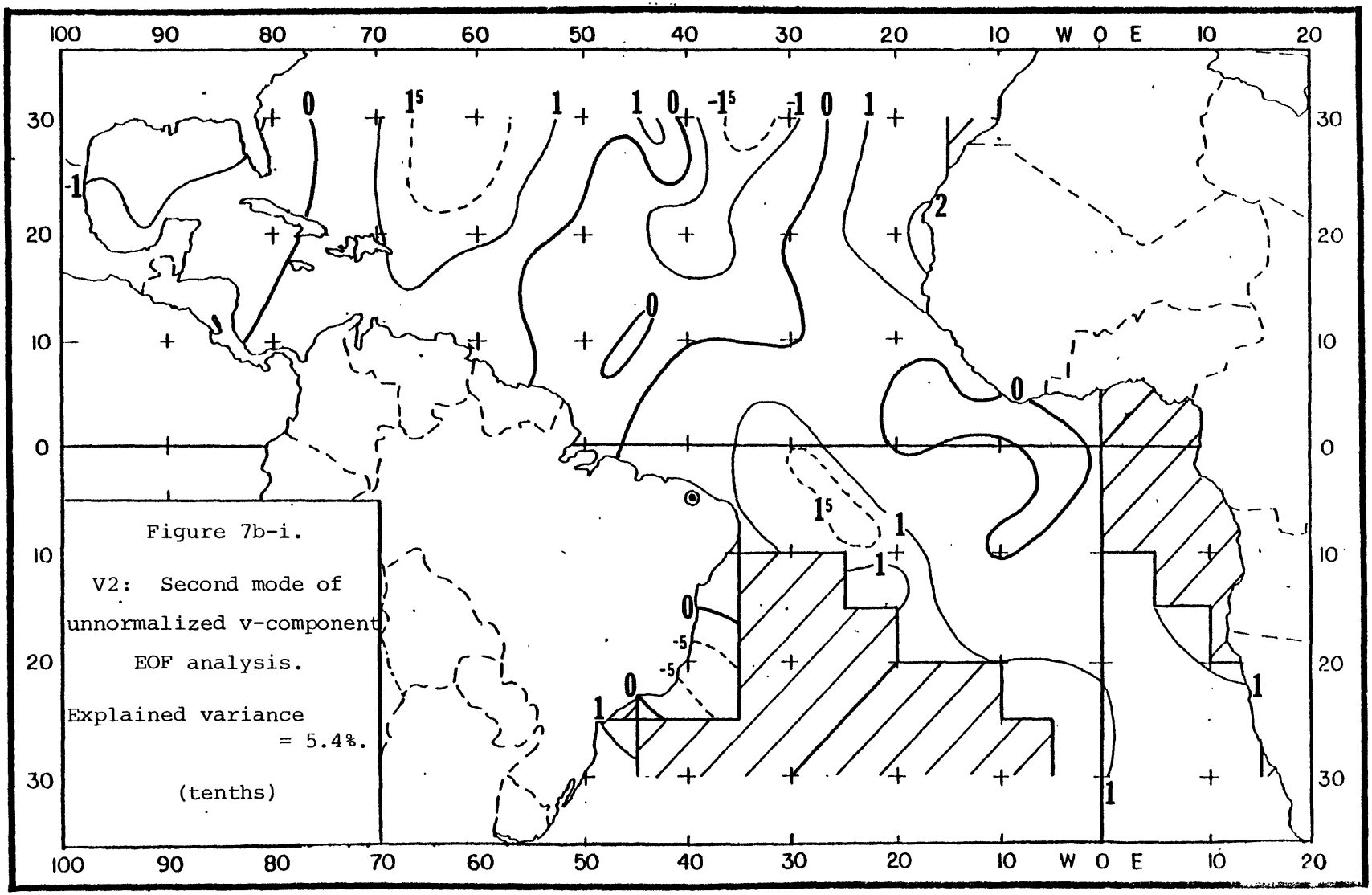
100 90 80 70 60 50 40 30 20 10 W 0 E 10 20
30 20 10 0 10 20 30
Figure 7b-i.
V2: Second mode of unnormalized v-component EOF analysis.
Explained variance = 5.4%.
(tenths)

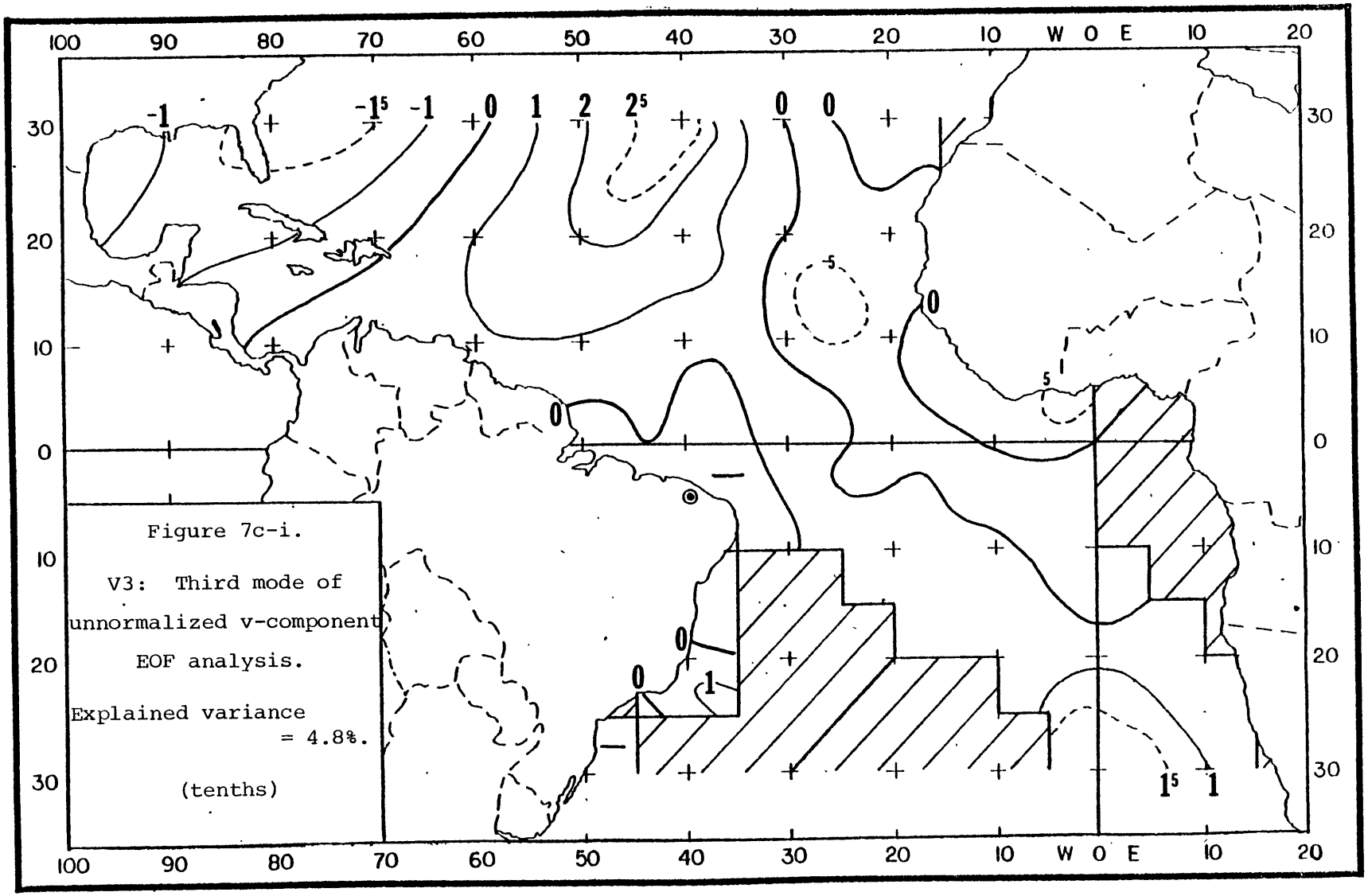
100 90 80 70 60 50 40 30 20 10 W 0 E 10 20
30
20
10
0
10
20
30
-1
-1⁵
-1
0
1
2
2⁵
0
0
-5
0
5
0
0
0
1
1⁵
1
Figure 7c-i.
V3: Third mode of unnormalized v-component EOF analysis.
Explained variance = 4.8%.
(tenths)

Figure 7c-ii. TSV3: Time series for V3. (knots)

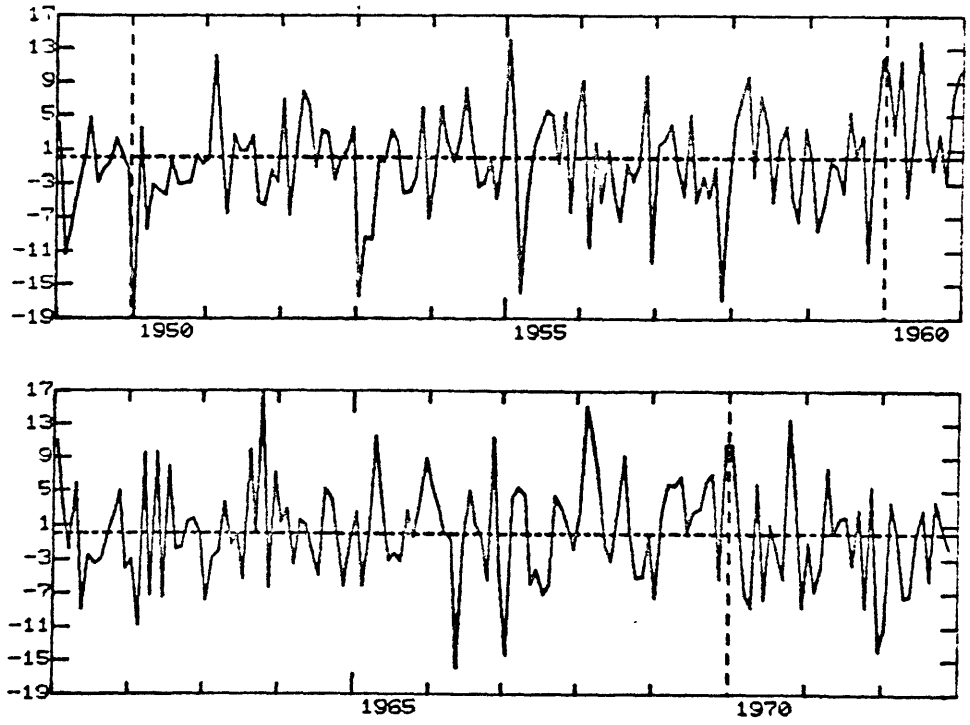

Figure 7d-ii. TSV4: Time series for V4. (knots)

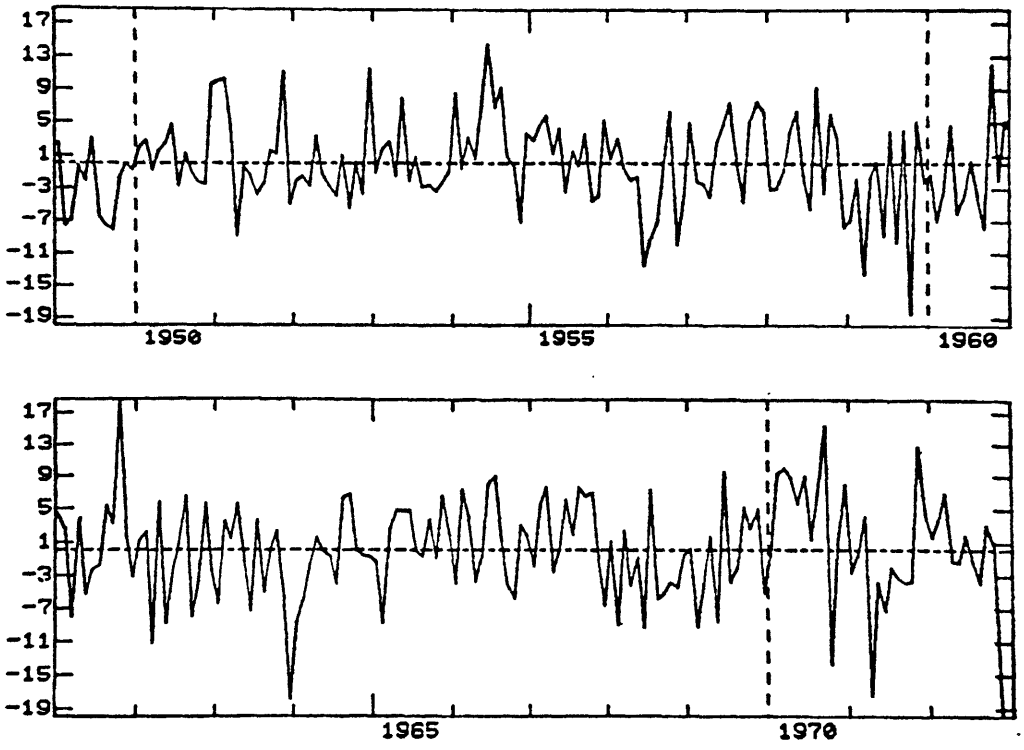

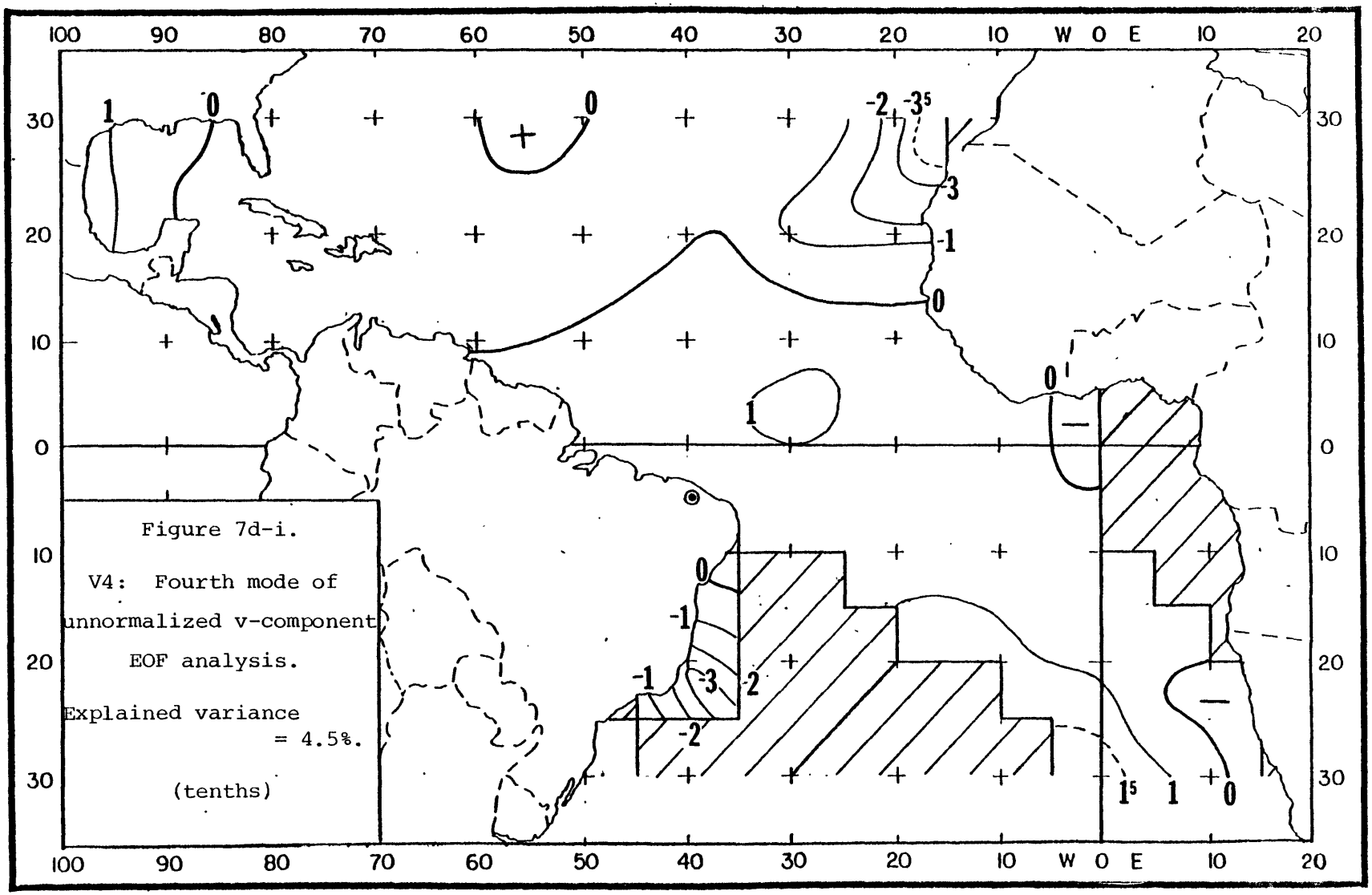
100 90 80 70 60 50 40 30 20 10 W 0 E 10 20
30
20
10
0
10
20
30
1
0
0
-2
-3.5
3
-1
0
0
1
0
-1
-1
-3
-2
-2
1.5
1
0
Figure 7d-i.
V4: Fourth mode of unnormalized v-component EOF analysis.
Explained variance = 4.5%.
(tenths)

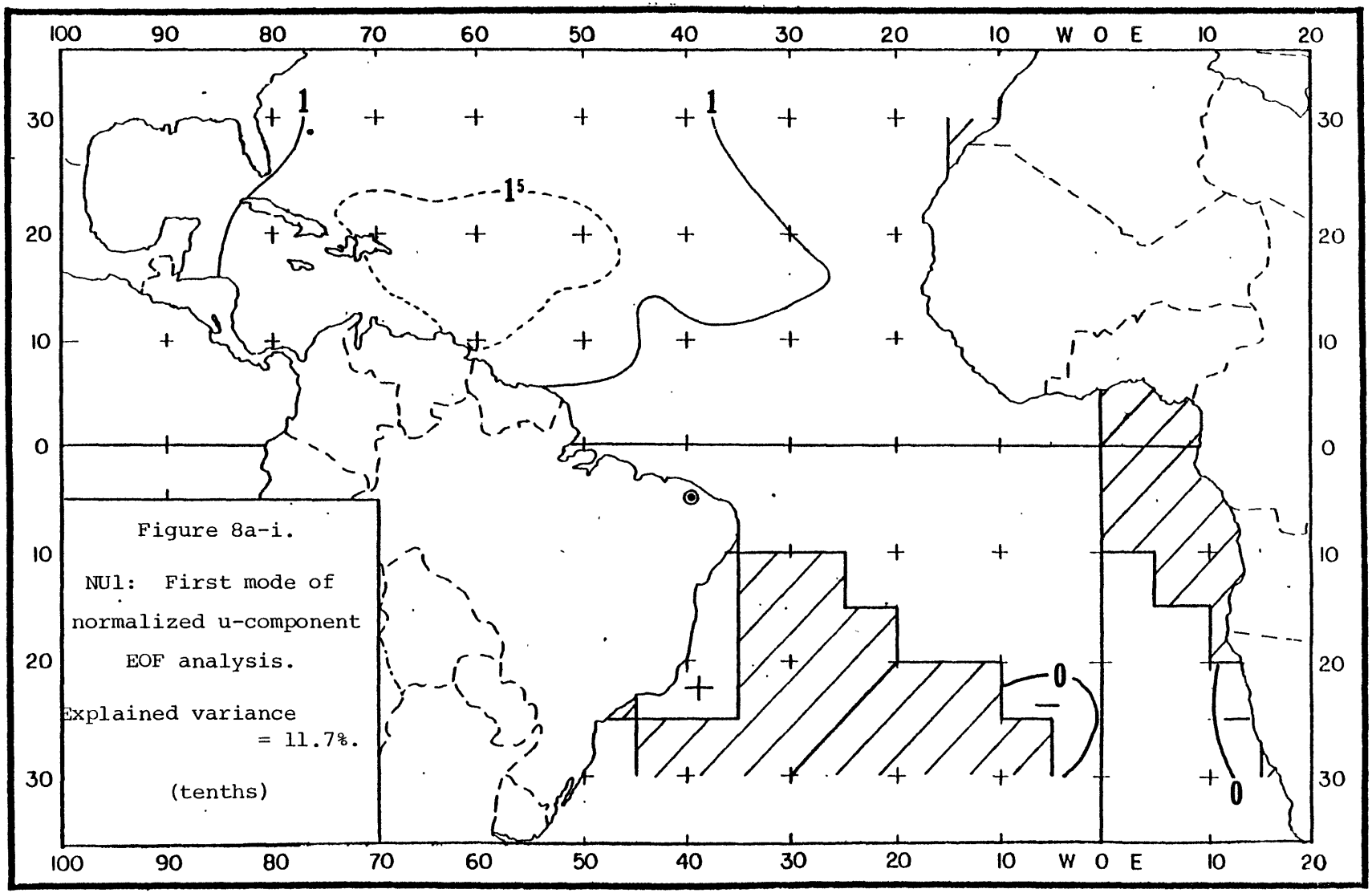
100 90 80 70 60 50 40 30 20 10 W 0 E 10 20
30
20
10
0
10
20
30
1
1
1.5
0
0
Figure 8a-i.
NU1: First mode of normalized u-component EOF analysis.
Explained variance = 11.7%.
(tenths)

Figure 8a-ii. TSNU1: Time series for NU1. (std dev's)

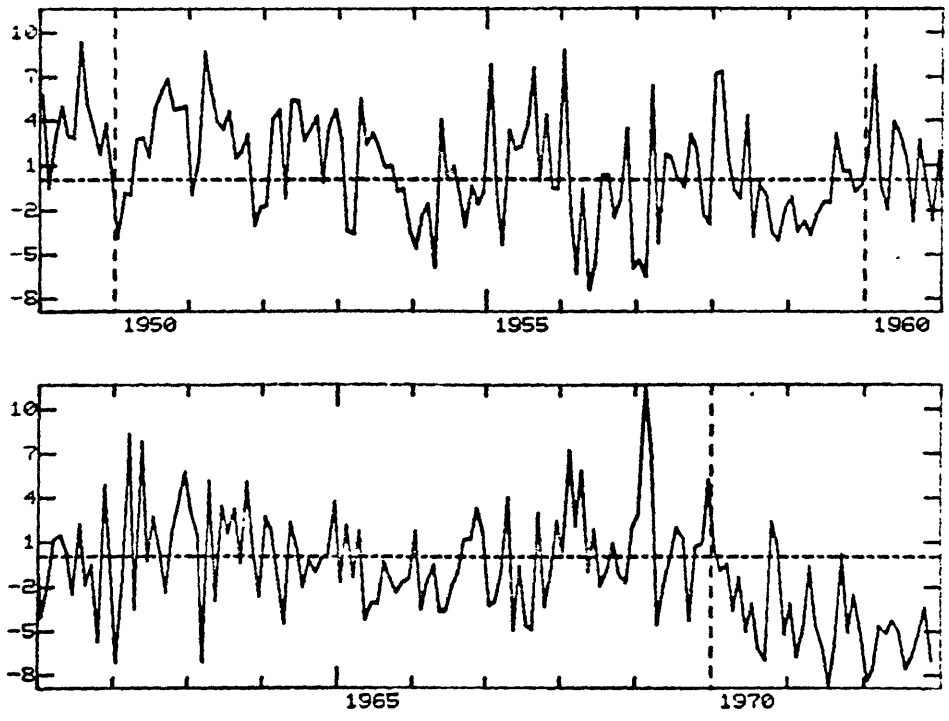

Figure 8b-ii. TSNU2: Time series for NU2. (std dev's)

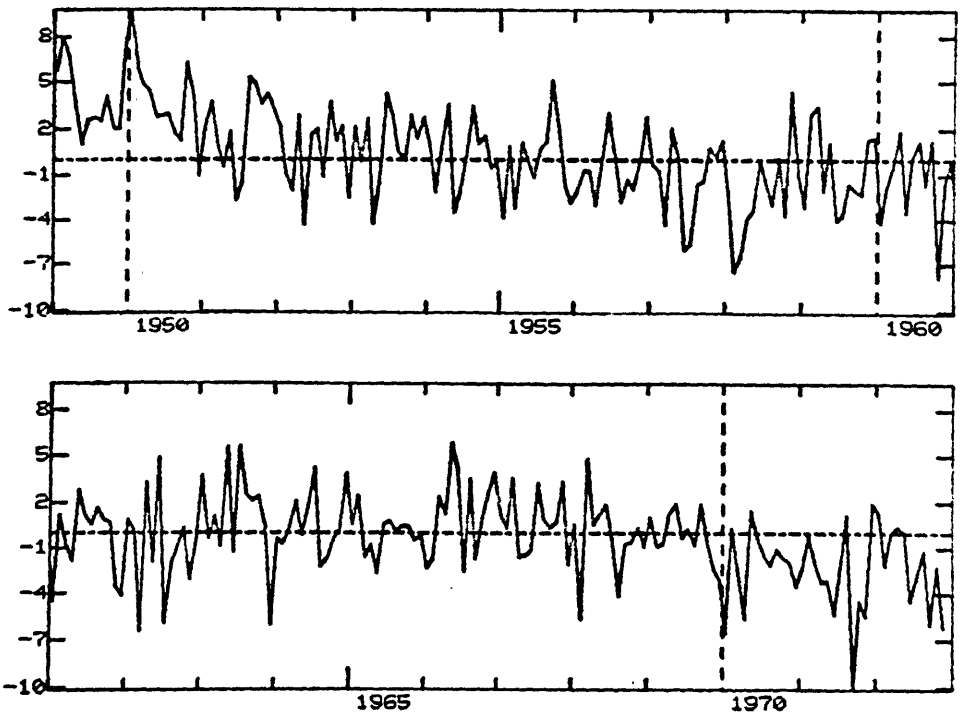

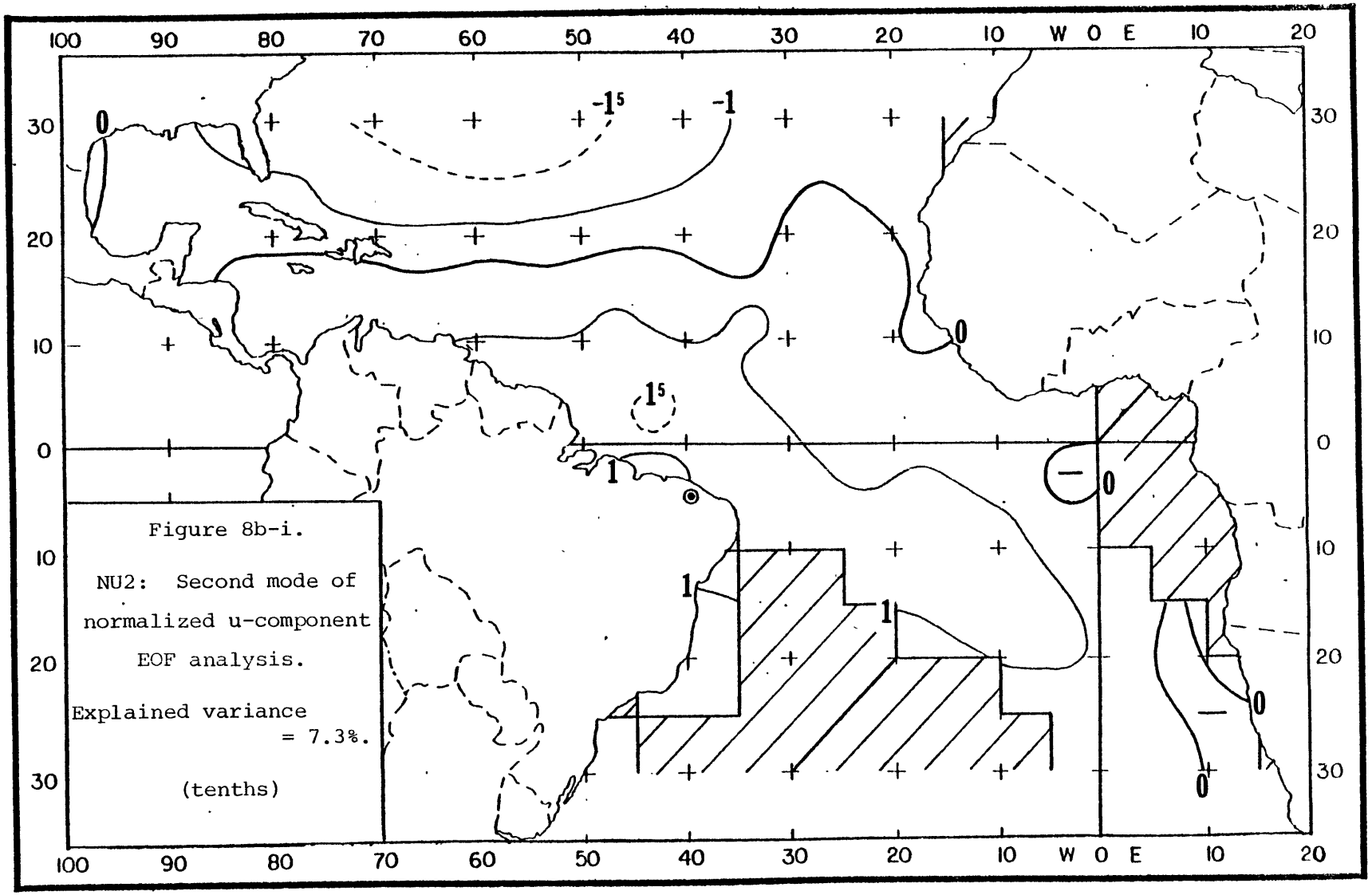
100 90 80 70 60 50 40 30 20 10 W 0 E 10 20
30
20
10
0
10
20
30
-1.5
-1
0
1.5
1
Figure 8b-i.
NU2: Second mode of normalized u-component EOF analysis.
Explained variance = 7.3%.
(tenths)

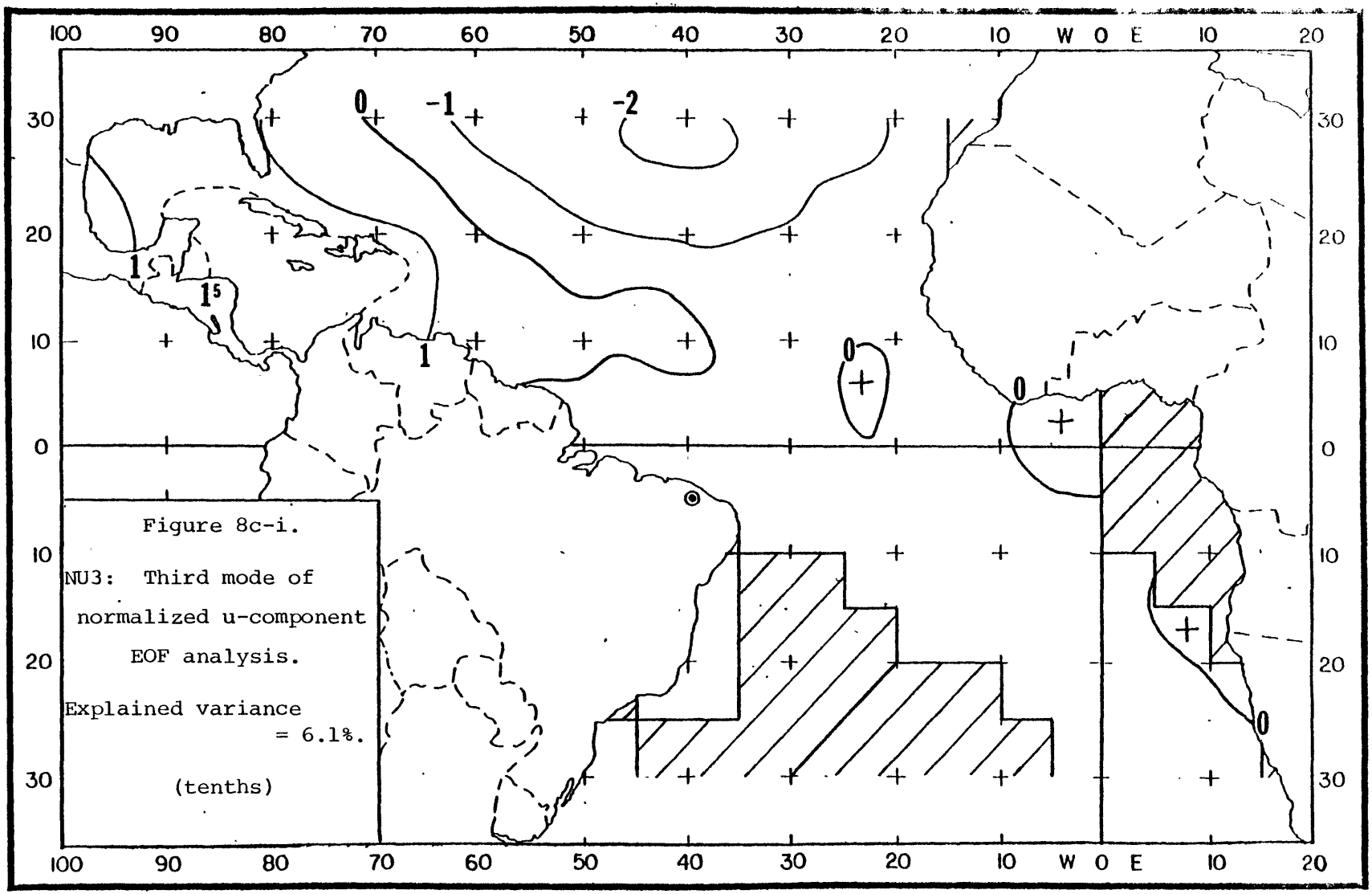
100 90 80 70 60 50 40 30 20 10 W 0 E 10 20
30
20
10
0
10
20
30
0
-1
-2
1
1.5
1
0
0
0
Figure 8c-i.
NU3: Third mode of normalized u-component EOF analysis.
Explained variance = 6.1%.
(tenths)

Figure 8c-ii. TSNU3: Time series for NU3. (std dev's)

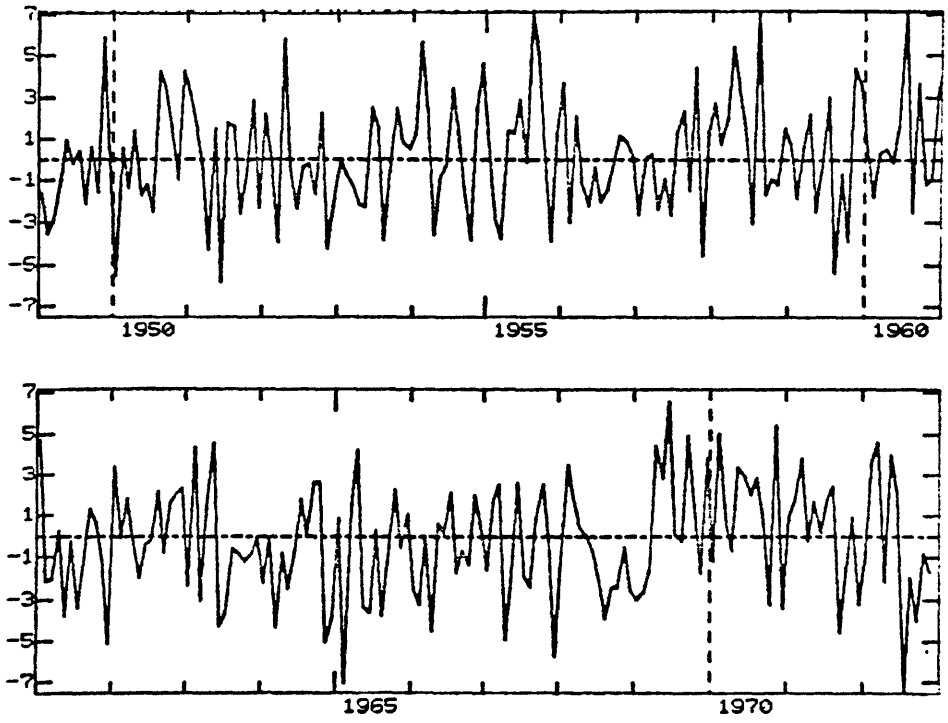

Figure 8d-ii. TSNU4: Time series for NU4. (std dev's)

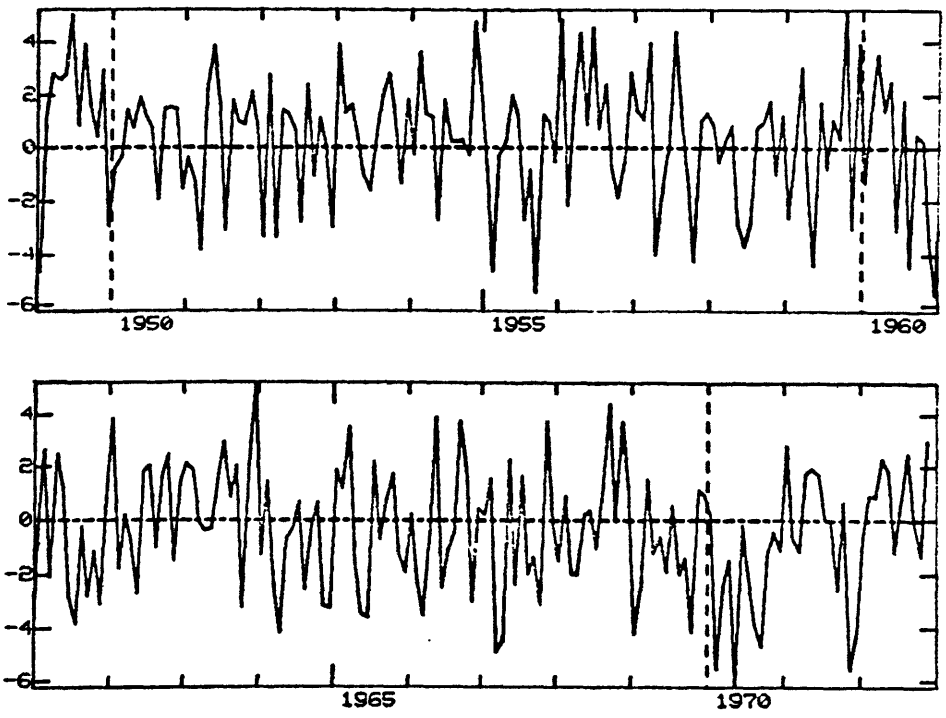

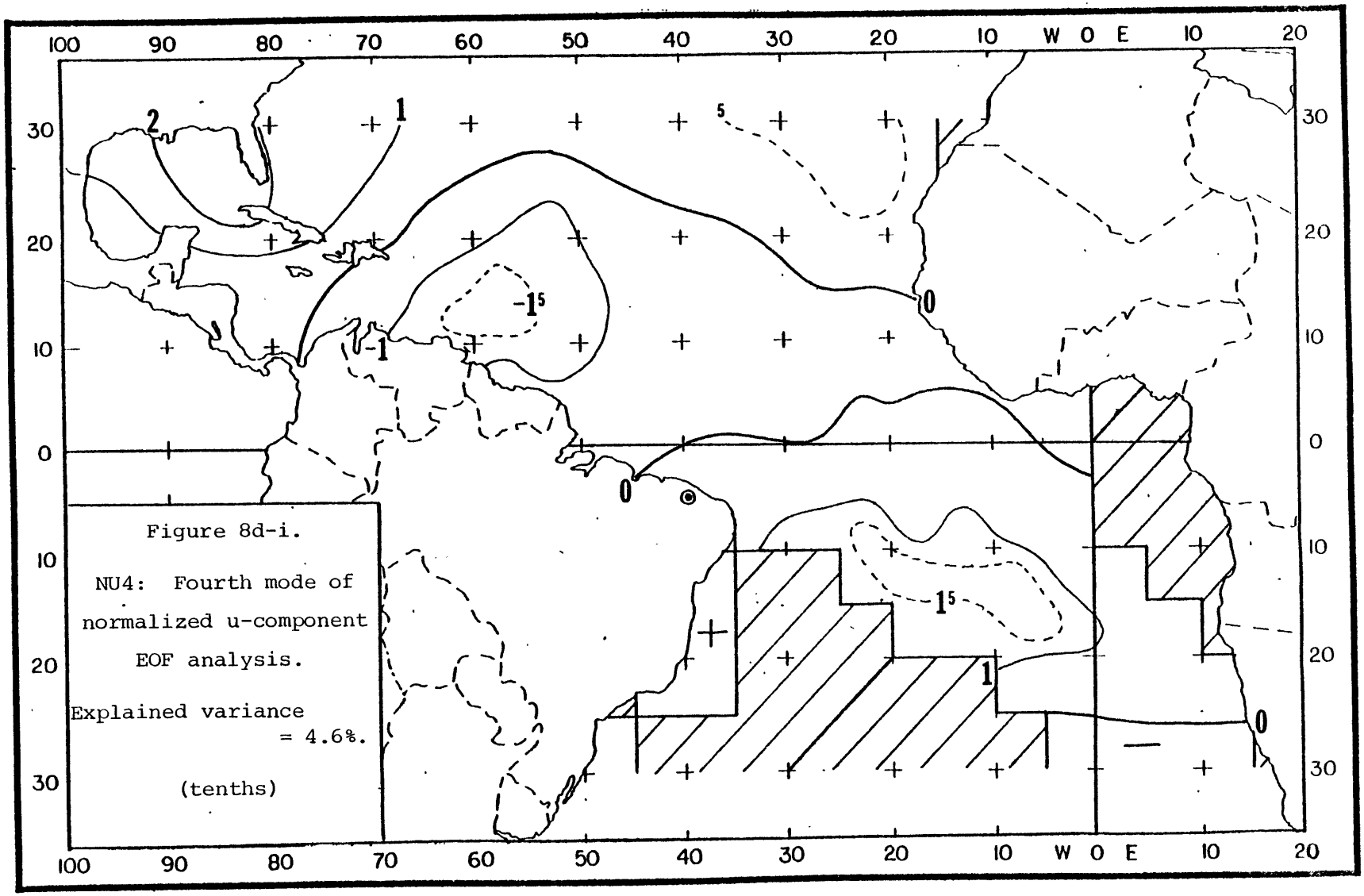
100 90 80 70 60 50 40 30 20 10 W 0 E 10 20
30
20
10
0
10
20
30
2
1
5
-1.5
-1
0
0
1.5
1
0
Figure 8d-i.
NU4: Fourth mode of normalized u-component EOF analysis.
Explained variance = 4.6%.
(tenths)

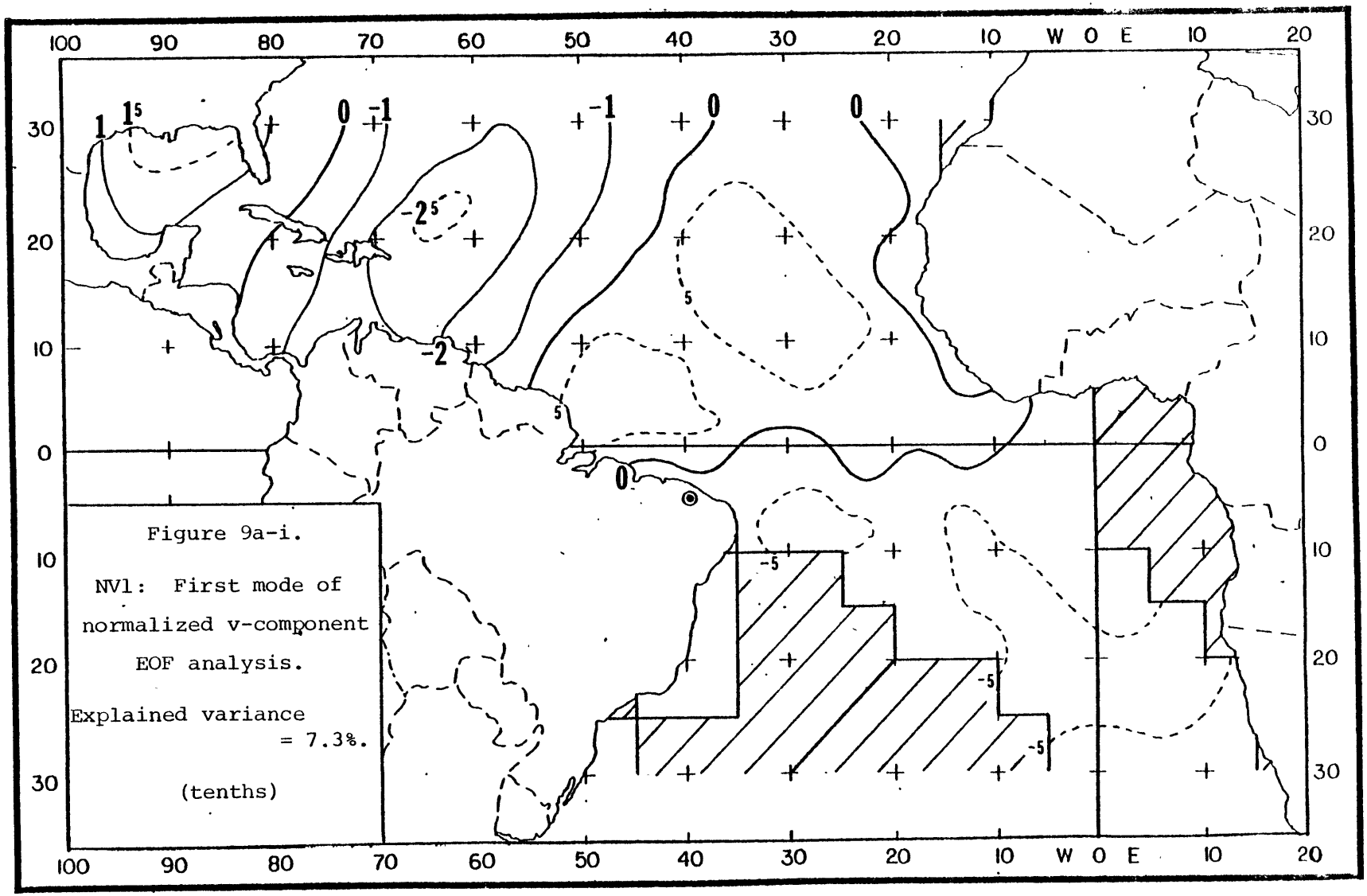
100 90 80 70 60 50 40 30 20 10 W 0 E 10 20
30
20
10
0
10
20
30
1
1.5
0
-1
-1
0
0
-2.5
-2
5
5
0
-5
-5
-5
Figure 9a-i.
NV1: First mode of normalized v-component EOF analysis.
Explained variance = 7.3%.
(tenths)

Figure 9a-ii. TSNV1: Time series for NV1. (std dev's)

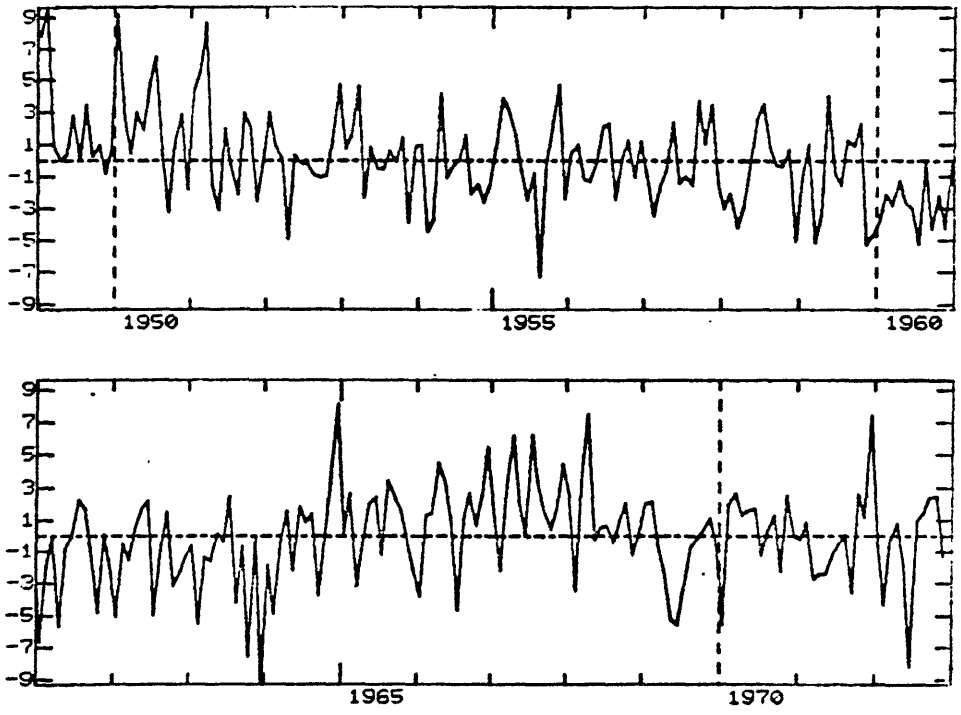

Figure 9b-ii. TSNV2: Time series for NV2. (std dev's)

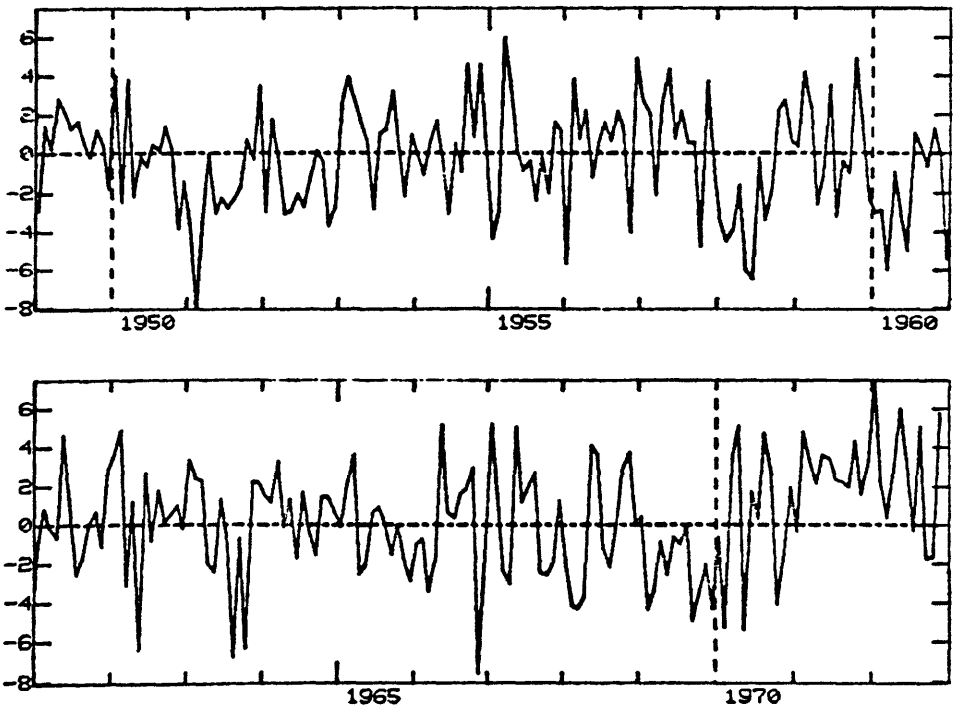

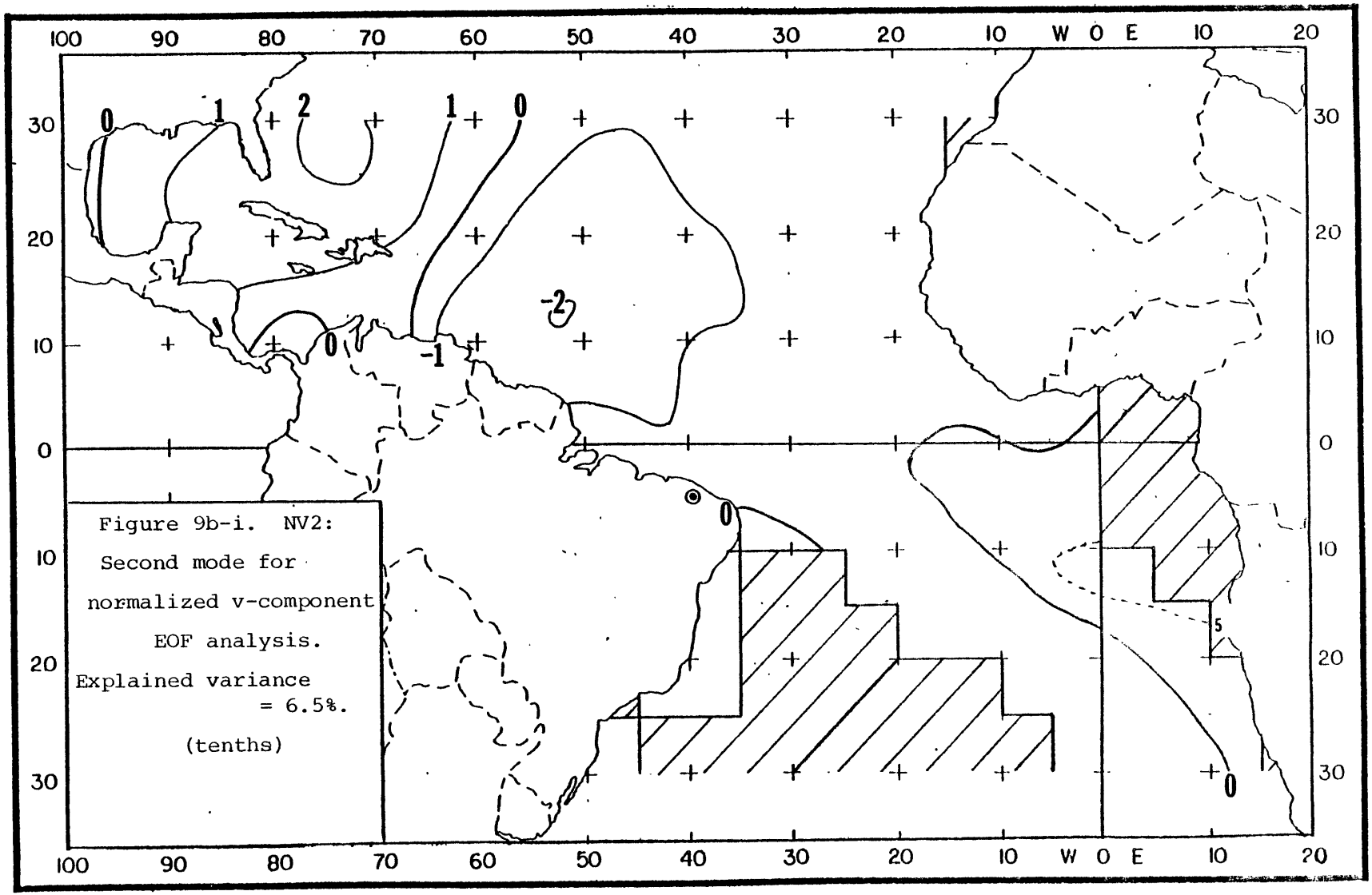
100 90 80 70 60 50 40 30 20 10 W 0 E 10 20
30
20
10
0
10
20
30
0
1
2
1
0
-2
0
-1
0
5
0
Figure 9b-i. NV2:
Second mode for
normalized v-component
EOF analysis.
Explained variance
= 6.5%.
(tenths)

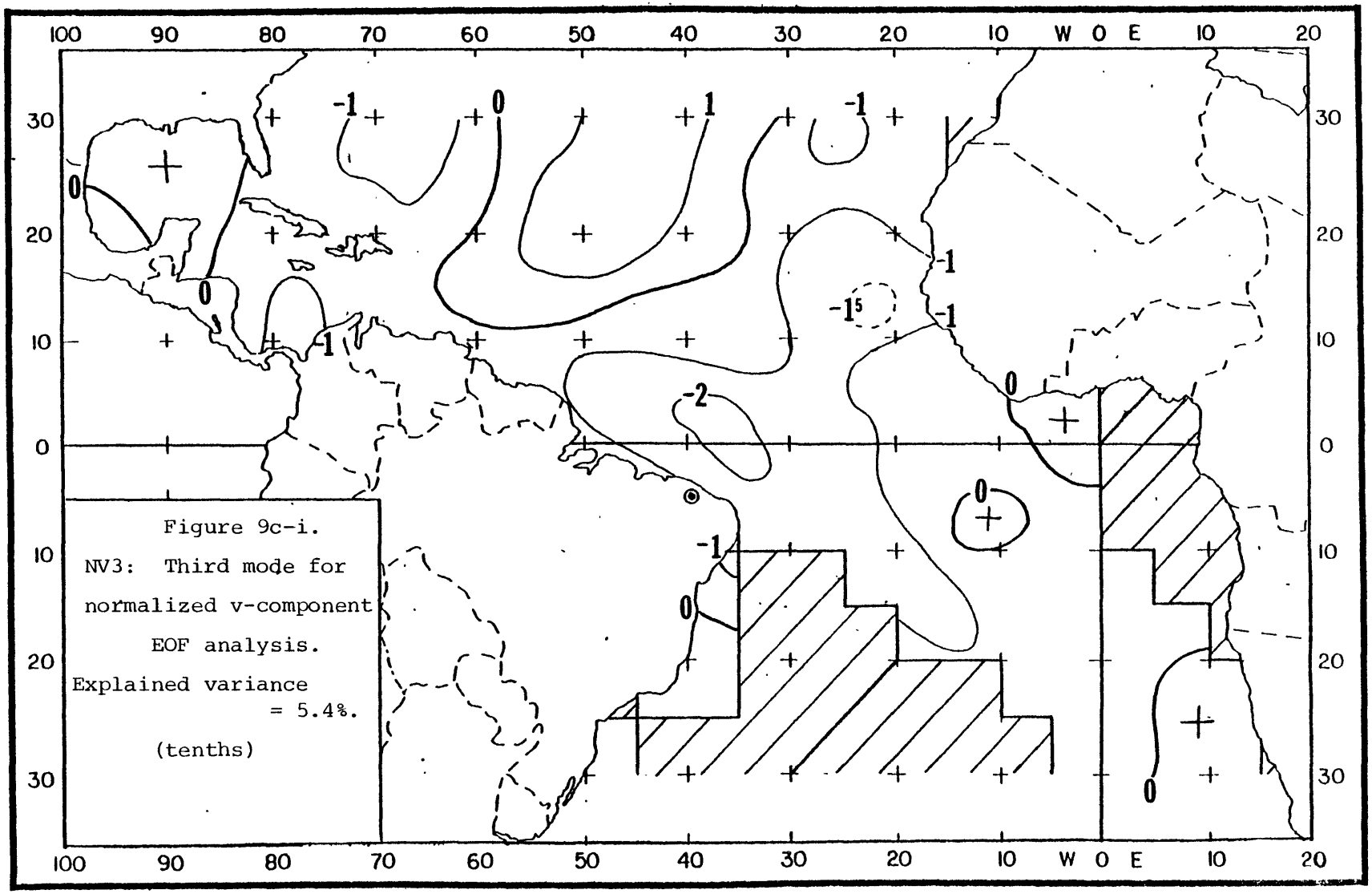

Figure 9c-i.
NV3: Third mode for normalized v-component EOF analysis.
Explained variance = 5.4%.
(tenths)

Figure 9c-ii. TSNV3: Time series for NV3. (std dev's)

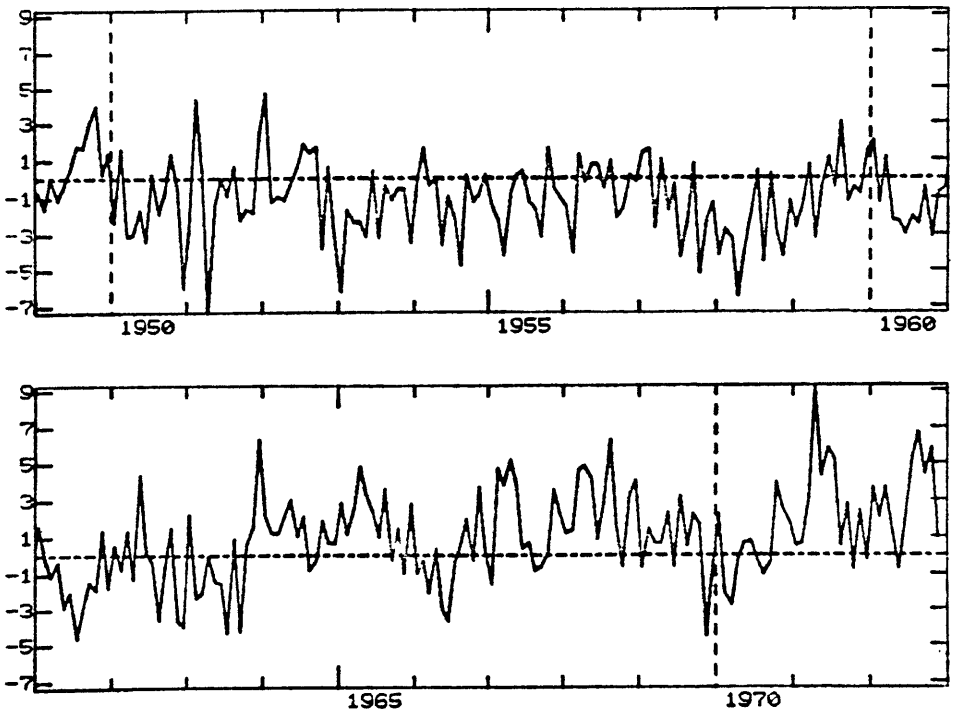

Figure 9d-ii. TSNV4: Time series for NV4. (std dev's)

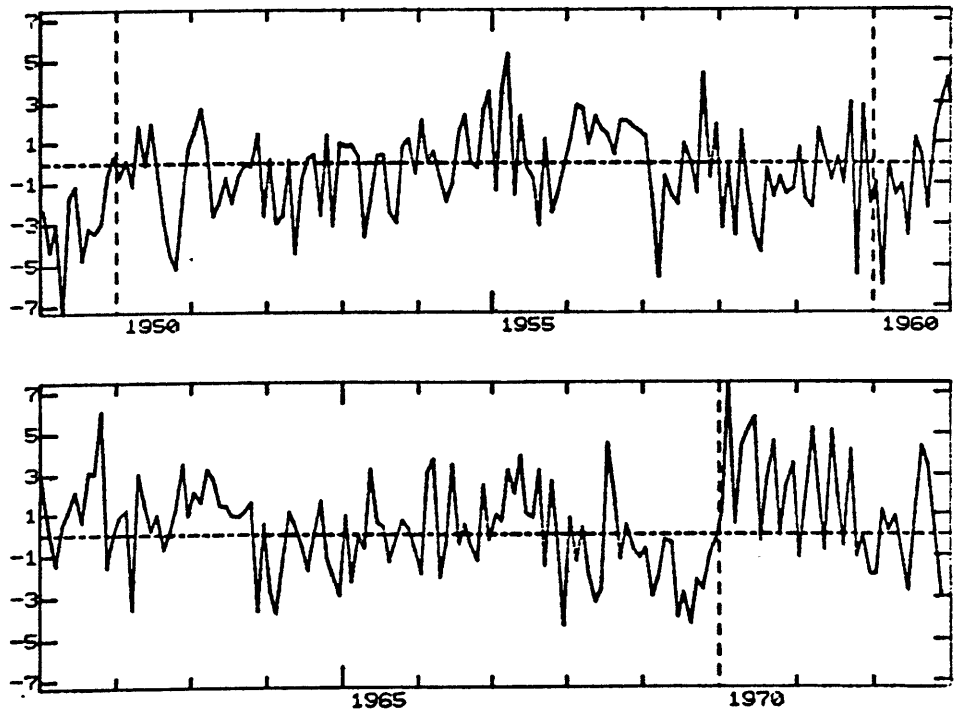

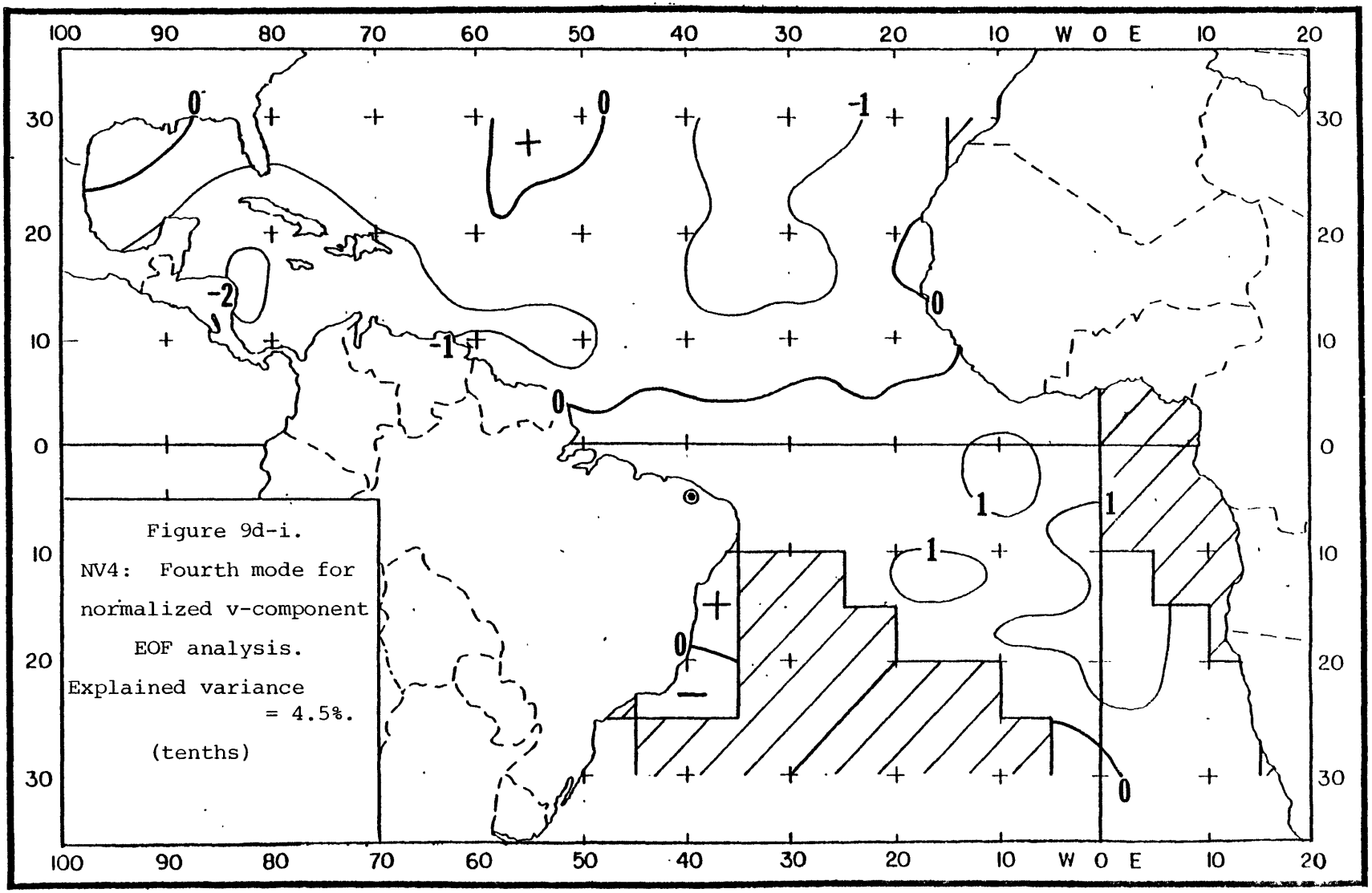

Figure 9d-i.
NV4: Fourth mode for normalized v-component EOF analysis.
Explained variance = 4.5%.
(tenths)

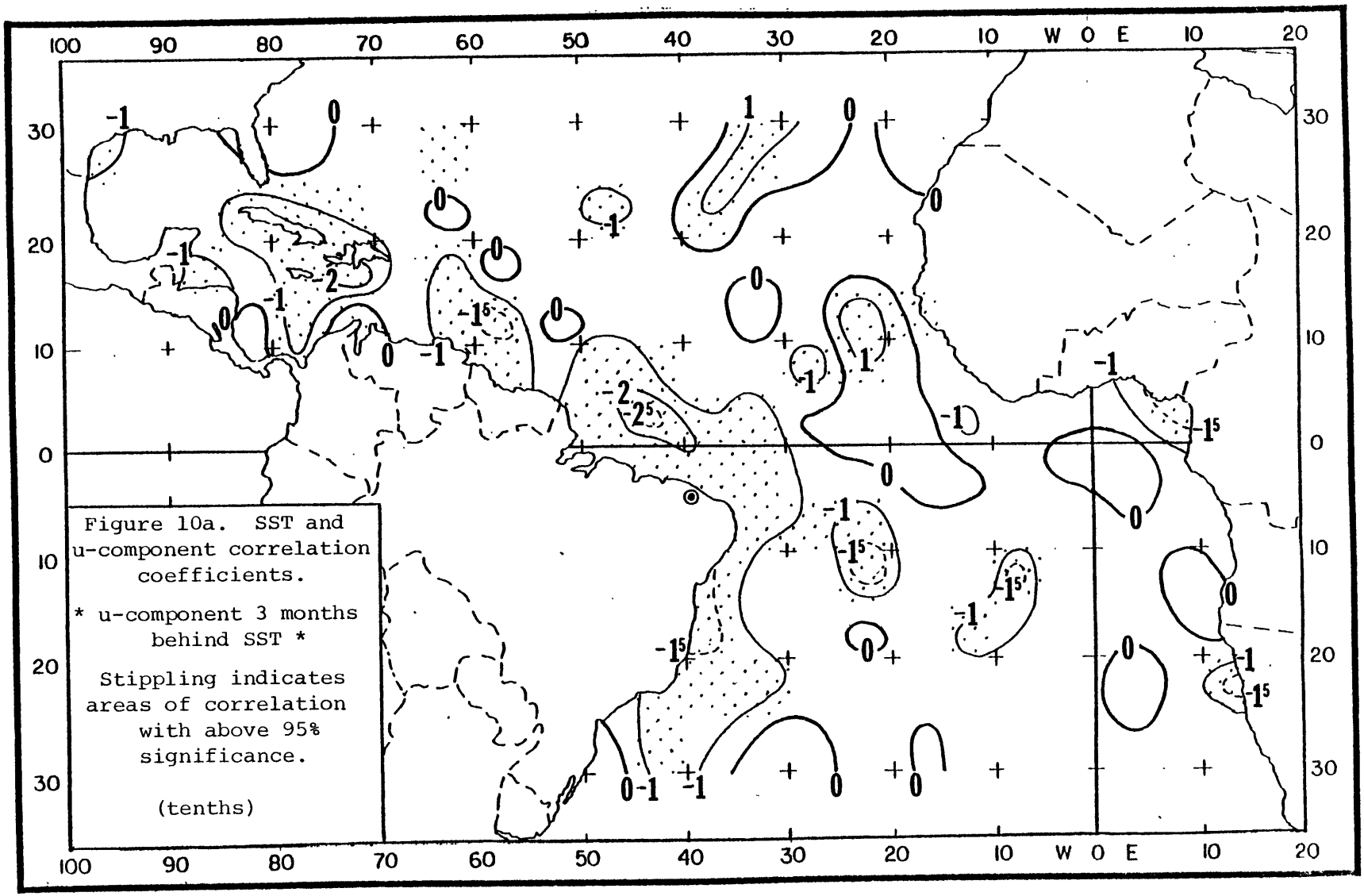
100 90 80 70 60 50 40 30 20 10 W 0 E 10 20
30
20
10
0
10
20
30
Figure 10a. SST and u-component correlation coefficients.
* u-component 3 months behind SST *
Stippling indicates areas of correlation with above 95% significance.
(tenths)

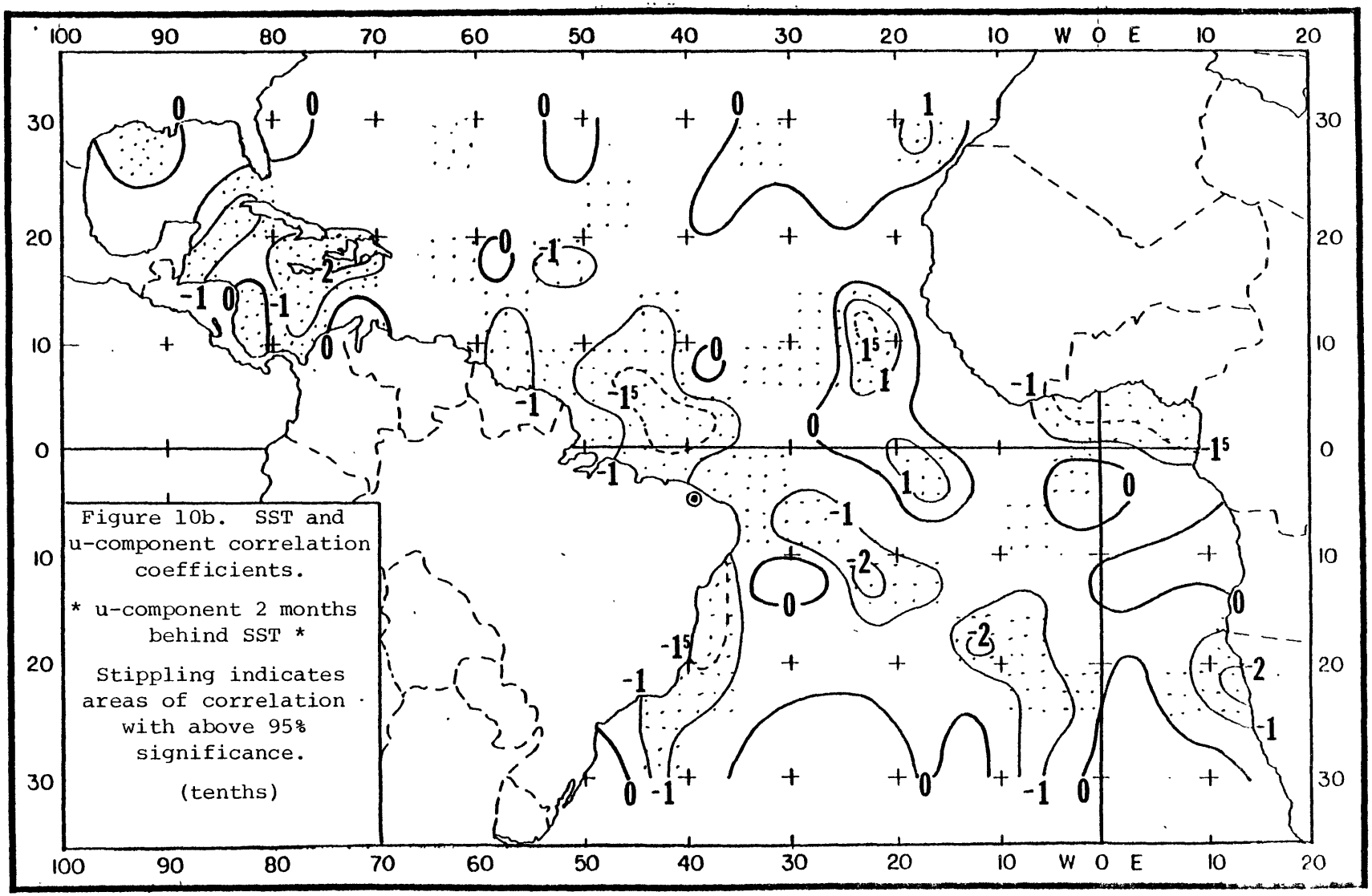
100 90 80 70 60 50 40 30 20 10 W 0 E 10 20
30
20
10
0
10
20
30
Figure 10b. SST and u-component correlation coefficients.
* u-component 2 months behind SST *
Stippling indicates areas of correlation with above 95% significance.
(tenths)

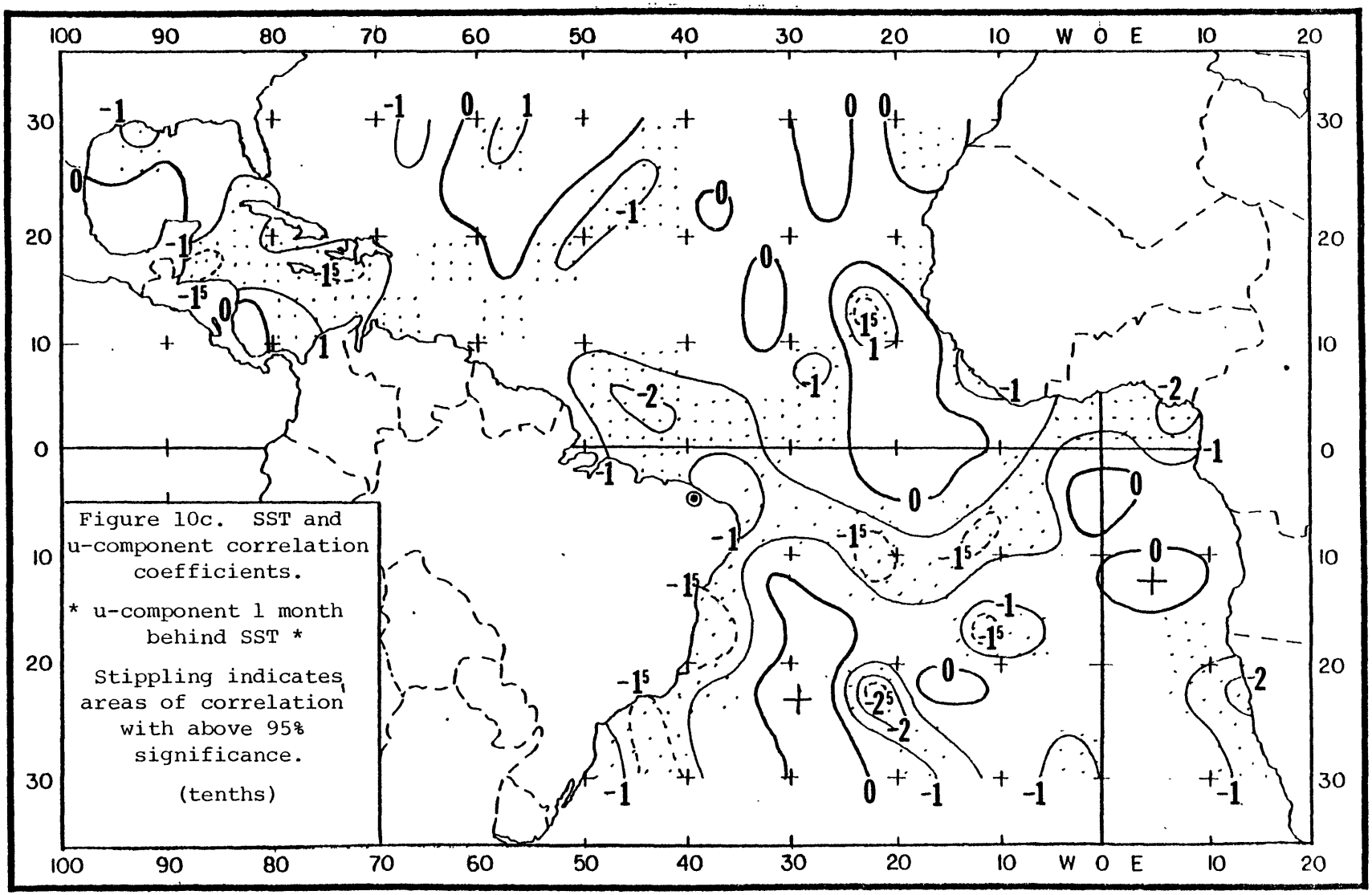
100 90 80 70 60 50 40 30 20 10 W 0 E 10 20
30 20 10 0 10 20 30
Figure 10c. SST and u-component correlation coefficients.
* u-component 1 month behind SST *
Stippling indicates areas of correlation with above 95% significance.
(tenths)

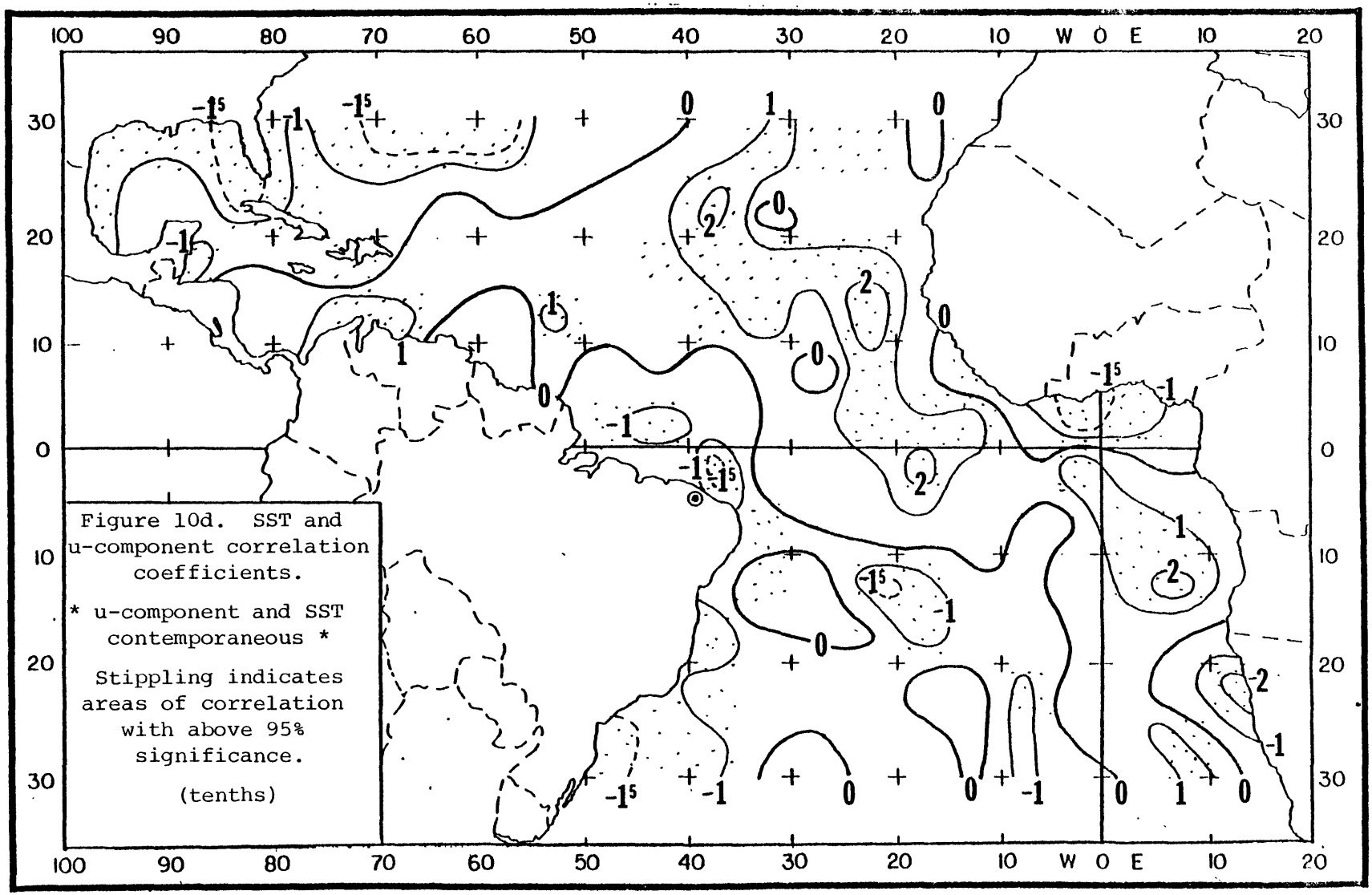
100 90 80 70 60 50 40 30 20 10 W 0 E 10 20
30
20
10
0
10
20
30
Figure 10d. SST and u-component correlation coefficients.
* u-component and SST contemporaneous *
Stippling indicates areas of correlation with above 95% significance.
(tenths)

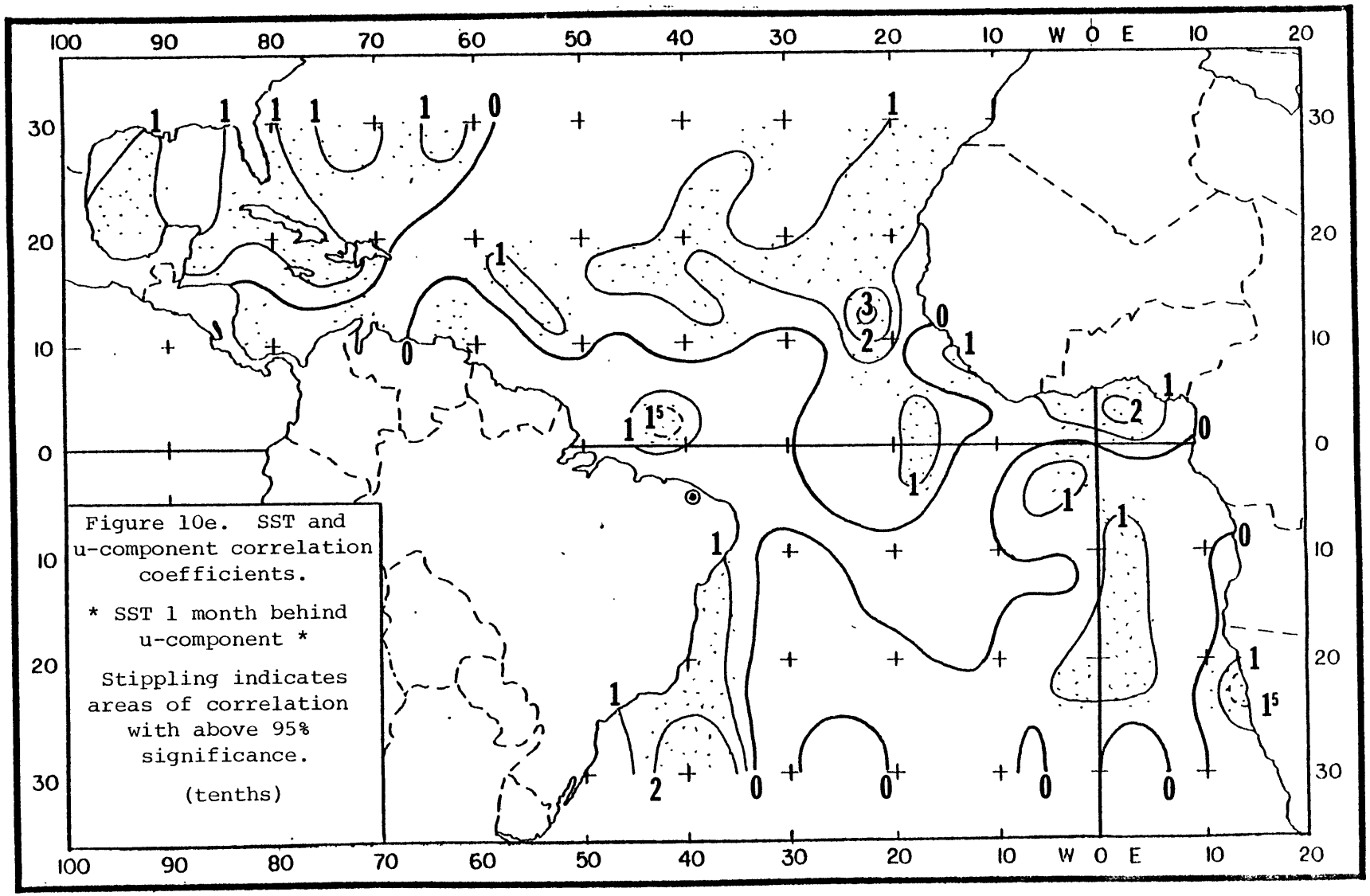
100 90 80 70 60 50 40 30 20 10 W 0 E 10 20
30
20
10
0
10
20
30
Figure 10e. SST and u-component correlation coefficients.
* SST 1 month behind u-component *
Stippling indicates areas of correlation with above 95% significance.
(tenths)

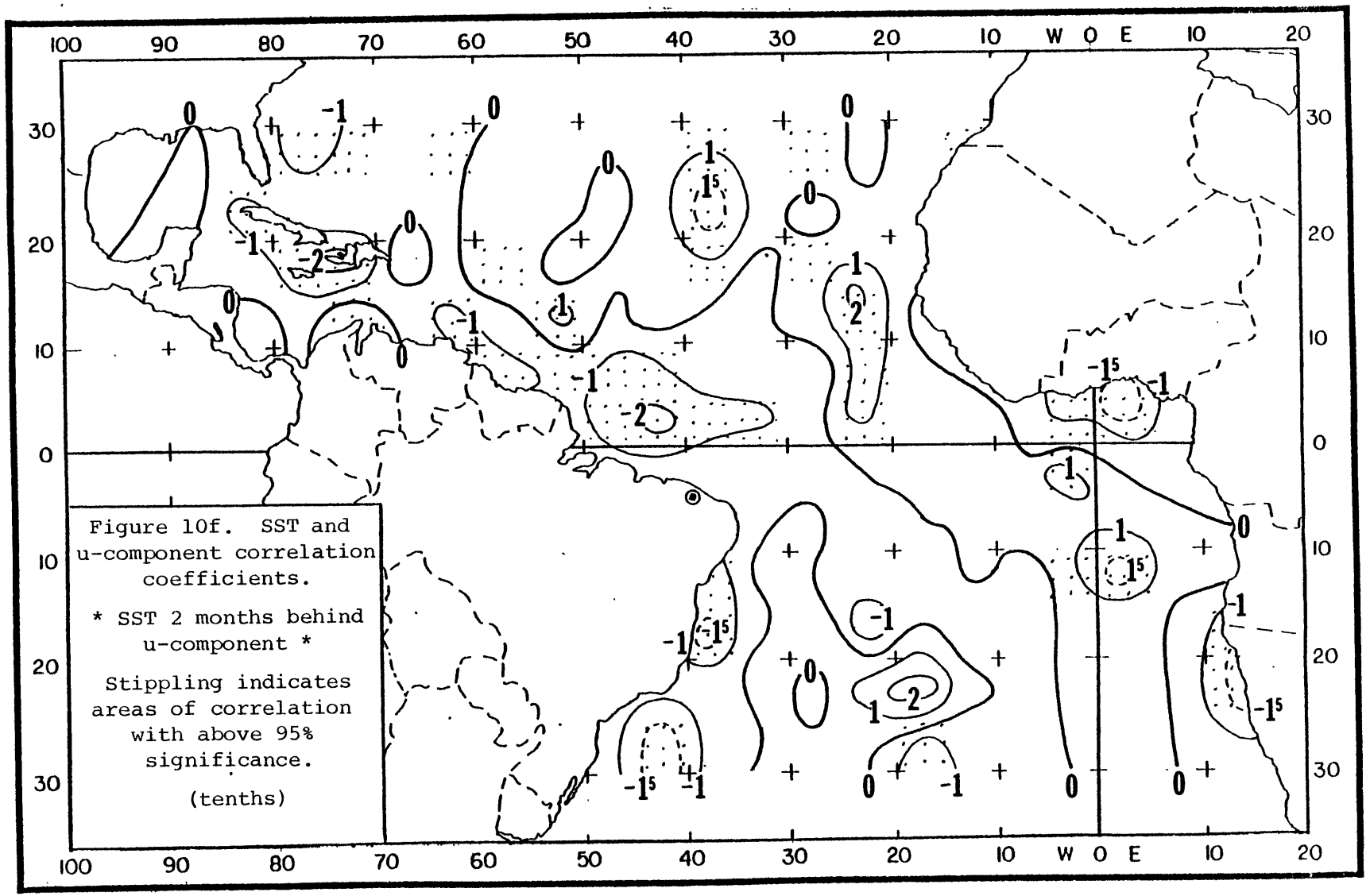
100 90 80 70 60 50 40 30 20 10 W 0 E 10 20
30
20
10
0
10
20
30
Figure 10f. SST and u-component correlation coefficients.
* SST 2 months behind u-component *
Stippling indicates areas of correlation with above 95% significance.
(tenths)

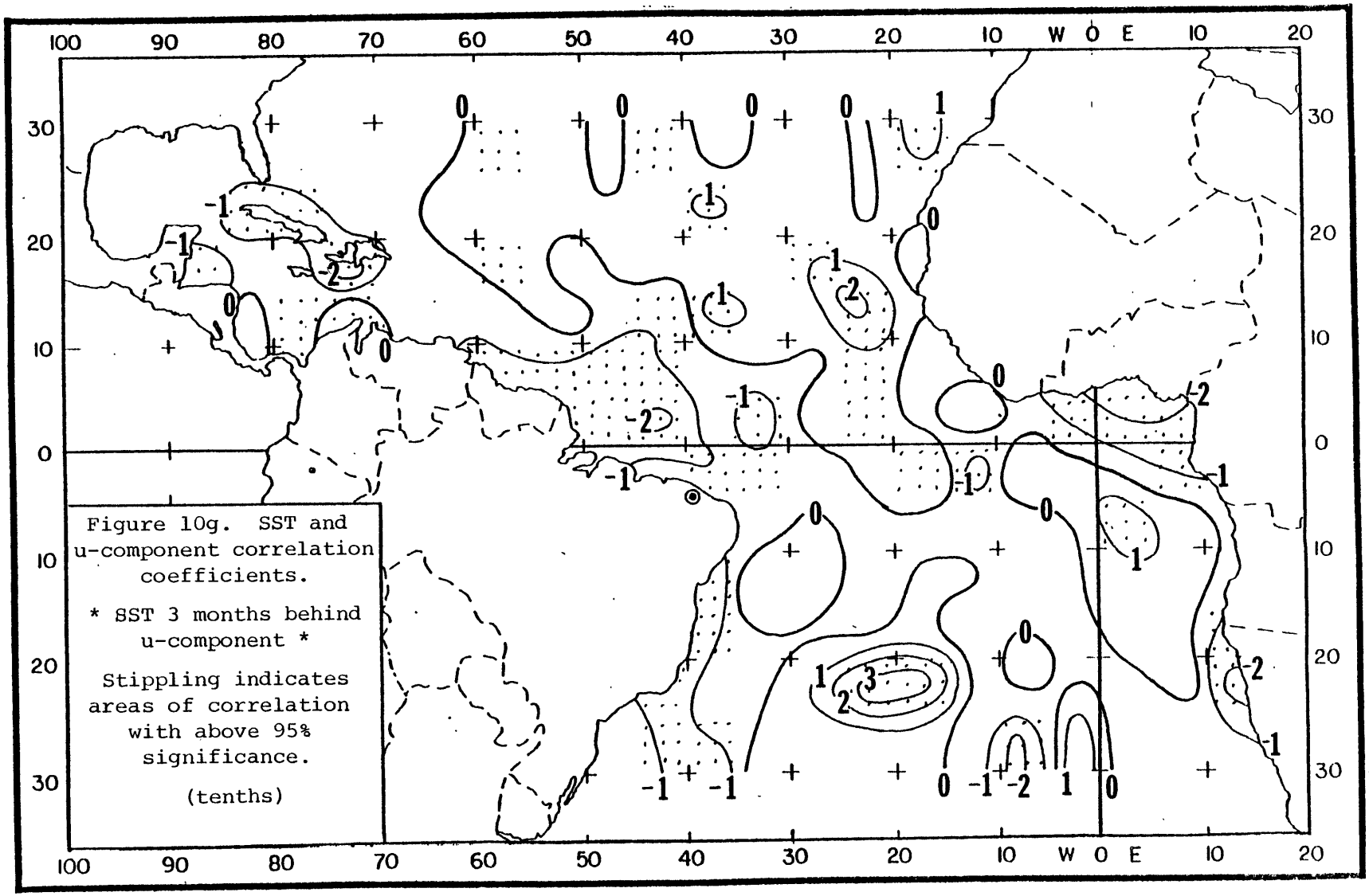
100 90 80 70 60 50 40 30 20 10 W 0 E 10 20
30 20 10 0 10 20 30
Figure 10g. SST and u-component correlation coefficients.
* SST 3 months behind u-component *
Stippling indicates areas of correlation with above 95% significance.
(tenths)

Figure 11.

Time series of Quixeramobim autumn precipitation, expressed as the monthly average for the three month season. (mm)

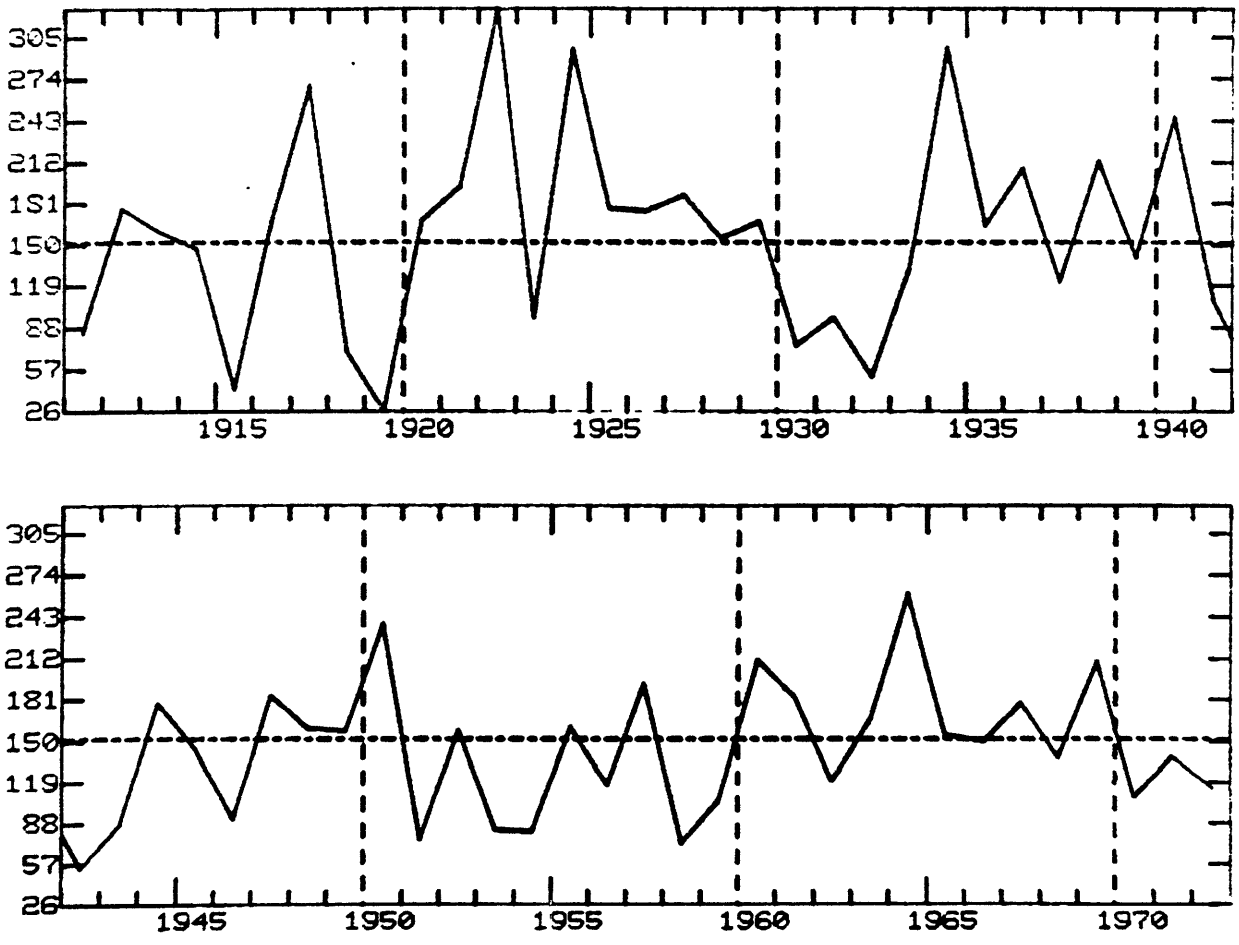

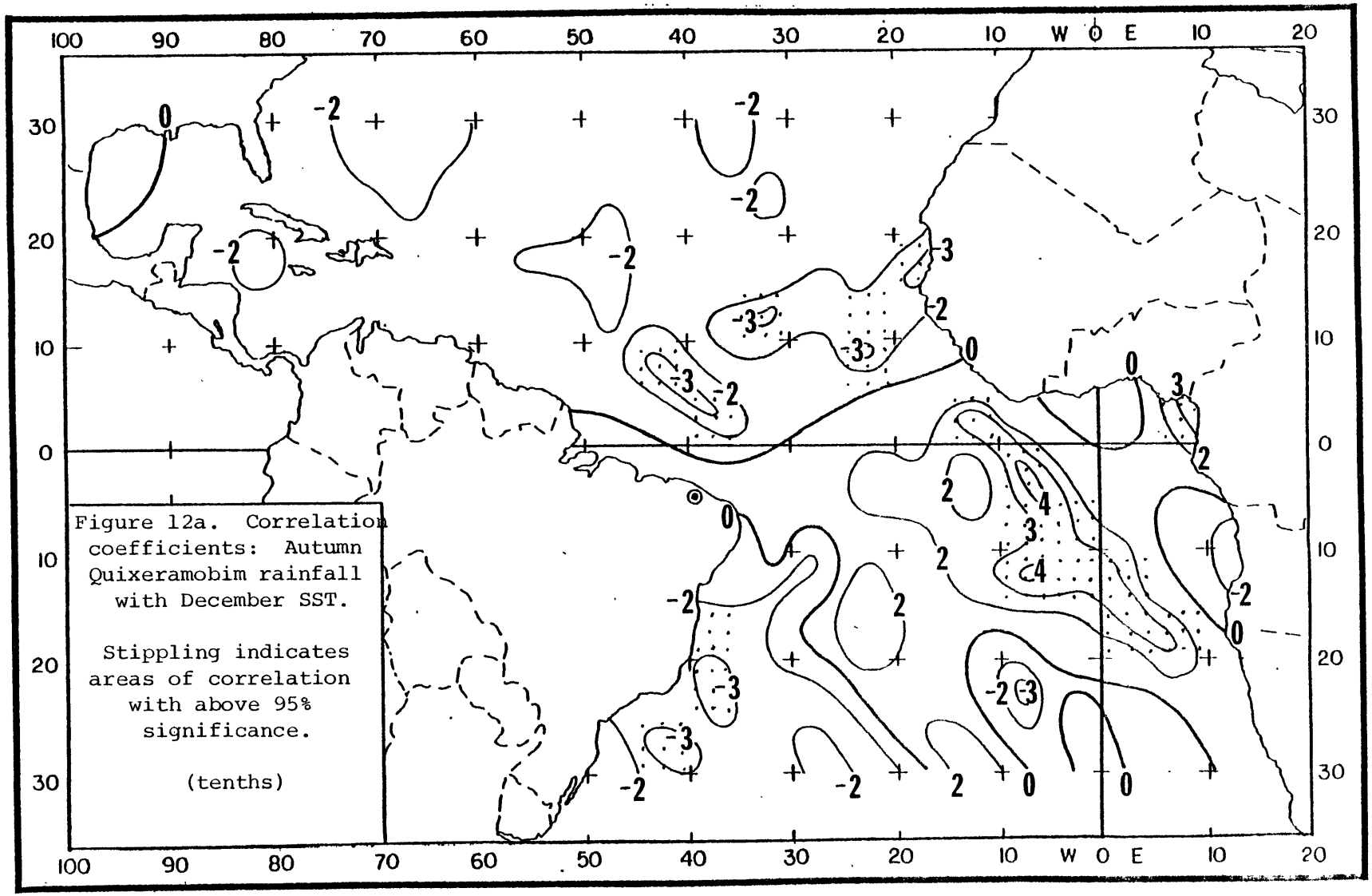
100 90 80 70 60 50 40 30 20 10 W 0 E 10 20
30 20 10 0 10 20 30
Figure 12a. Correlation coefficients: Autumn Quixeramobim rainfall with December SST.
Stippling indicates areas of correlation with above 95% significance.
(tenths)

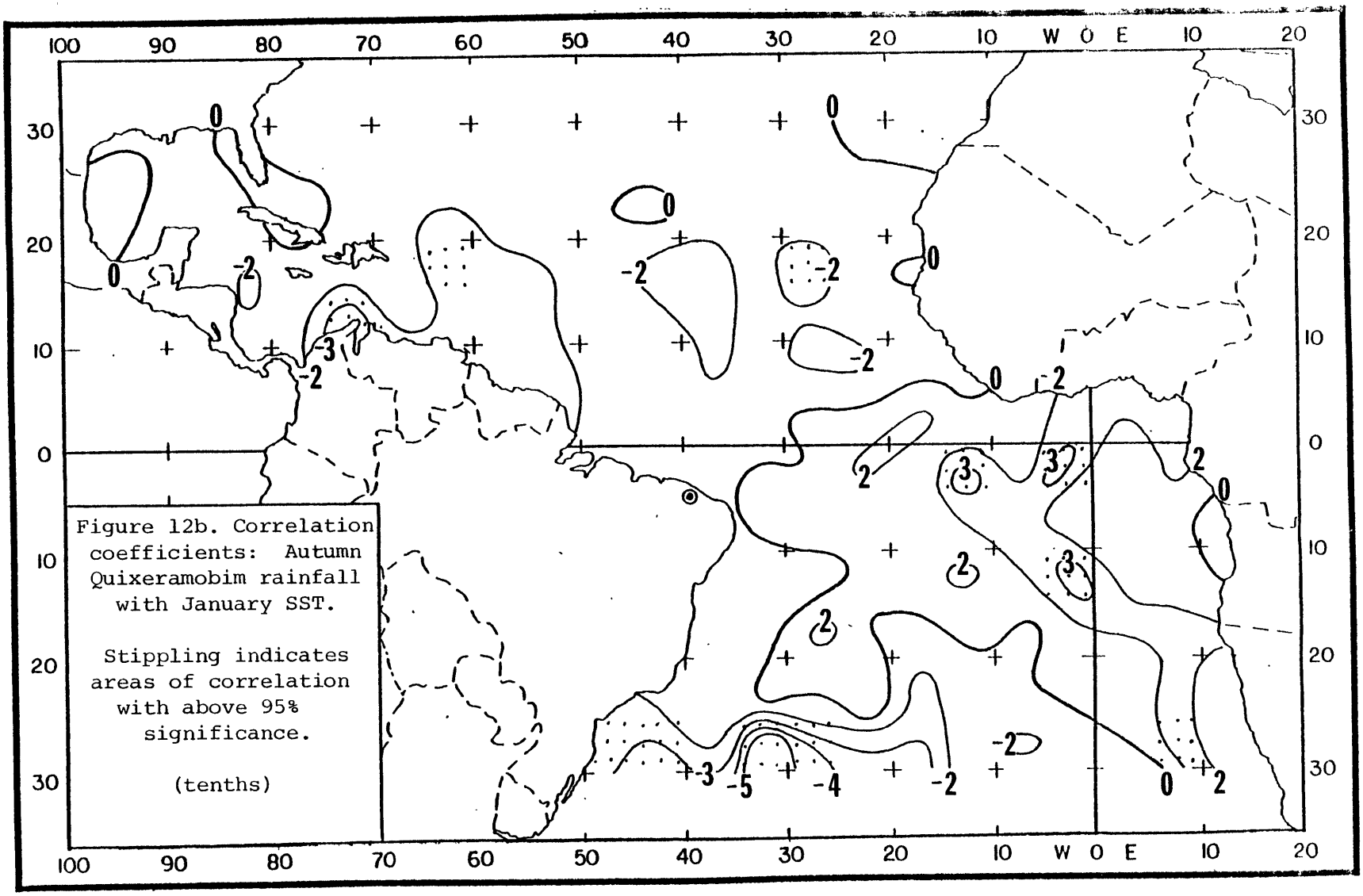
100 90 80 70 60 50 40 30 20 10 W 0 E 10 20
30 20 10 0 10 20 30
Figure 12b. Correlation coefficients: Autumn Quixeramobim rainfall with January SST.
Stippling indicates areas of correlation with above 95% significance.
(tenths)

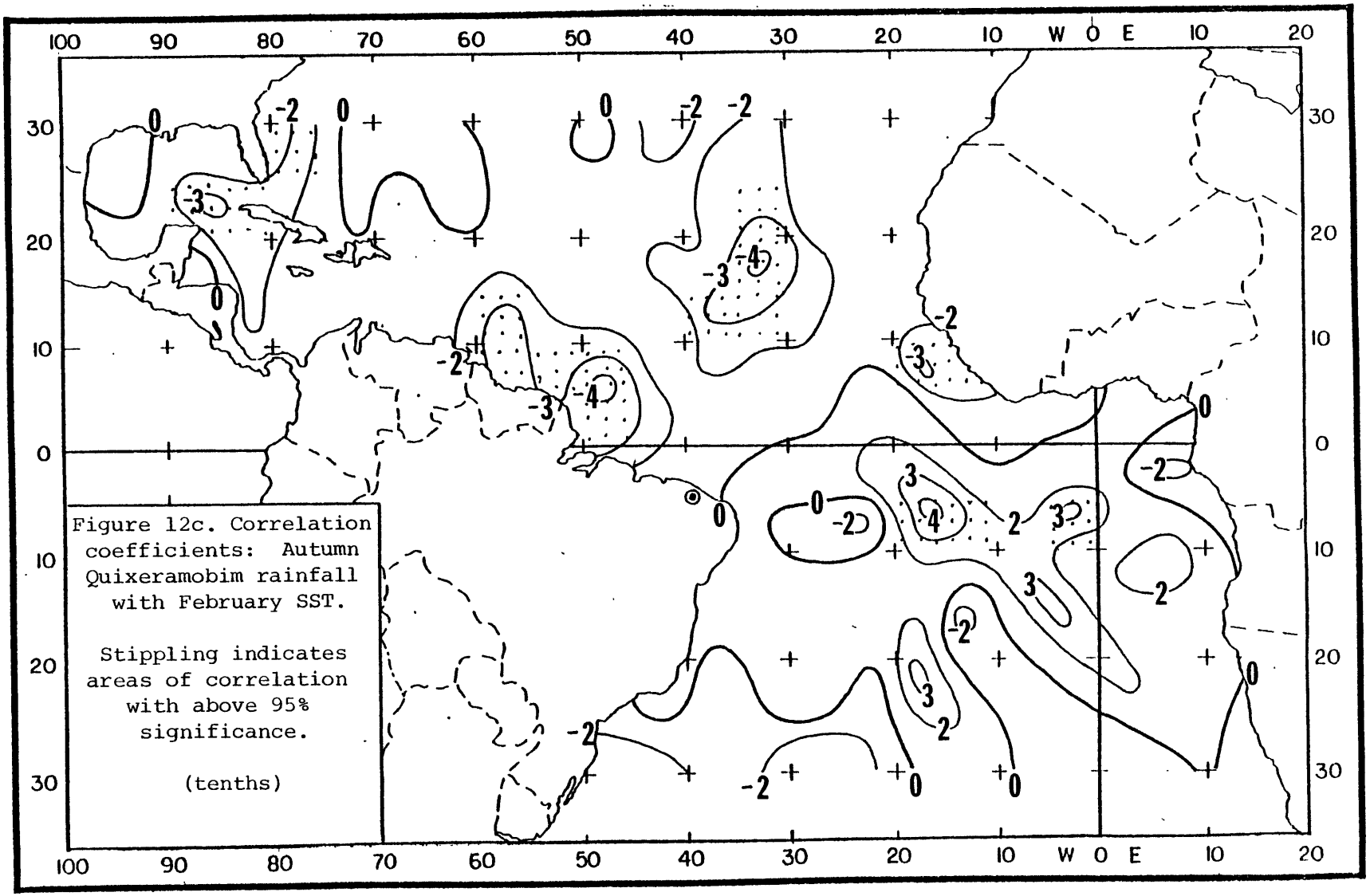
100 90 80 70 60 50 40 30 20 10 W 0 E 10 20
30 20 10 0 10 20 30
Figure 12c. Correlation coefficients: Autumn Quixeramobim rainfall with February SST.
Stippling indicates areas of correlation with above 95% significance.
(tenths)

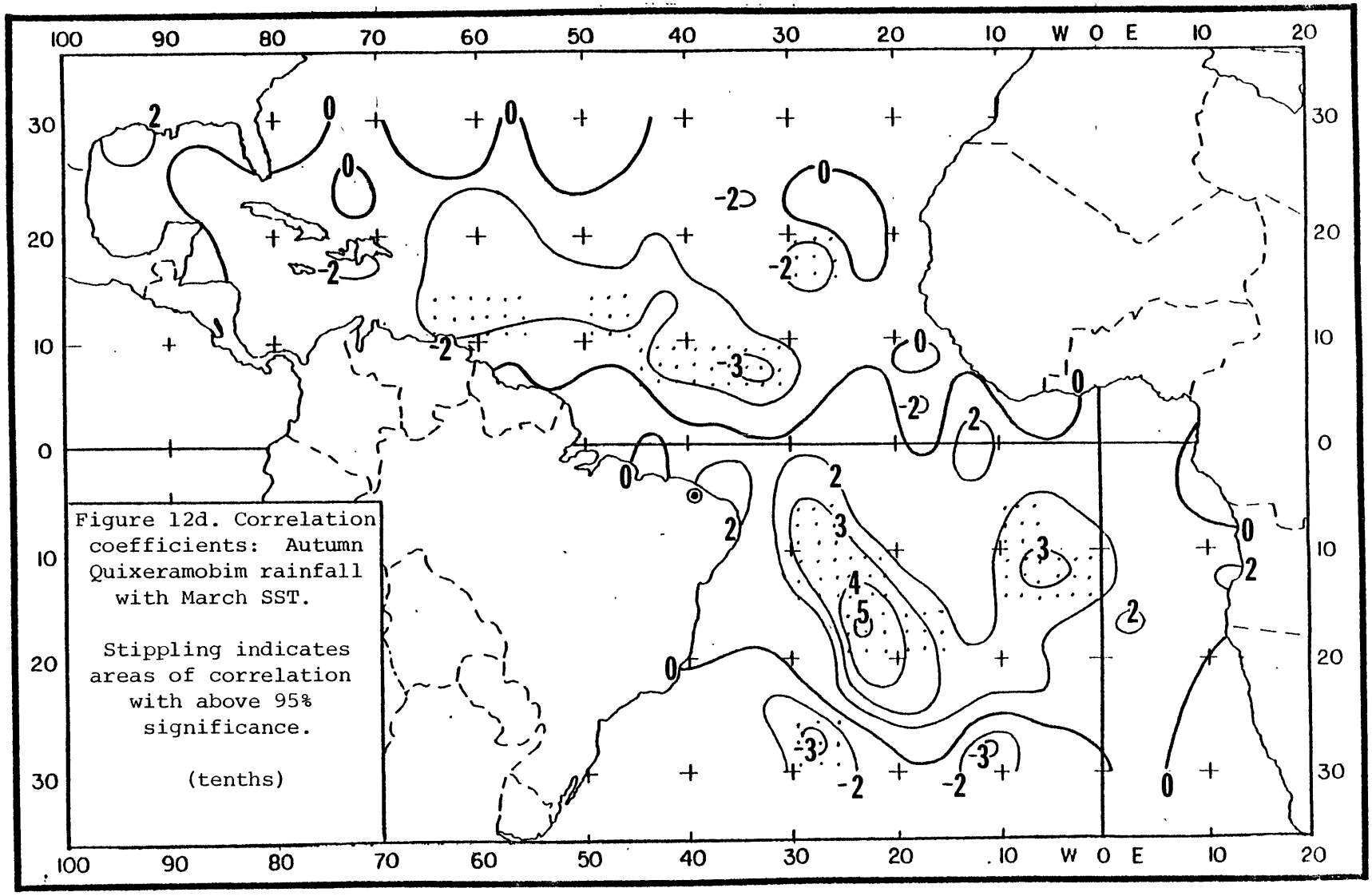
100 90 80 70 60 50 40 30 20 10 W 0 E 10 20
30 20 10 0 10 20 30
Figure 12d. Correlation coefficients: Autumn Quixeramobim rainfall with March SST.
Stippling indicates areas of correlation with above 95% significance.
(tenths)

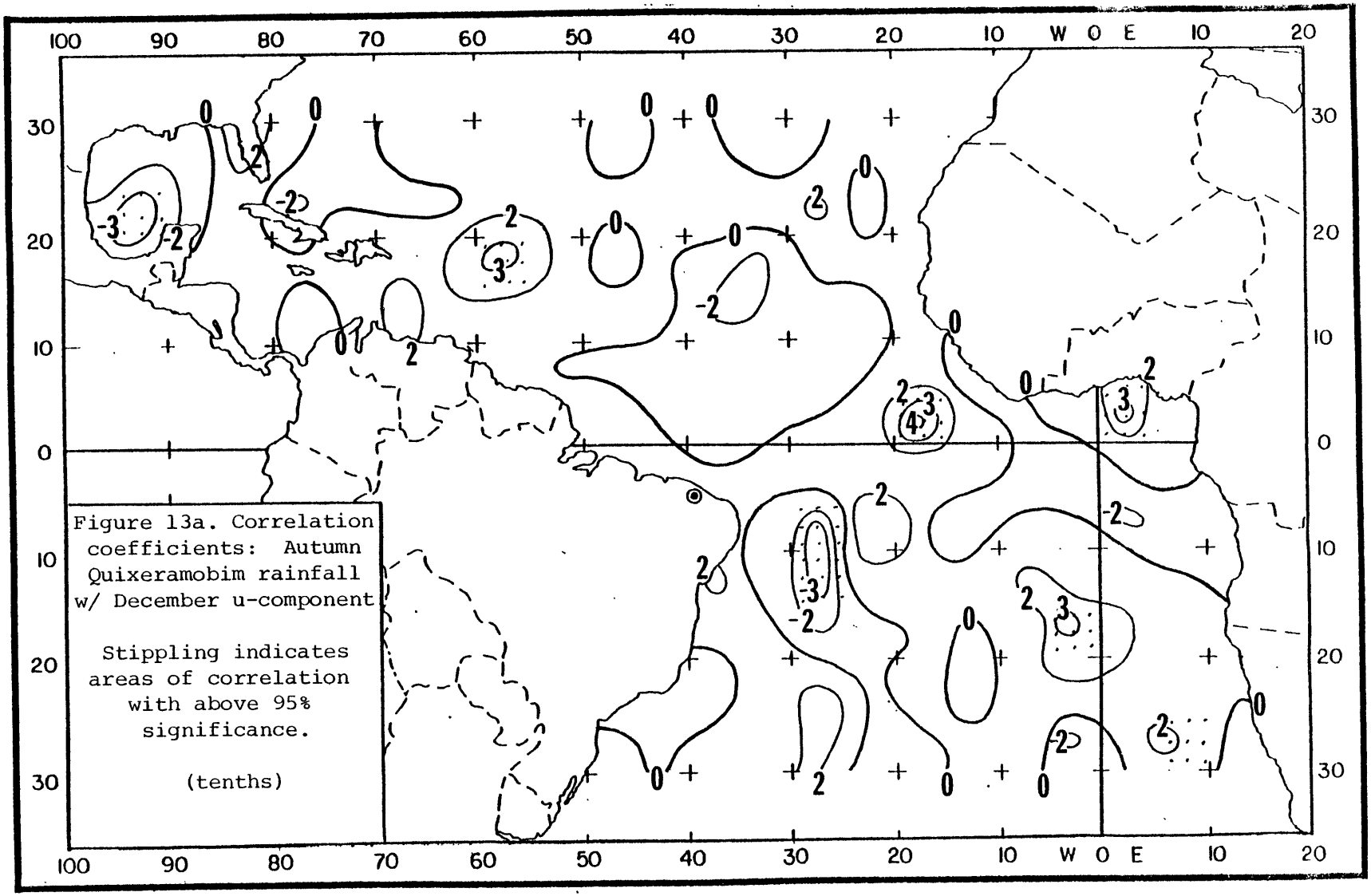
100 90 80 70 60 50 40 30 20 10 W 0 E 10 20
30 20 10 0 10 20 30
Figure 13a. Correlation coefficients: Autumn Quixeramobim rainfall w/ December u-component
Stippling indicates areas of correlation with above 95% significance.
(tenths)

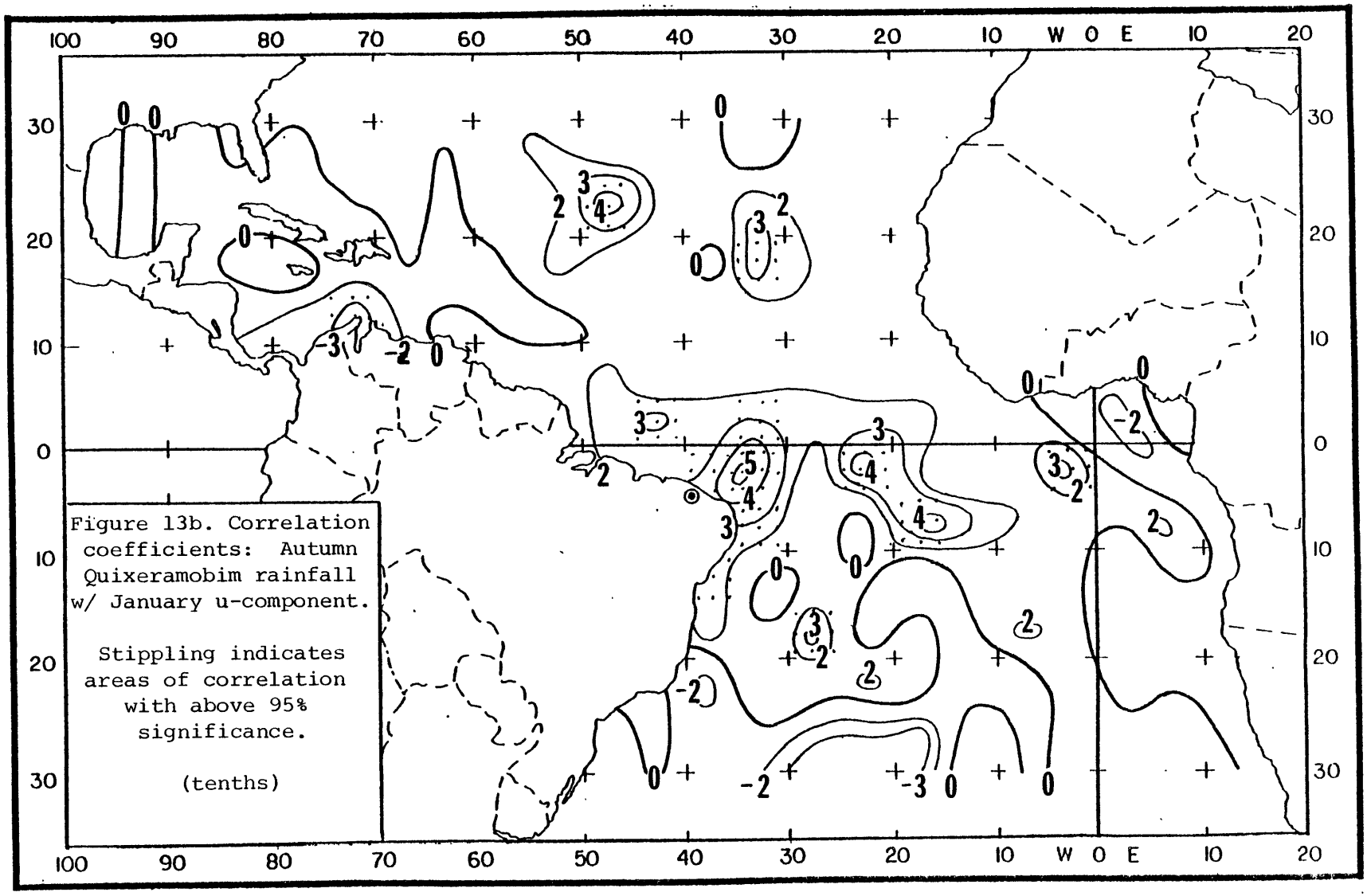
100 90 80 70 60 50 40 30 20 10 W 0 E 10 20
30 20 10 0 10 20 30
Figure 13b. Correlation coefficients: Autumn Quixeramobim rainfall w/ January u-component.
Stippling indicates areas of correlation with above 95% significance.
(tenths)

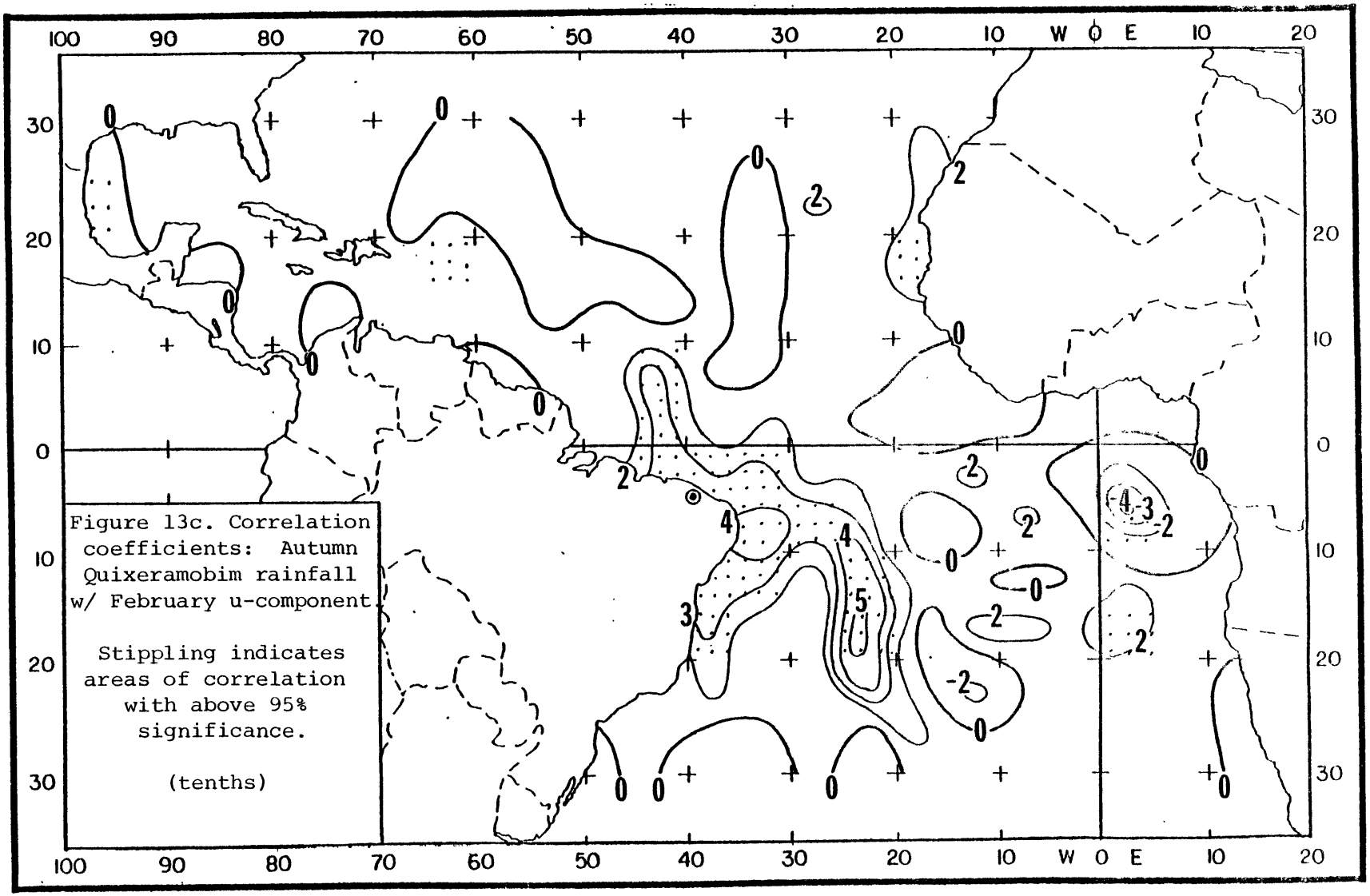
100 90 80 70 60 50 40 30 20 10 W 0 E 10 20
30 20 10 0 10 20 30
Figure 13c. Correlation coefficients: Autumn Quixeramobim rainfall w/ February u-component.
Stippling indicates areas of correlation with above 95% significance.
(tenths)

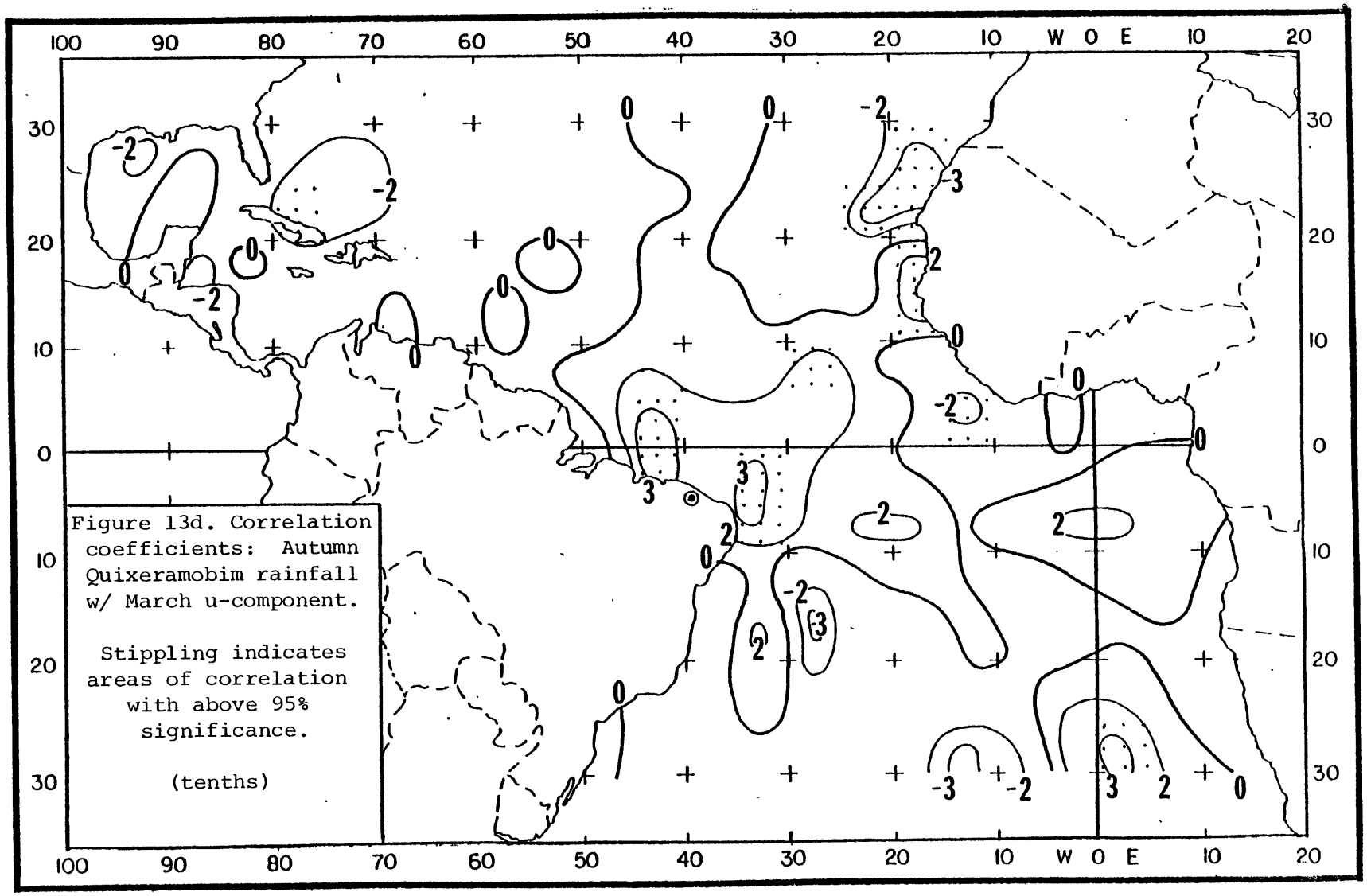
100 90 80 70 60 50 40 30 20 10 W 0 E 10 20
30
20
10
0
10
20
30
Figure 13d. Correlation coefficients: Autumn Quixeramobim rainfall w/ March u-component.
Stippling indicates areas of correlation with above 95% significance.
(tenths)

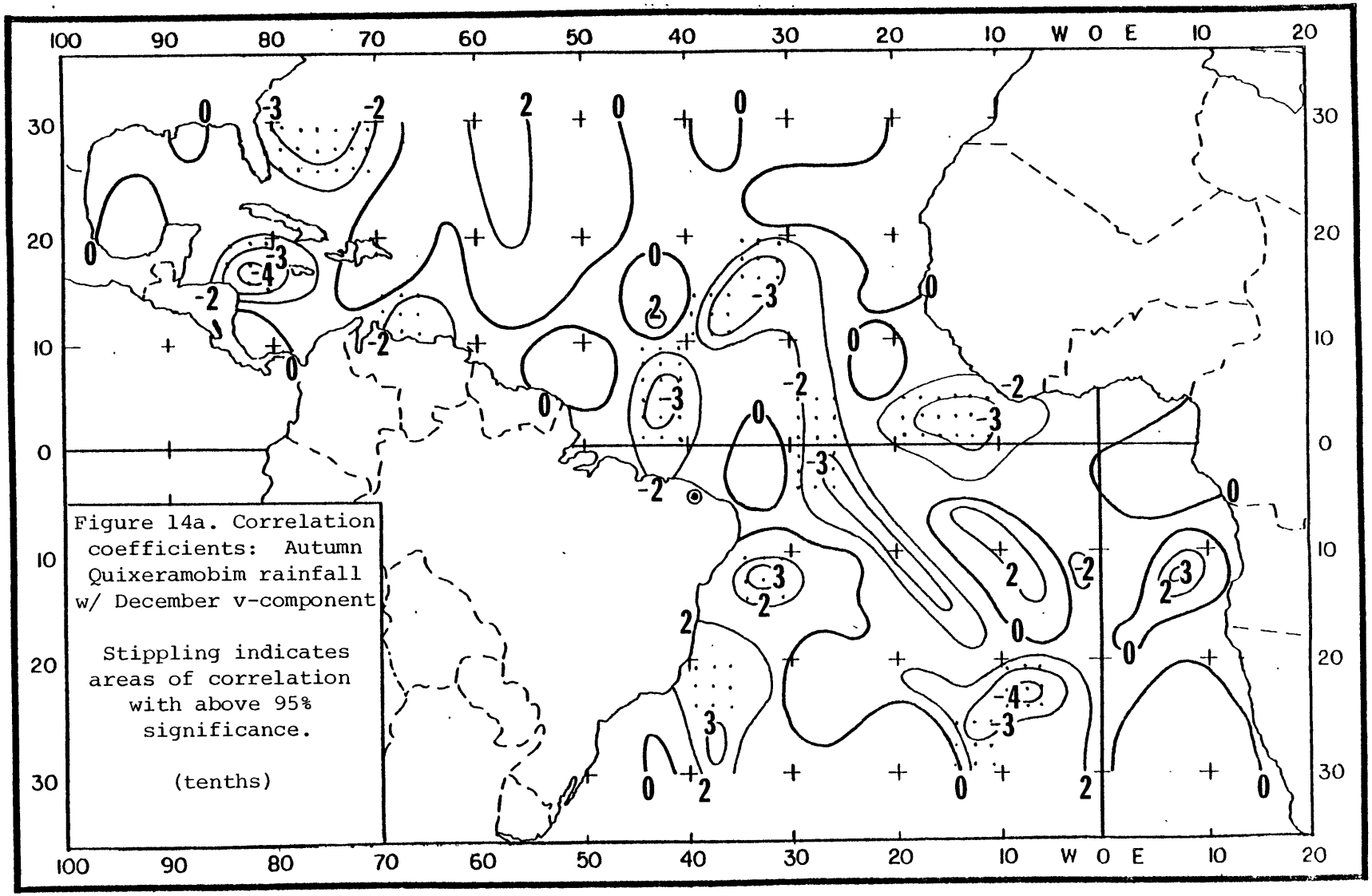
100 90 80 70 60 50 40 30 20 10 W 0 E 10 20
30
20
10
0
10
20
30
Figure 14a. Correlation coefficients: Autumn Quixeramobim rainfall w/ December v-component
Stippling indicates areas of correlation with above 95% significance.
(tenths)

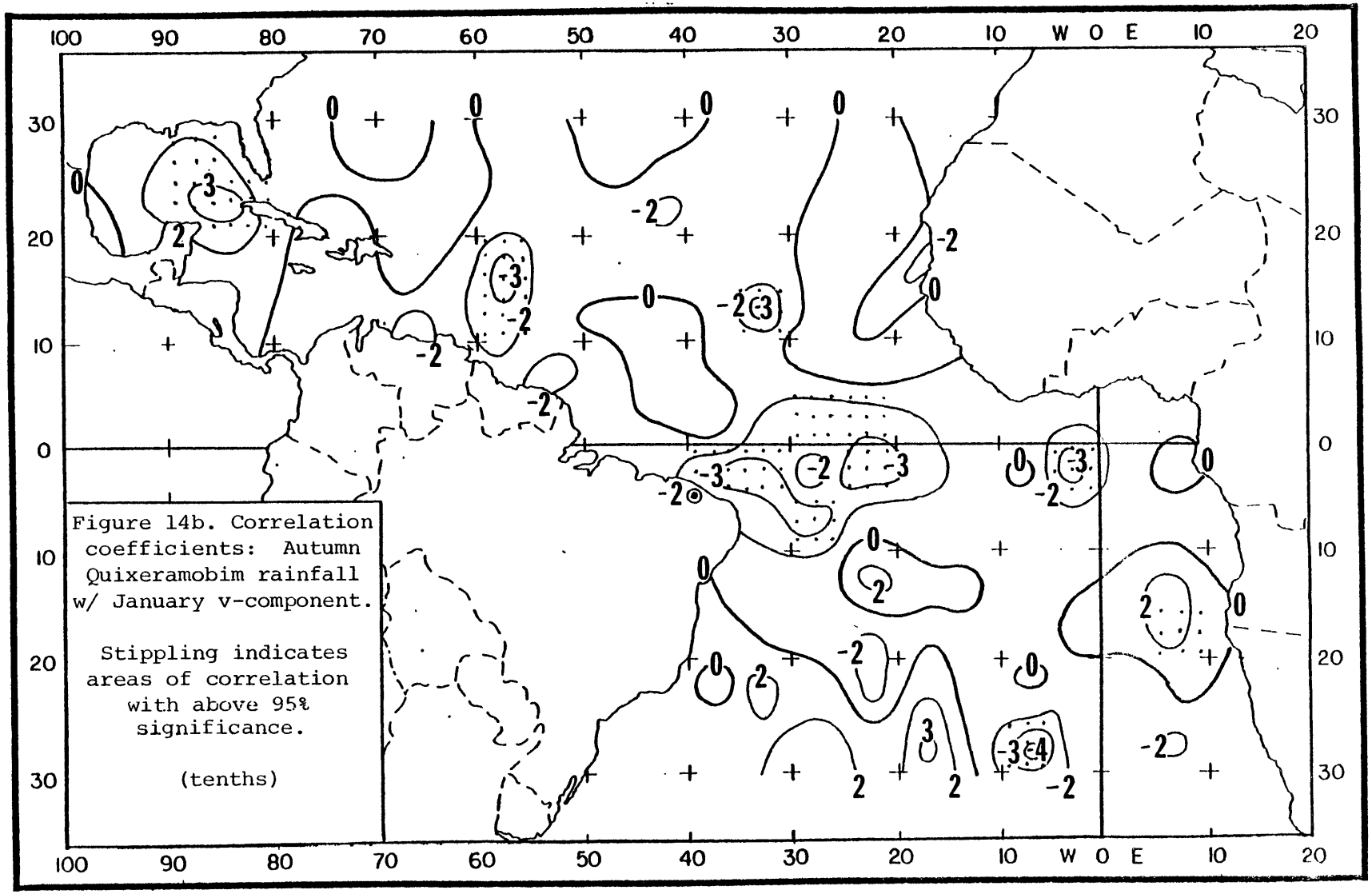
100 90 80 70 60 50 40 30 20 10 W 0 E 10 20
30 20 10 0 10 20 30
Figure 14b. Correlation coefficients: Autumn Quixeramobim rainfall w/ January v-component.
Stippling indicates areas of correlation with above 95% significance.
(tenths)

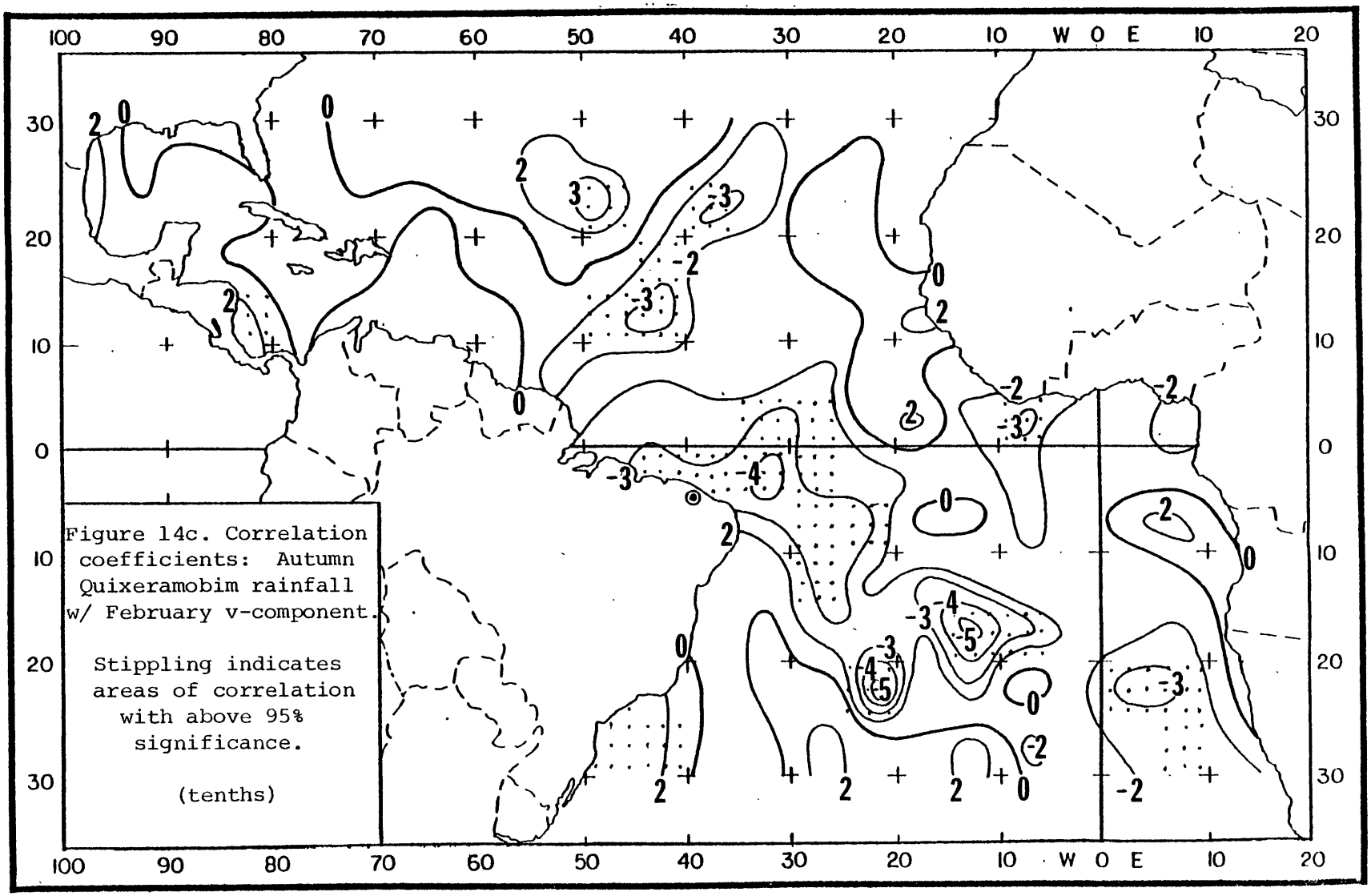
100 90 80 70 60 50 40 30 20 10 W 0 E 10 20
30
20
10
0
10
20
30
Figure 14c. Correlation coefficients: Autumn Quixeramobim rainfall w/ February v-component.
Stippling indicates areas of correlation with above 95% significance.
(tenths)

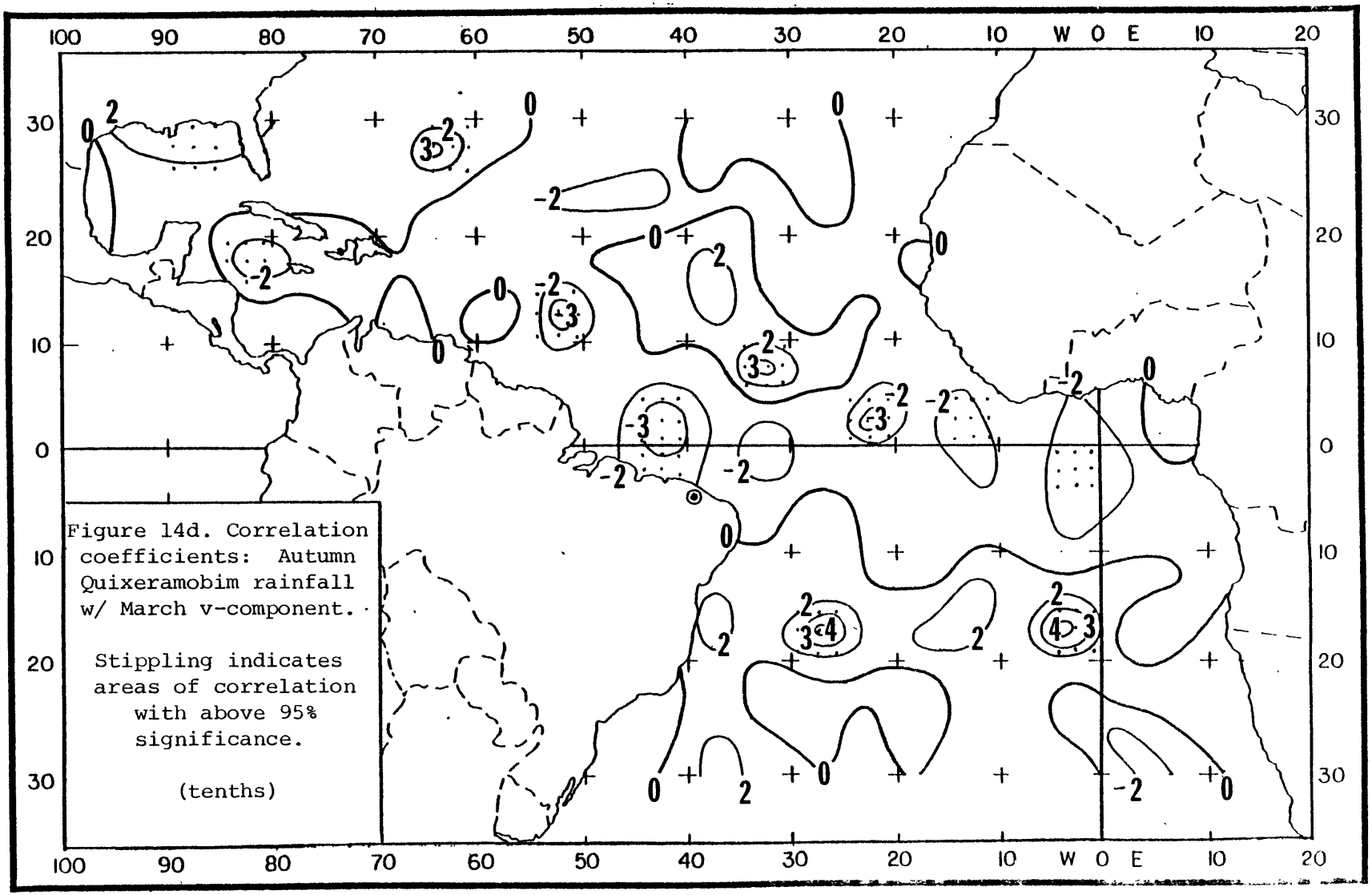
100 90 80 70 60 50 40 30 20 10 W 0 E 10 20
30
20
10
0
10
20
30
Figure 14d. Correlation coefficients: Autumn Quixeramobim rainfall w/ March v-component.
Stippling indicates areas of correlation with above 95% significance.
(tenths)

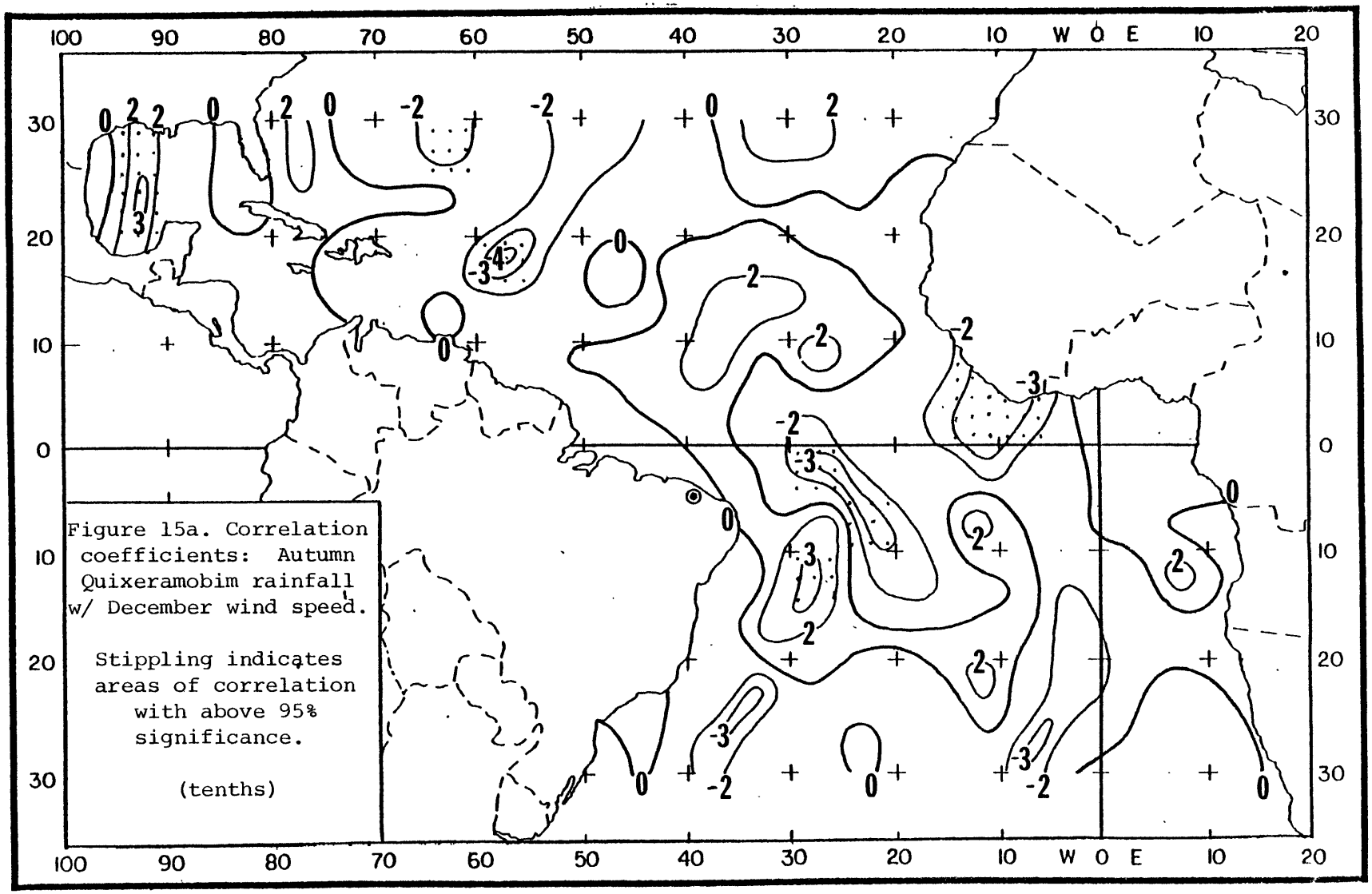
100 90 80 70 60 50 40 30 20 10 W 0 E 10 20
30
20
10
0
10
20
30
Figure 15a. Correlation coefficients: Autumn Quixeramobim rainfall w/ December wind speed.
Stippling indicates areas of correlation with above 95% significance.
(tenths)

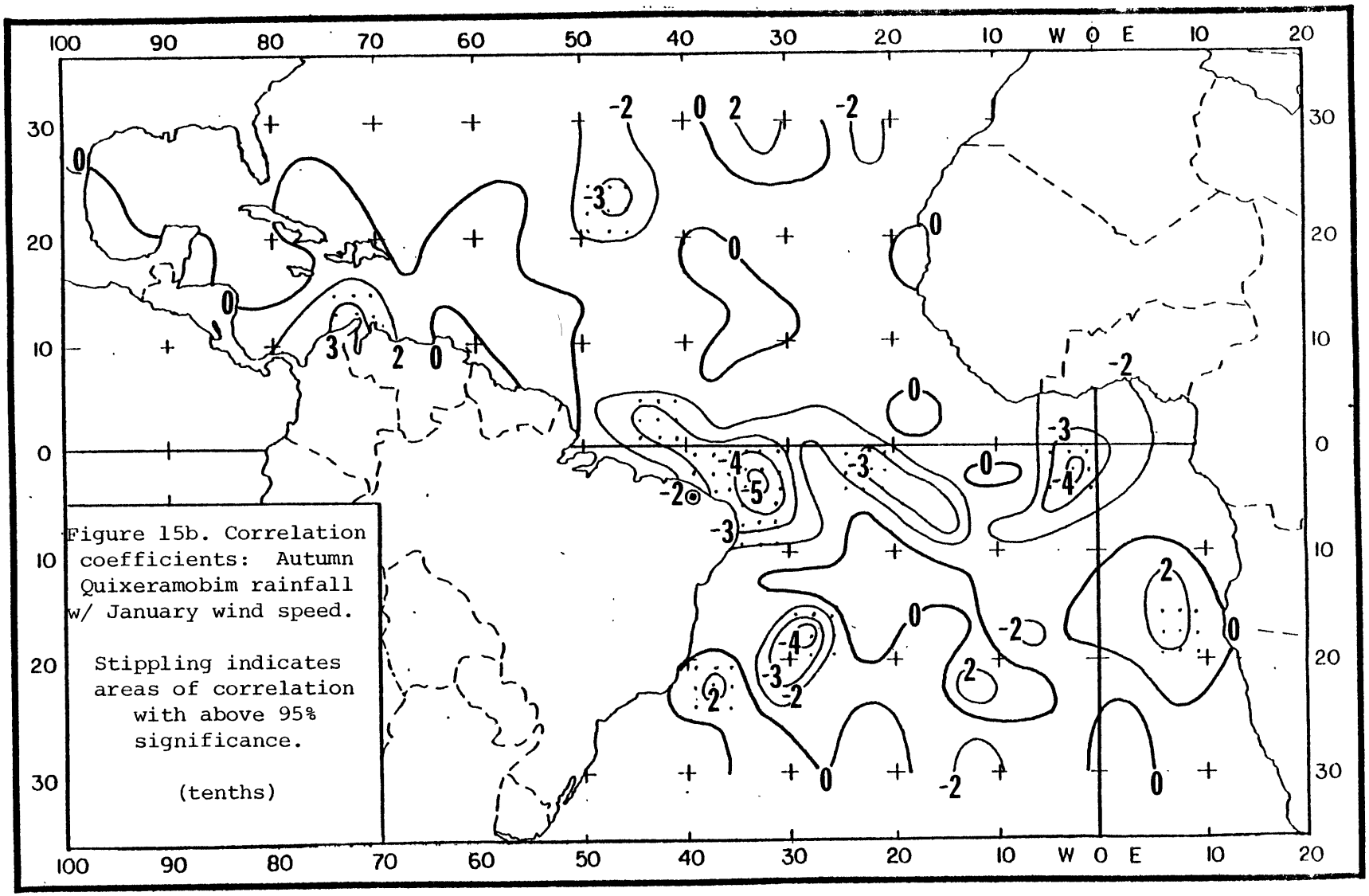
100 90 80 70 60 50 40 30 20 10 W 0 E 10 20
30 20 10 0 10 20 30
Figure 15b. Correlation coefficients: Autumn Quixeramobim rainfall w/ January wind speed.
Stippling indicates areas of correlation with above 95% significance.
(tenths)

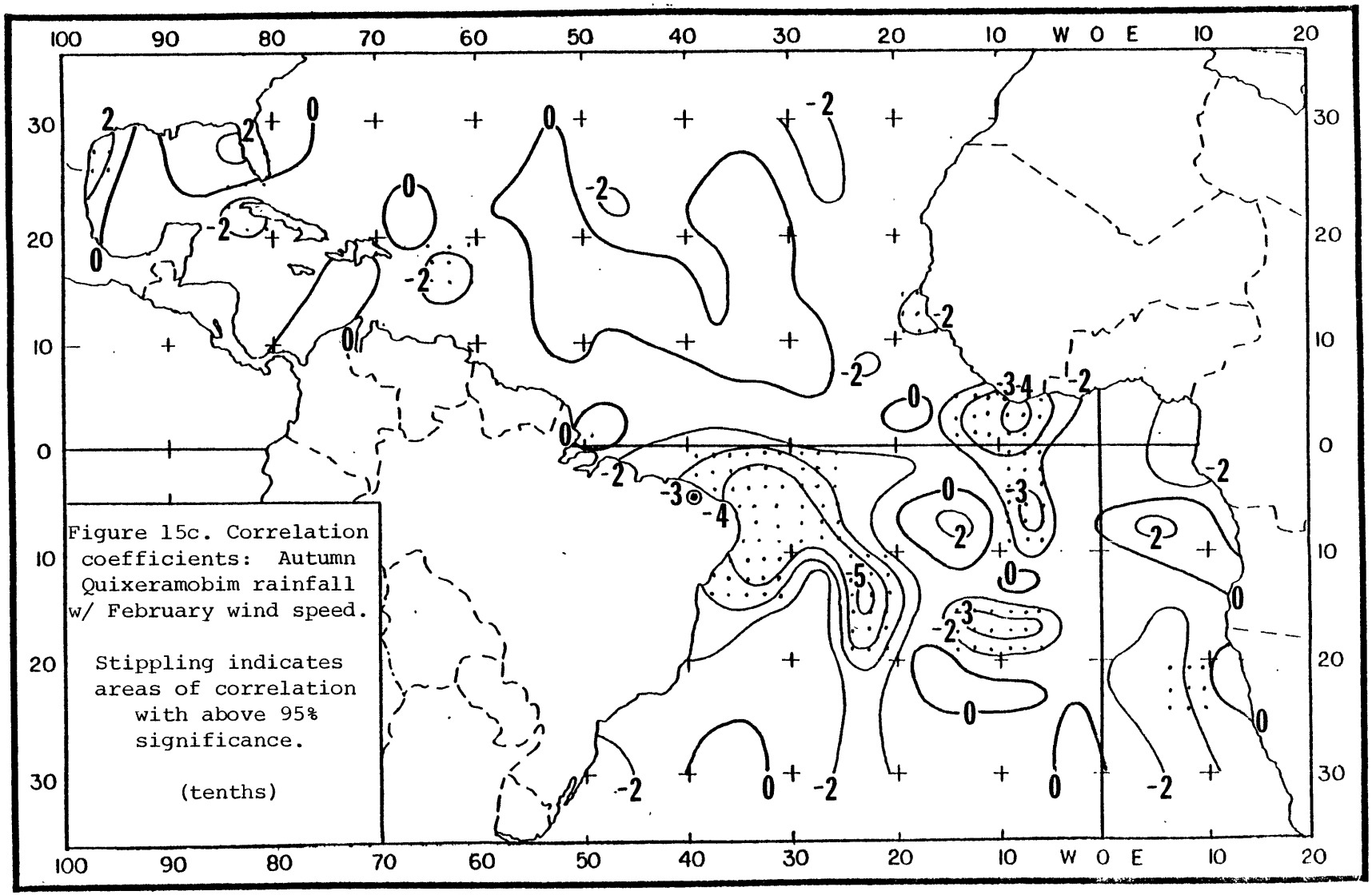
100 90 80 70 60 50 40 30 20 10 W 0 E 10 20
30
20
10
0
10
20
30
Figure 15c. Correlation coefficients: Autumn Quixeramobim rainfall w/ February wind speed.
Stippling indicates areas of correlation with above 95% significance.
(tenths)

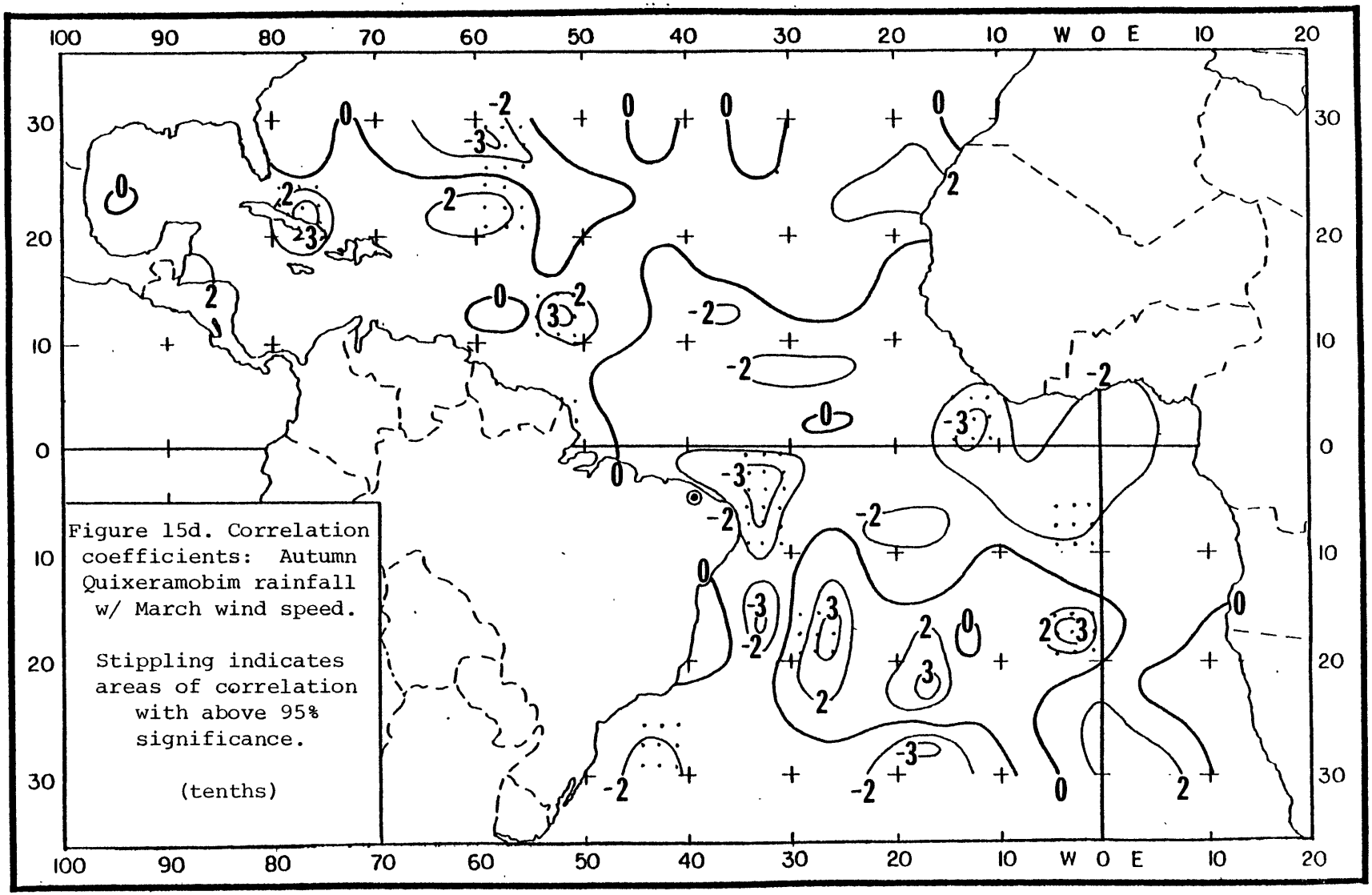
100 90 80 70 60 50 40 30 20 10 W 0 E 10 20
30
20
10
0
10
20
30
Figure 15d. Correlation coefficients: Autumn Quixeramobim rainfall w/ March wind speed.
Stippling indicates areas of correlation with above 95% significance.
(tenths)

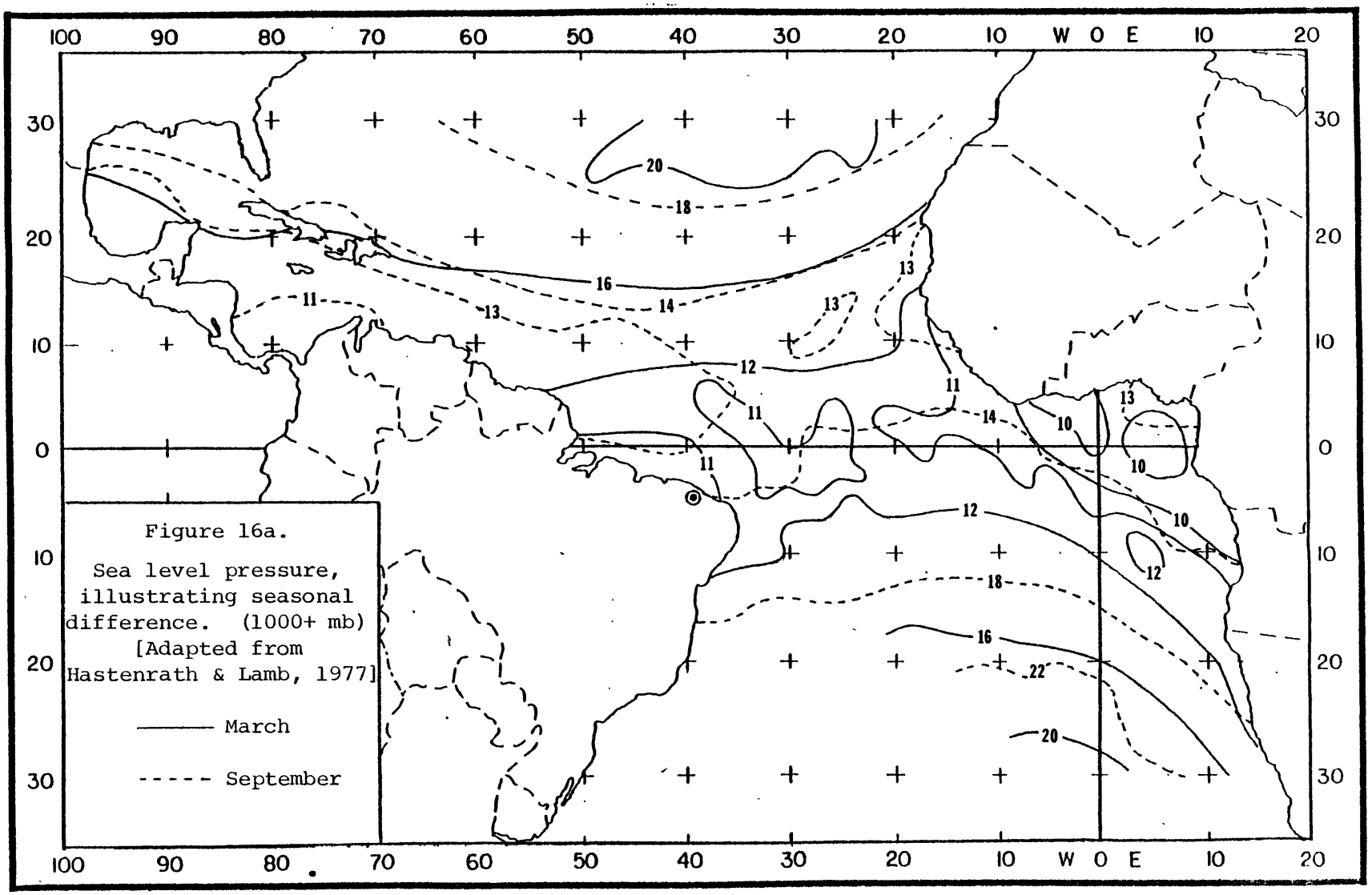
100 90 80 70 60 50 40 30 20 10 W 0 E 10 20
30
20
10
0
10
20
30
20
18
16
14
13
12
11
10
22
Figure 16a.
Sea level pressure, illustrating seasonal difference. (1000+ mb) [Adapted from Hastenrath & Lamb, 1977]
March
September

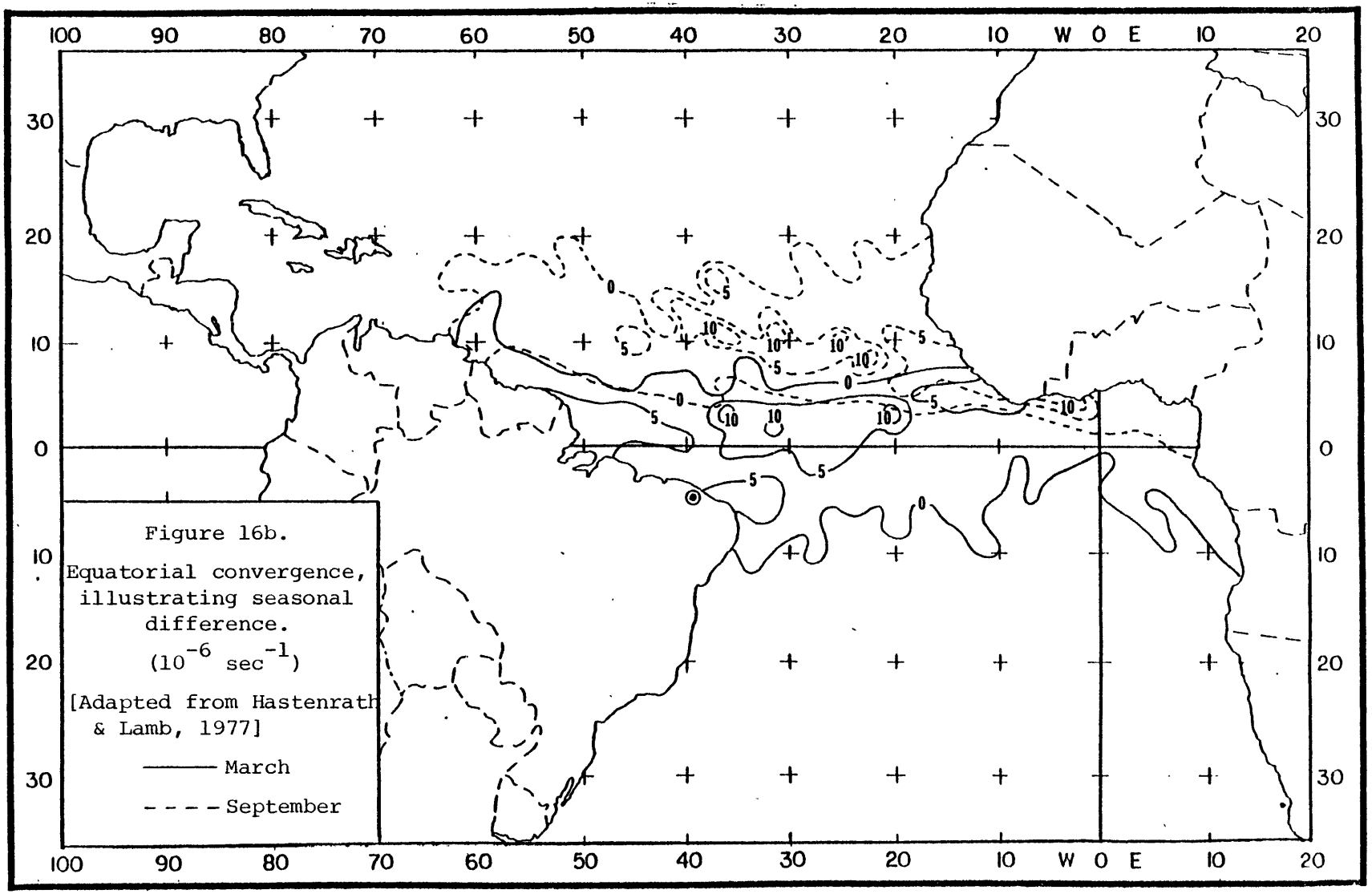
100 90 80 70 60 50 40 30 20 10 W 0 E 10 20
30
20
10
0
10
20
30
0
5
10
-5
Figure 16b.
Equatorial convergence, illustrating seasonal difference.
(10^{-6} sec^{-1})
[Adapted from Hastenrath & Lamb, 1977]
——— March
- - - - September

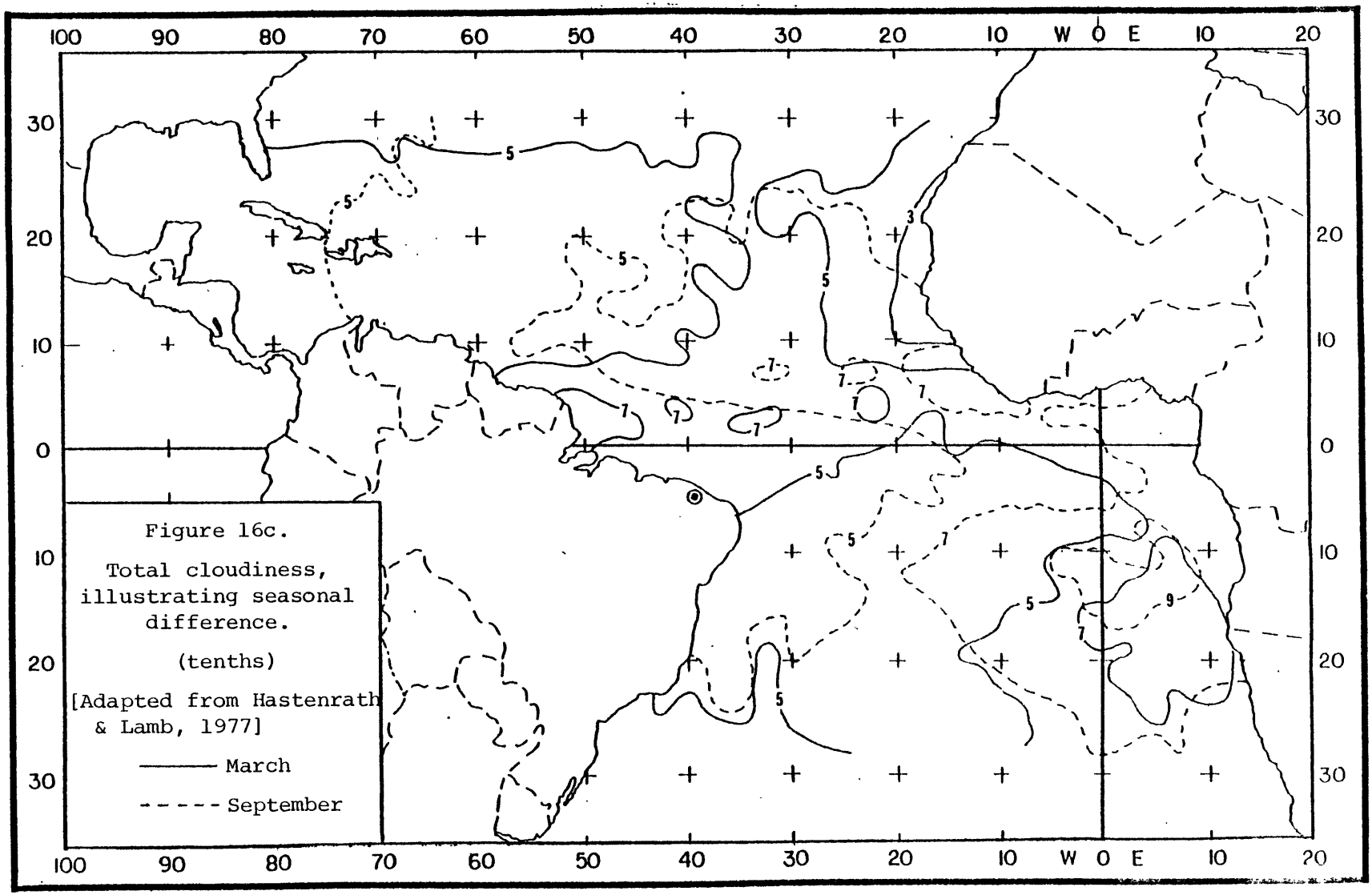
100 90 80 70 60 50 40 30 20 10 W 0 E 10 20
30
20
10
0
10
20
30
Figure 16c.
Total cloudiness, illustrating seasonal difference.
(tenths)
[Adapted from Hastenrath & Lamb, 1977]
March
September

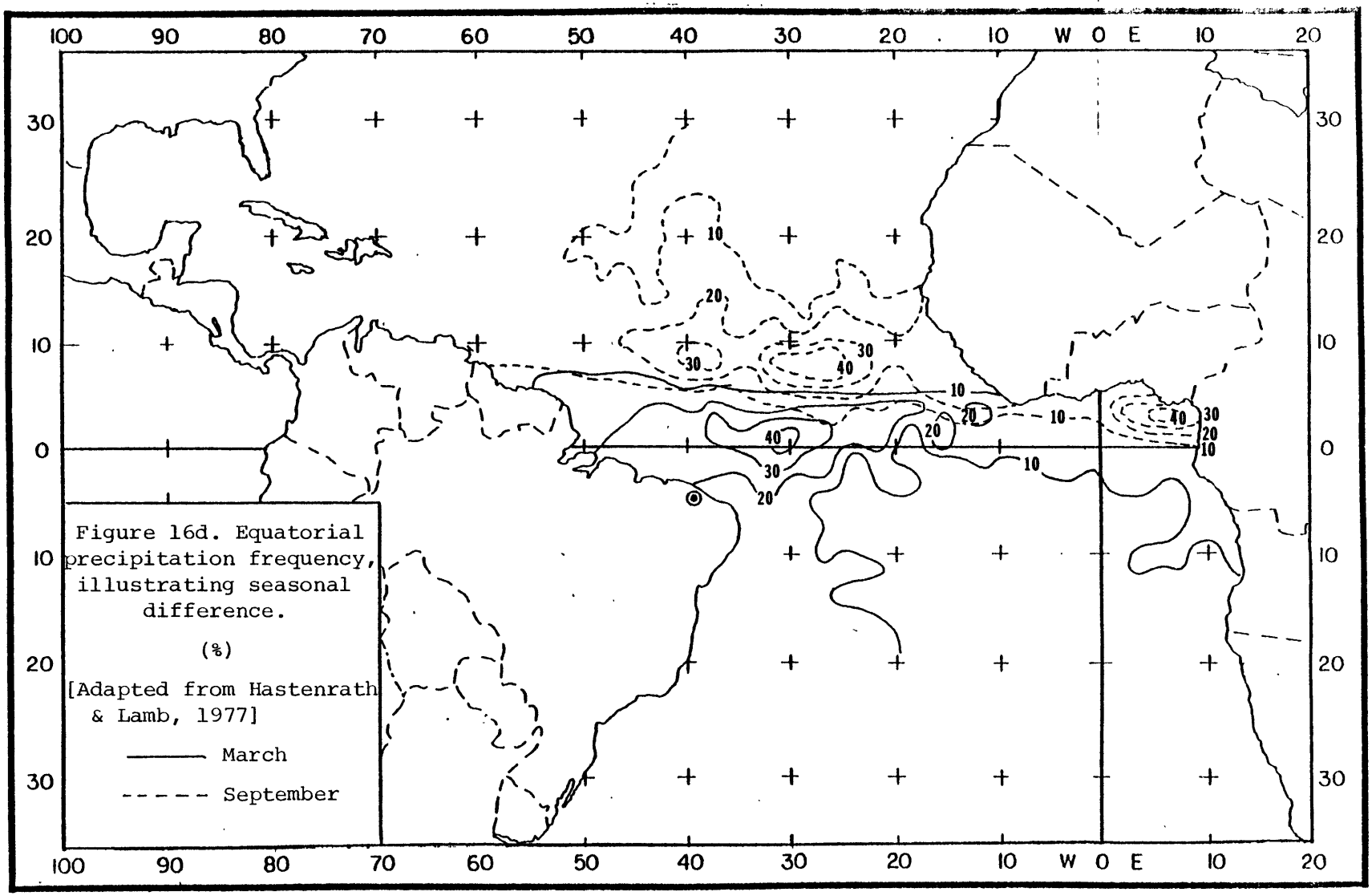

Figure 16d. Equatorial precipitation frequency, illustrating seasonal difference.

(%)

[Adapted from Hastenrath & Lamb, 1977]

Figure 17.

Longitudinal cross sections of simple convergence index using only v-components of wind. (knots)

———— Mean of 15 dry years.

— — — — Mean of 11 wet years.

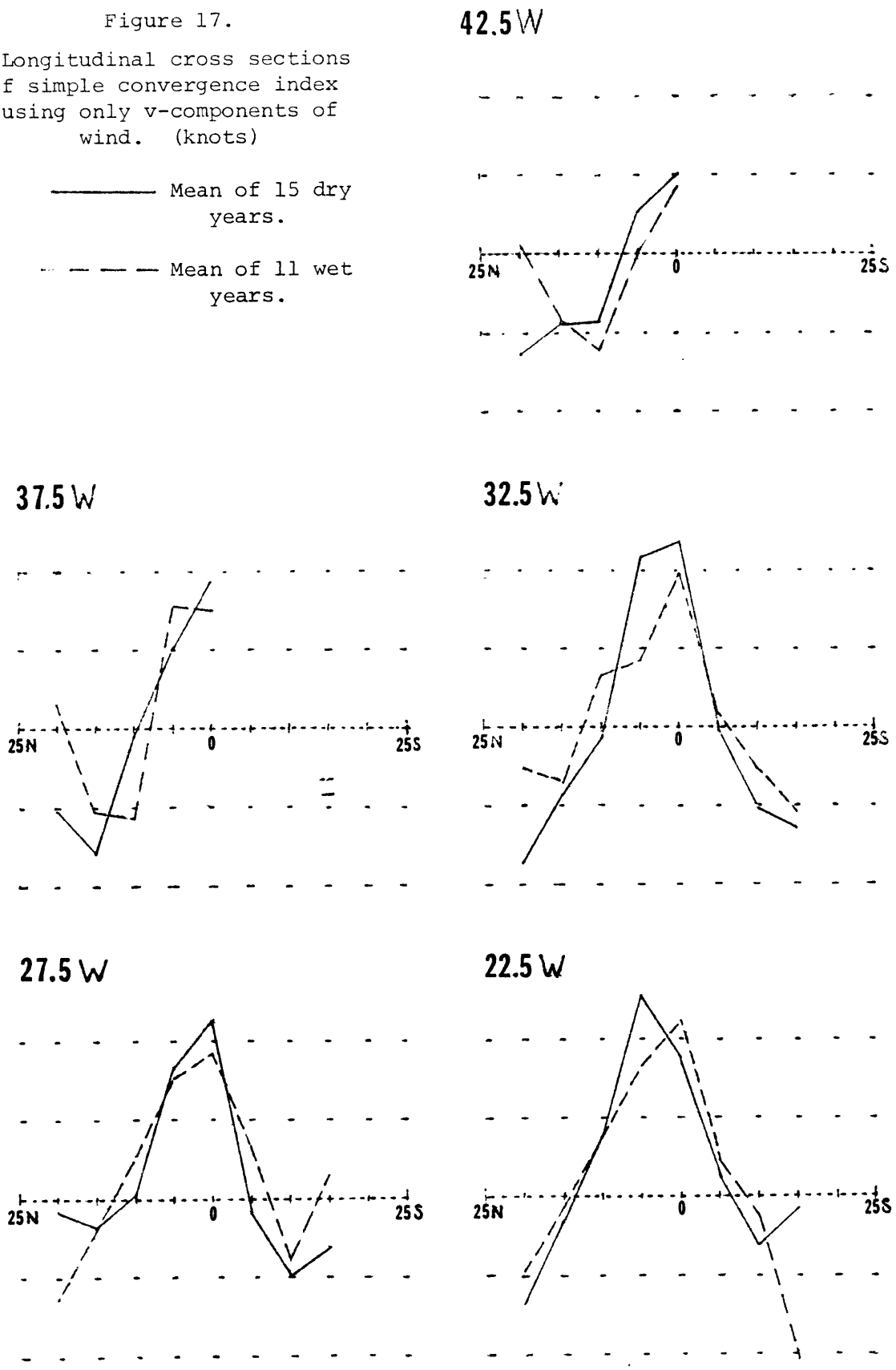

Figure 18.

Longitudinal cross sections of second convergence index using both u- and v-components, and accounting for meridional convergence. (knots)

———— Mean of 15 dry years.

— — — — Mean of 11 wet years.

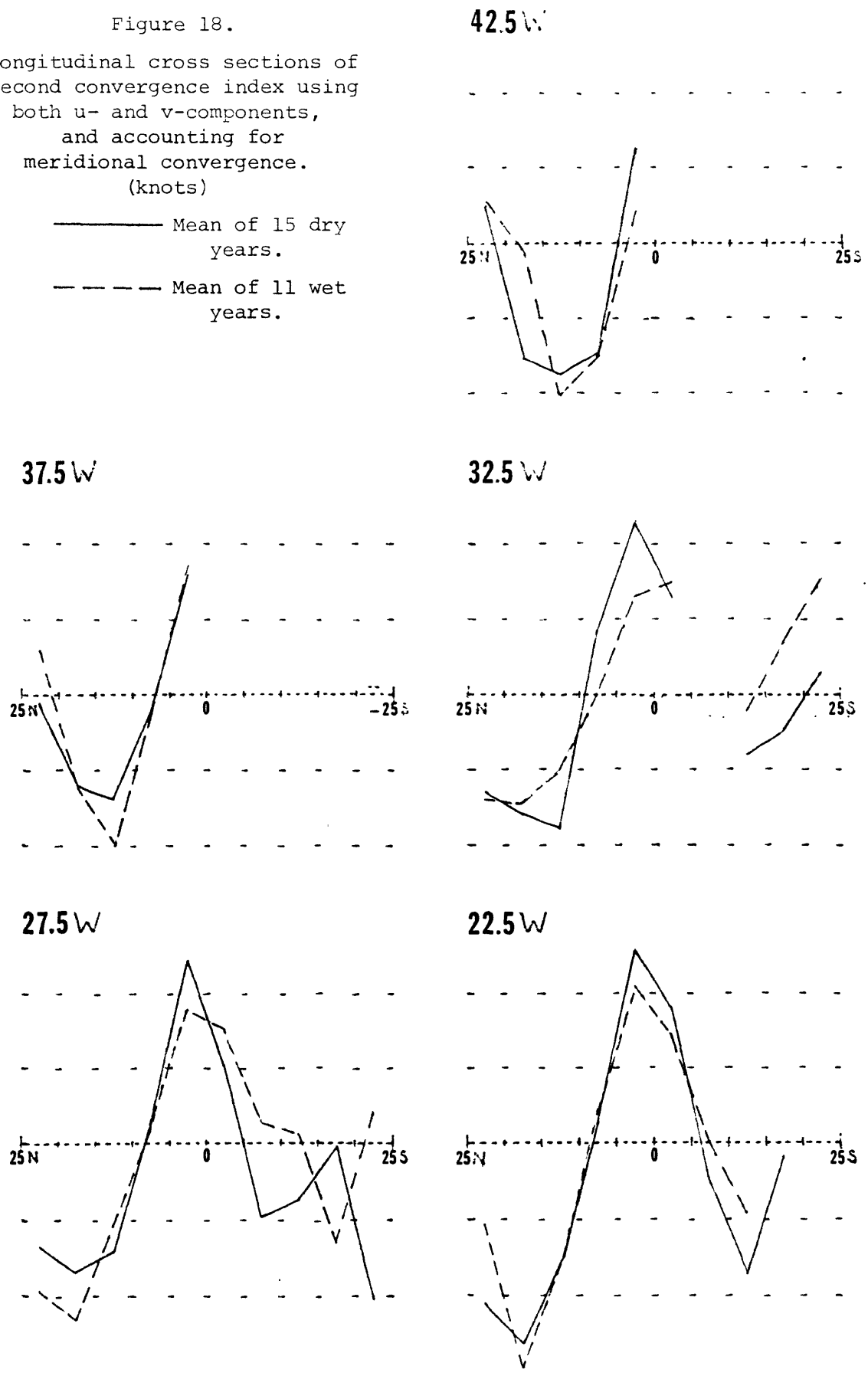

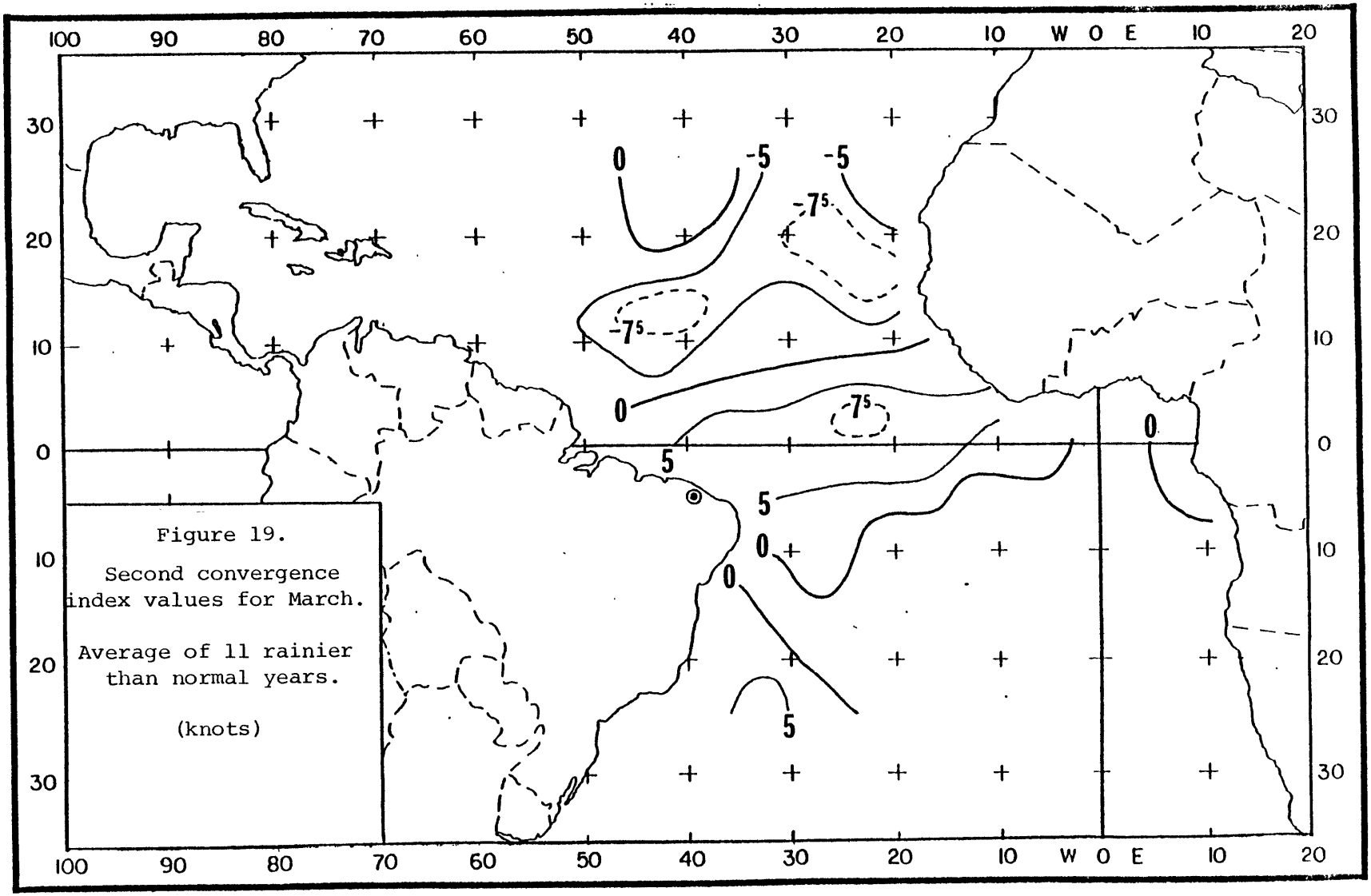
100 90 80 70 60 50 40 30 20 10 W 0 E 10 20
30
20
10
0
10
20
30
0
-5
-5
-7.5
-7.5
-7.5
0
0
5
5
0
0
5
Figure 19.
Second convergence index values for March.
Average of 11 rainier than normal years.
(knots)

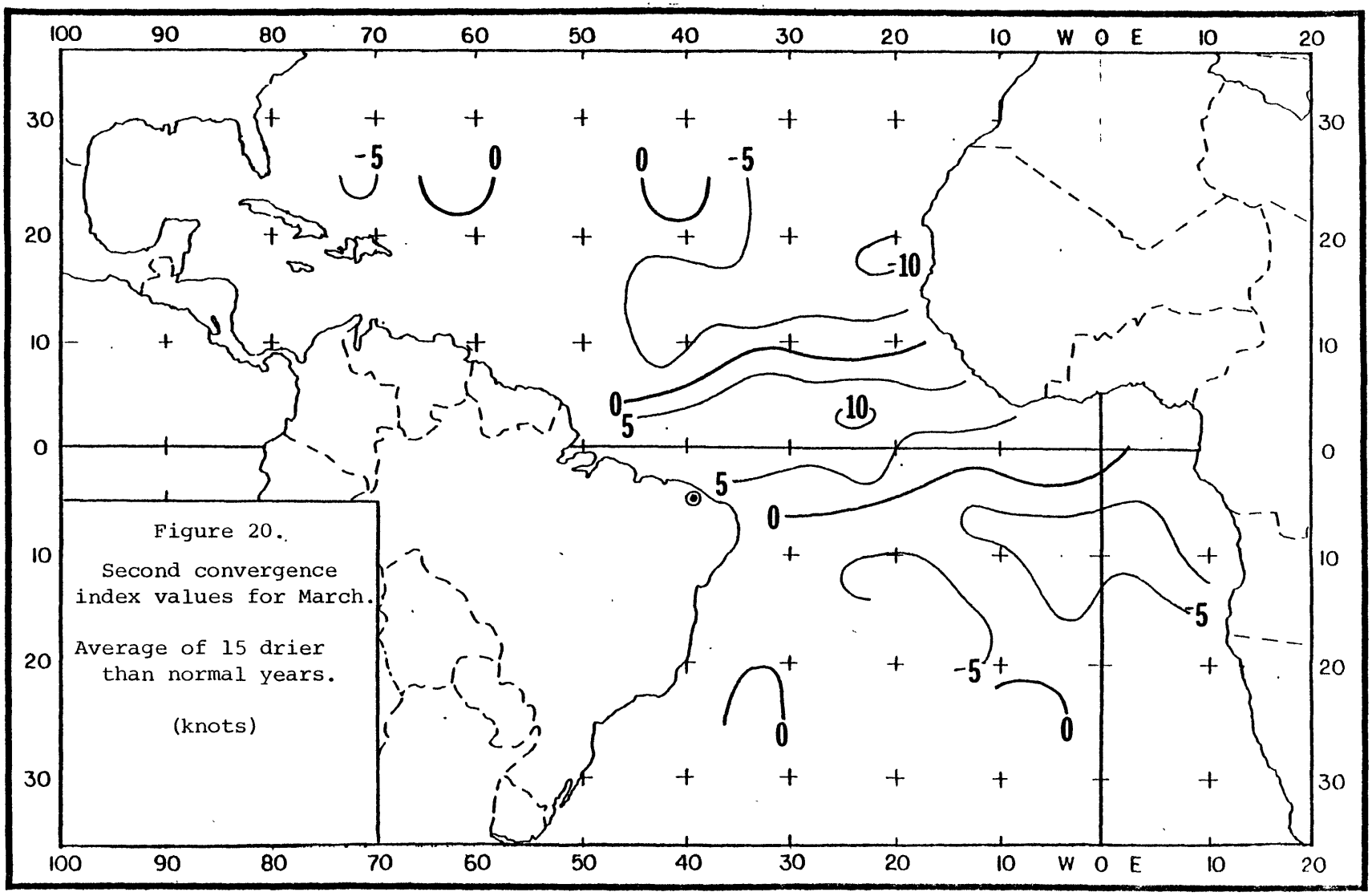

Figure 20.

Second convergence index values for March.

Average of 15 drier than normal years.

(knots)